THE ANTENNA LABORATORY

RESEARCH ACTIVITIES in ---

Antenna Control *Antennas* *Echo Area Studies*
Microwave Circuits *Aeronautics* *E M Field Theory*
Terrain Investigations *Radomes* *Systems Analysis*
Wave Propagation *Submillimeter Applications*

AD 641197

A FIRST ORDER APPROACH TO RADOME BORESIGHT ANALYSIS AND DESIGN

R. E. Van Doeren

Contract Number NOw-64-0293-d

1894-6 15 March 1966

DDC
NOV 3 1966
A

Prepared for:
Department of the Navy
Bureau of Naval Weapons
Washington, D.C.

Department of ELECTRICAL ENGINEERING

Code 1
CLEARINGHOUSE
FOR FEDERAL SCIENTIFIC AND
TECHNICAL INFORMATION
Hardcopy $3.00 | Microfiche $0.75 | 79 pp
ARCHIVE COPY

THE OHIO STATE UNIVERSITY
RESEARCH FOUNDATION
Columbus, Ohio

REPORT 1804-6

REPORT
by
THE OHIO STATE UNIVERSITY RESEARCH FOUNDATION
COLUMBUS, OHIO 43212

Sponsor	Department of the Navy Bureau of Naval Weapons Washington, D. C.
Contract Number	NOw-64-0293-d
Investigation of	Electronic Polarization Control
Subject of Report	A First Order Approach to Radome Boresight Analysis and Design
Submitted by	R. E. Van Doeren Antenna Laboratory Department of Electrical Engineering
Date	15 March 1966

Release to Defense Document Center (formerly ASTIA) without Restriction.
Release by the Office of Technical Service, Department of Commerce, is approved.

ABSTRACT

A simplified first-order theory of radome boresight error is derived and applied to prediction and design problems. Reasonable predictive results are obtained for radomes with known boresight error.

The dependence of boresight error on the derivatives of IPD and $|T|$ with respect to incidence angle is shown and the significance of polarization in light of the theory is discussed. Polarization control is shown to reduce boresight error when used with an appropriate radome wall design.

The possibility of a "cancellation" design for a radome, wherein the errors due to phase tapering and to differential attenuation tend to cancel each other is pointed out. The concept of artificially introduced loss to achieve such cancellation is discussed. A design example is included.

Radome design curves giving $|T|^2$, IPD, $d/d\theta(\text{IPD})$, and $d/d\theta|T|$ for several important radome wall structures are also included.

TABLE OF CONTENTS

TABLE OF CONTENTS (cont)

A FIRST ORDER APPROACH TO RADOME BORESIGHT ANALYSIS AND DESIGN

I. INTRODUCTION

A protective radome is usually necessary to shield track and guidance radars from the elements. The radome, however, introduces phase and amplitude perturbations to the antenna fields which act to reduce the radar's accuracy and range.

For most practical radome wall structures, the incidence angle is less than 80°. A significant improvement in the power transmission coefficient, and hence the range,[1] could be realized if one were able to maintain parallel polarization incident on the radome for all antenna positions. Investigation of the possibility that polarization control might provide similar improvement in boresight error is the main topic of this report.

As a basis for determining polarization effects, a first-order theory of in-plane boresight error of a two dimensional radome is developed. The first-order boresight theory presented here has the advantage of being simpler than most previous approaches.[2-8] Moreover, it focuses attention on the principal boresight error parameters.

Design curves for several practical radome wall structures are included. Application of these curves to radome boresight analysis and design is discussed. Conclusions regarding polarization effects on boresight error are drawn. The design curves depart from other work on plane-wave, plane-sheet transmission[8-10] by inclusion of the calculated derivatives of both the transmission coefficient and IPD, in addition to the usual data on $|T|^2$ and IPD.

Justification of the first-order boresight theory is provided by comparing predicted boresight error with the experimentally measured boresight error of two radomes. The comparison is reasonable and it is concluded that guidelines drawn from the theory and the design curves are valid.

II. FIRST-ORDER THEORY OF TRACK RADAR BORESIGHT ERRORS

The function of a track radar is to provide accurate target position information to a weapons system. At the present time the most accurate track information is obtained by positioning the radar antenna so that the

target is located in a sharp, well-defined null, the angular position of which is accurately known. There are two distinct kinds of null-type tracking radars, i.e., amplitude comparison radars and phase comparison radars. The principles of operation and the first-order boresight theories of each are discussed separately.

A. Amplitude Comparison Radars

1. Theory of operation

Amplitude comparison radars utilize two squinted beams in each of two (usually orthogonal) planes. The target responses of the two beams in a given plane are compared and the antenna pointed such that the target is maintained at the crossover point, the angle at which the beam responses are equal. The apparent boresight direction is that of the crossover point; the deviation of the apparent boresight direction from the true pointing direction of the antenna is called the boresight error.

In amplitude monopulse radars the steering information is obtained from the monopulse ratio

$$r(\phi) = \frac{F_1(\phi) - F_2(\phi)}{F_1(\phi) + F_2(\phi)} \quad , \tag{1}$$

where $F_1(\phi)$ and $F_2(\phi)$ are the patterns of the individual beams. A method for obtaining the sum and the differences of the beam responses is shown in Fig. 1.

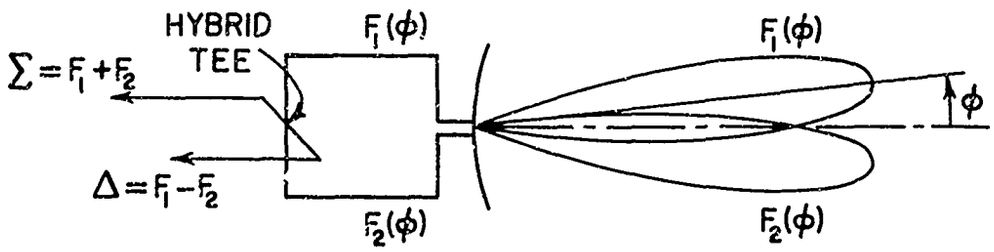

Fig. 1. Sum and difference network for amplitude monopulse.

The phase centers of the two antenna beams are assumed coincident for monopulse, and the two patterns are assumed identical without a radome. The effects of non-coincidence of the phase centers and of a constant phase difference between the two beams (at a given frequency) are to fill in the null of $r(\phi)$ and thus degrade the monopulse system performance. However, the location of the minimum of $r(\phi)$ is not perturbed and thus the boresight direction is not affected by the above errors.

In multipulse amplitude comparison radars, such as conical scan and sequential lobing radars, the steering information is obtained by some direct comparison of the amplitude responses of the two squinted beams in a particular plane. Thus, non-coincidence of the beam phase centers or phase differences between the beams does not affect the performance.

The boresight error of interest here is the deviation of crossover from the true pointing direction. The boresight error analysis of both monopulse and multipulse amplitude comparison radomes is thus the same.

2. Amplitude comparison boresight error

The crossover point can be shifted by two effects. First, there is a beam-bending error caused by a tilted phase front. This effect shifts the entire two-beam pattern. Second, there is a differential attenuation error which simply changes the angle at which one beam's response equals that of the other. The total boresight error is the algebraic sum of the preceding two errors; both are discussed in detail below.

a. Beam-bending boresight error

If an aperture with uniform phase is used with a radome which has nonuniform insertion phase delay, the aperture's beam will be bent; i.e., it will no longer be directed normal to the aperture face. If, for example, a beam is directed through a radome with continuous variation of incidence angle of the rays from the aperture, the transmitted phase across the aperture can be expanded in a Taylor series in powers of the increment in incidence angle from the center of the aperture to either side. Figure 2 shows the geometry of the two-dimensional aperture and radome wall which are the bases for the boresight criteria developed. At any point outside the radome we can therefore write the new aperture phase as follows:

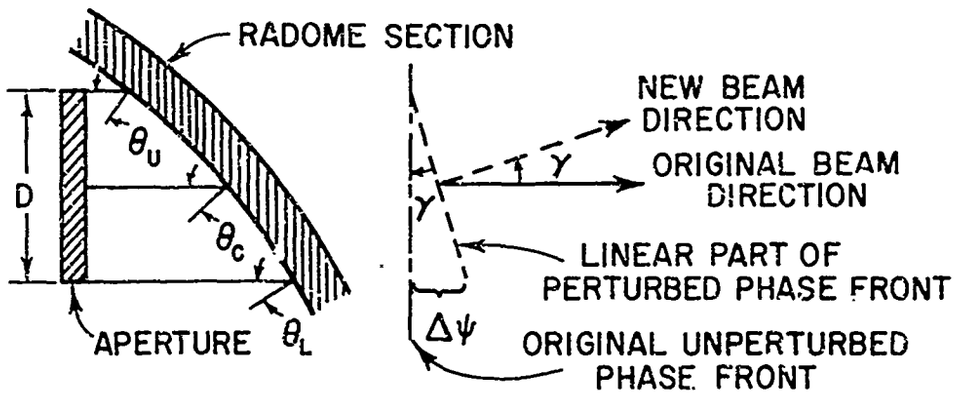

Fig. 2. Two-dimensional antenna-radome geometry used in the boresight analysis.

$$(2) \qquad \psi = \psi_o + \frac{\partial(\mathrm{IPD})}{\partial\theta}\bigg|_{\theta_c} (\theta - \theta_c) + \frac{\partial^2(\mathrm{IPD})}{\partial\theta^2}\bigg|_{\theta_c} \frac{(\theta - \theta_c)^2}{2!}$$

$$+ \frac{\partial^3(\mathrm{IPD})}{\partial\theta^3}\bigg|_{\theta_c} \frac{(\theta - \theta_c)^3}{3!} + - - - - - - .$$

For a smooth radome, the second-degree term is very nearly symmetrical and therefore does not contribute a beam-bending phase slope. In practice, the first derivative of the IPD with respect to incidence angle is at least two orders of magnitude greater than the third derivative. Thus, so long as $(\theta - \theta_c)$ is less than about ten degrees, the third-order term may be neglected in making a first-order approximation to the linear component of the phase slope.*

---

* For many radome walls, the first derivative is three orders of magnitude larger than the third, and still larger increments of incidence angle can be tolerated in the approximation.

Thus, the first-order approximation of the linear phase taper introduced across the aperture by the radome is given by

$$\Delta\psi = \left.\frac{\partial(\mathrm{IPD})}{\partial\theta}\right|_{\theta_c} (\theta_U - \theta_L) . \tag{3}$$

Reference to Fig. 2 shows that we can approximate the new beam direction, γ (the beam-bending angle), by considering the original aperture to have the linear phase taper $\Delta\psi$ across it. Adopting this approach, we find

$$\tan\gamma = \frac{\Delta\psi}{2\pi\frac{D}{\lambda}} , \quad \Delta\psi \text{ in radians;} \tag{4}$$

$$\tan\gamma = \frac{\Delta\psi}{360\frac{D}{\lambda}} , \quad \Delta\psi \text{ in degrees .} \tag{5}$$

The beam-bending angle is rarely greater (for practical radomes) than a few degrees and we can therefore replace $\tan\gamma$ by γ. By using the expression for $\Delta\psi$ in degrees we have, then,

$$\gamma = \frac{\Delta\psi}{360\frac{D}{\lambda}} , \quad \gamma \text{ in radians.} \tag{6}$$

If we rewrite the beam-bending boresight error as m_{bb} in milliradians (1 radian = 10^3 milliradian), we find

$$m_{bb} = \gamma \times 10^3 = 2.78 \frac{\Delta\psi}{D/\lambda} . \tag{7}$$

But, using Eq. (3) in Eq. (7), we get

$$m_{bb} = \frac{2.78}{D/\lambda} \left.\frac{\partial(\mathrm{IPD})}{\partial\theta}\right|_{\theta_c} (\theta_U - \theta_L) . \tag{8}$$

In Eq. (8) $(\theta_U - \theta_L)$ is in degrees (see Fig. 2), $\partial(\text{IPD})/\partial\theta$ may be in degrees/degree or radians/radian, and m_{bb} is in milliradians. A positive error is directed toward the beam axis of $F_1(\dot{\phi})$ and a negative error toward $F_2(\dot{\phi})$.

b. Differential attenuation boresight error

The crossover point of two identical, squinted beams determines the boresight direction observed by an amplitude radar. Attenuation of one beam relative to the other will clearly change the angle at which the two beams have equal amplitude. If intially identical beams are squinted through an angle δ, as shown in Fig. 3, we have, if $F(\dot{\phi})$ is an even function,

$$(9) \qquad \begin{cases} F_1(\dot{\phi}) = F(\dot{\phi} - \delta/2) \\ F_2(\dot{\phi}) = F(\dot{\phi} + \delta/2) \\ F(\dot{\phi}) = F(-\dot{\phi}) \end{cases}$$

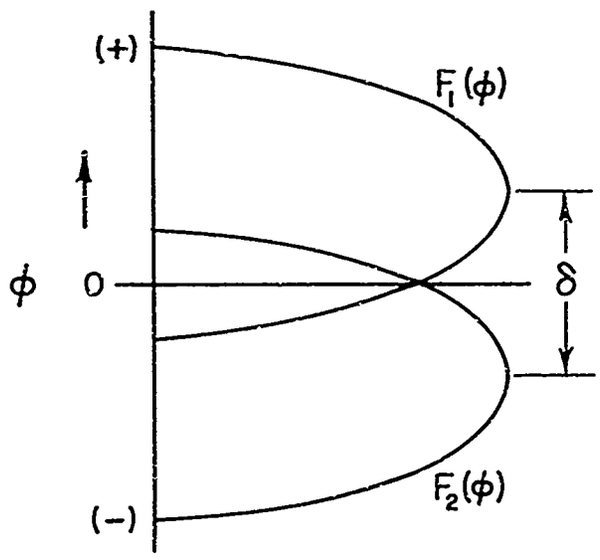

Fig. 3. Squinted beam geometry.

The unperturbed boresight direction is given by

$$F_1(\phi) - F_2(\phi) = F(\phi - \delta/2) - F(\phi + \delta/2) = 0 .$$

If an amplitude perturbation factor, α, is inserted, the perturbed boresight direction (crossover point) is given by

(10) $$\alpha\, F(\phi - \delta/2) - F(\phi + \delta/2) = 0.$$

In practice, α is not very different from unity and the boresight errors are small enough so that they can be quite closely approximated using straight line representations of $F_1(\phi)$ and $F_2(\phi)$ at the crossover point. If s is chosen to be the positive slope of $F_1(\phi)$ at $\phi = 0$ (original cross-over point), then near $\phi = 0$, we have.

(11) $$F_1(\phi) = F_0 + s\,\phi$$
$$F_2(\phi) = F_0 - s\,\phi \quad ,$$

where F_0 is the amplitude level at which the patterns cross. Using Eq. (11) in Eq. (10), we get the following equation for the new boresight direction:

$$\alpha(F_0 + s\phi_0) - (F_0 - s\phi_0) = 0 \quad ,$$

which gives for ϕ_0, the new, apparent, boresight direction

(12) $$\phi_0 (1 + \alpha) s = F_0(1 - \alpha)$$

$$\phi_0 = \frac{F_0}{s} \frac{1 - \alpha}{1 + \alpha} \quad .$$

By restricting our concern to small boresight errors we are able to consider only those values of α such that $0.9 \leq \alpha < 1.1$. For α in this range, the following approximation is within 5% :

$$\frac{1-\alpha}{1+\alpha} \approx \frac{1-\alpha}{2} \quad .$$

Thus, for small boresight errors, the new boresight location, ϕ_0, is given by

$$(13) \qquad \phi_0 = (1 - \alpha)\ \frac{F_0}{2s} \quad .$$

If we put ϕ_0 in milliradians and re-label it m_a, and put s in units per milliradian, we can write the following for the boresight error resulting from differential attenuation:

$$(14) \qquad m_a = (1 - \alpha)\ \frac{F_0}{2s} \quad .$$

The perturbation (attenuation) factor α is related to the variation of transmission coefficient by the following discussion.

Let θ_1 be the average incidence angle for beam 1, θ_2 that for beam 2, and θ_{AVG} the average of the two. Write the magnitude of the transmission coefficients of the respective beams as follows:

$$(15) \qquad |T_1| = |T(\theta_{AVG})| + \left.\frac{\partial T}{\partial \theta}\right|_{\theta_{AVG}} (\theta_1 - \theta_{AVG}) + \left.\frac{\partial^2 T}{\partial \theta^2}\right|_{\theta_{AVG}} \frac{(\theta_1 - \theta_{AVG})^2}{2!} + \ldots .$$

and

$$(16) \qquad |T_2| = |T(\theta_{AVG})| + \left.\frac{\partial T}{\partial \theta}\right|_{\theta_{AVG}} (\theta_2 - \theta_{AVG}) + \left.\frac{\partial^2 T}{\partial \theta^2}\right|_{\theta_{AVG}} \frac{(\theta_2 - \theta_{AVG})^2}{2!} + \ldots . \quad .$$

Neglecting second-order terms and higher, and subtracting Eq. (15) from Eq. (16), we find

$$\Delta|T| = |T_2| - |T_1| = |T_2|\,(1 - \alpha)$$

$$\Delta|T| = -\frac{\partial T}{\partial \theta}\bigg|_{\theta_{AVG}} (\theta_1 - \theta_2) \quad .$$

The result for $(1 - \alpha)$ is, therefore,

$$(1 - \alpha) = \frac{-1}{|T_2|}\,\frac{\partial T}{\partial \theta}\bigg|_{\theta_{AVG}} (\theta_1 - \theta_2) \quad . \tag{17}$$

Using Eq. (17) in Eq. (14), we obtain the result for the boresight error due to differential attenuation

$$m_a = -\frac{F_0}{2s}\,\frac{1}{|T_2|}\,\frac{\partial |T|}{\partial \theta}\,(\theta_1 - \theta_2) \quad , \tag{18}$$

where

F_0 = normalized nominal cross-over amplitude;

s = positive slope of the individual patterns at $\phi = 0$ $[F(\phi) = F_0]$ in units per milliradian; and

$(\theta_1 - \theta_2)$ is consistent in units with $\partial|T|/\partial\theta$ and θ_1 is the average incidence angle of beam 1 and θ_2 that of beam 2.

The total first-order boresight error for an amplitude comparison radar (monopulse or multipulse) is thus given by

$$m = \frac{2.78}{D/\lambda}\,\frac{d(IPD)}{d\theta}\bigg|_{\theta_c} (\theta_U - \theta_L) - \frac{F_0}{2s}\,\frac{1}{|T_2|}\,\frac{d|T|}{d\theta}\,(\theta_1 - \theta_2) \quad , \tag{19}$$

where all the symbols are defined in the text just after Eq. (8) and Eq. (18). The partial derivatives have been replaced by the regular derivatives since this is the notation used in the curves of Appendix A.

The presence of two terms in Eq. (19) provides for the possibility of one term reducing or even cancelling the other. More is said later about the significance of this so-called cancellation design.

B. Phase Comparison Track Radars

1. Theory of operation

A track radar using phase comparison is inherently a monopulse radar since the required coherency of the electromagnetic waves can be obtained only within a single pulse. An in-plane phase monopulse radar uses two side-by-side parallel-directed antennas as shown in Fig. 4.

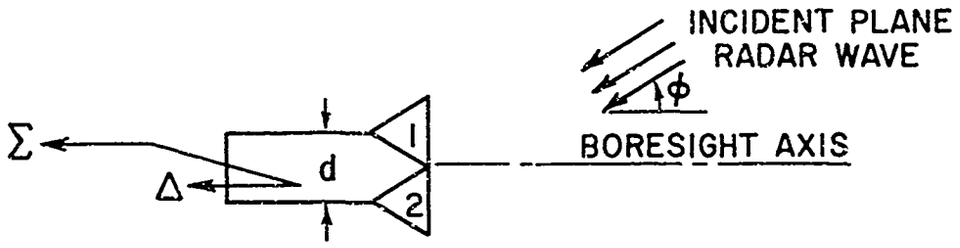

Fig. 4. Sum and difference network for phase monopulse.

The steering information in a phase monopulse radar is also obtained from the monopulse ratio which is given by

$$r(\phi) = \frac{e^{j\left(k\frac{d}{2}\sin\phi + \frac{\pi}{2}\right)} + e^{-j\left(k\frac{d}{2}\sin\phi + \frac{\pi}{2}\right)}}{e^{j\left(k\frac{d}{2}\sin\phi\right)} + e^{-j\left(k\frac{d}{2}\sin\phi\right)}} = \frac{\Delta}{\Sigma} \quad , \tag{20}$$

where d is the phase center spacing and k is the free-space propagation constant, $2\pi/\lambda_0$. The monopulse ratio reduces to,

$$r(\phi) = \frac{\cos\left(\pi\frac{d}{\lambda_0}\sin\phi + \frac{\pi}{2}\right)}{\cos\left(\pi\frac{d}{\lambda_0}\sin\phi\right)} = -\tan\left(\pi\frac{d}{\lambda_0}\sin\phi\right) \quad . \tag{21}$$

Equation (21) gives the response of an ideal phase monopulse radar. $r(\phi)$ contains all the steering information necessary to position the antenna so that the target is in the null. If non-ideal conditions prevail, such as non-identical patterns or existence of an extraneous relative retardation in phase, the character of $r(\phi)$ will be altered and the system performance changed.

2. Phase comparison boresight error

If the functional form of the antenna patterns remains the same, the effect of reduction of the amplitude of one beam with respect to the other is to fill in the null of the monopulse ratio but not to change the position of the minimum of $r(\phi)$. Hence, differential attenuation does not result in boresight error for a phase monopulse radar.

The effect of an extraneous phase shift, however, is another story. If such a relative phase shift, η, exists, advancing antenna 2 relative to 1, it must be included in the exponentials of Eq. (20). $r(\phi)$ then becomes

$$r(\phi) = -\tan\left(\pi \frac{d}{\lambda_0} \sin\phi - \frac{\eta}{2}\right) . \tag{22}$$

Hence, when such a phase advance exists, the electrical boresight direction $[r(\phi_0) = 0]$ is obtained from Eq. (22) as

$$\sin\phi_0 = \frac{\eta}{2\pi \frac{d}{\lambda_0}} . \tag{23}$$

In Eq. (23), ϕ_0 is the boresight error. In practice, ϕ_0 is small and Eq. (23) can be written

$$\phi_0 = \frac{\eta}{2\pi \frac{d}{\lambda_0}} . \tag{24}$$

In Eq. (24), ϕ_0 and η are in radians. A more convenient expression gives ϕ_0 (re-labeled m) in milliradians and η in degrees:

$$m = 2.78 \frac{\eta}{d/\lambda_0} \quad . \tag{25}$$

For the case of a radome in place over the phase monopulse radar, a phase error of the type described above can be introduced by a difference in insertion phase delay through the radome for the two antennas. If ψ_0 is the insertion phase delay (IPD) at the average angle of incidence for the two antennas, the average IPD for the individual antennas can be expressed as follows:

$$\psi_2 = \psi_0 + \frac{\partial \psi}{\partial \theta}\Big|_{\theta_{AVG}} (\theta_2 - \theta_{AVG}) + \frac{\partial^2 \psi}{\partial \theta}\Big|_{\theta_{AVG}} \frac{(\theta_2 - \theta_{AVG})^2}{2!} + \cdots \tag{26}$$

and

$$\psi_1 = \psi_0 + \frac{\partial \psi}{\partial \theta}\Big|_{\theta_{AVG}} (\theta_1 - \theta_{AVG}) + \frac{\partial^2 \psi}{\partial \theta}\Big|_{\theta_{AVG}} \frac{(\theta_1 - \theta_{AVG})^2}{2!} + \cdots \quad . \tag{27}$$

To find the relative phase advance of antenna 2 relative to antenna 1, Eq. (26) is subtracted from Eq. (27) and only the first-degree terms are retained:

$$\eta = \psi_1 - \psi_2 = \frac{\partial \psi}{\partial \theta}\Big|_{\theta_{AVG}} (\theta_1 - \theta_2) \quad . \tag{28}$$

θ_1 is the average incidence angle for antenna 1 and θ_2 that for antenna 2. The first-order formula for boresight error in a phase monopulse radar is, therefore,

$$m = \frac{2.78}{d/\lambda_0} \frac{\partial(\text{IPD})}{\partial \theta}\Big|_{\theta_{AVG}} (\theta_1 - \theta_2) \quad , \tag{29}$$

m = boresight error in milliradian,

$\theta_1-\theta_2$ = difference in average angle of incidence seen by the two antennas in degrees, and

d/λ_0 = phase center separation of the two antennas.

III. BORESIGHT ERROR PREDICTION

Approximate equations are derived in Section II for the boresight error of a streamlined two-dimensional radome. The predictive potency of these equations for a three-dimensional radome is not expected to be great although reasonable predictions should be expected, at least away from the nose region. Pressel[11] has pointed out that application of two-dimensional analysis to three-dimensional radomes gives surprisingly good results. In any case, justification of Eqs. (8) and (18), specifically, will be attempted by predicting the boresight error of two radomes for which the boresight error has been reported. Both radomes in question house amplitude comparison radars.

In Eq. (8), the value of D/λ_0 used for the calculations is that of an equivalent uniformly excited circular aperture having the same 3 dB beamwidth as the actual antenna. Use of this "equivalence" is appropriate since the low-amplitude tapers at the edge of the aperture contribute very little to formation of the main beam (the region of interest in boresight analysis) but act largely to inhibit sidelobe development.

The equations of Section II were derived for a smoothly varying radome wall. Application of the beam bending equation (Eq. (8)) to the nose region of a radome involves a rather arbitrary method of averaging. At the look angle such that one-half the equivalent aperture has its rays symmetrically disposed about the nose (as shown in Fig. 5) the beam bending boresight error is computed using the following qualitative technique . It is noted that the half-aperture looking through the nose has a nearly symmetrical incidence angle distribution; the beam of this half aperture will therefore experience no bending. This result is interpreted as being equivalent to a constant incidence angle of zero degrees for this half. The average incidence angle for the other half aperture is found. Then the average incidence angle of the averages of the two half-apertures is found and used for $(\theta_U - \theta_L)$ in Eqs. (8) and (19). This amounts to using one-half the average incidence angle of the upper half aperture (see Fig. 5) for $(\theta_U - \theta_L)$

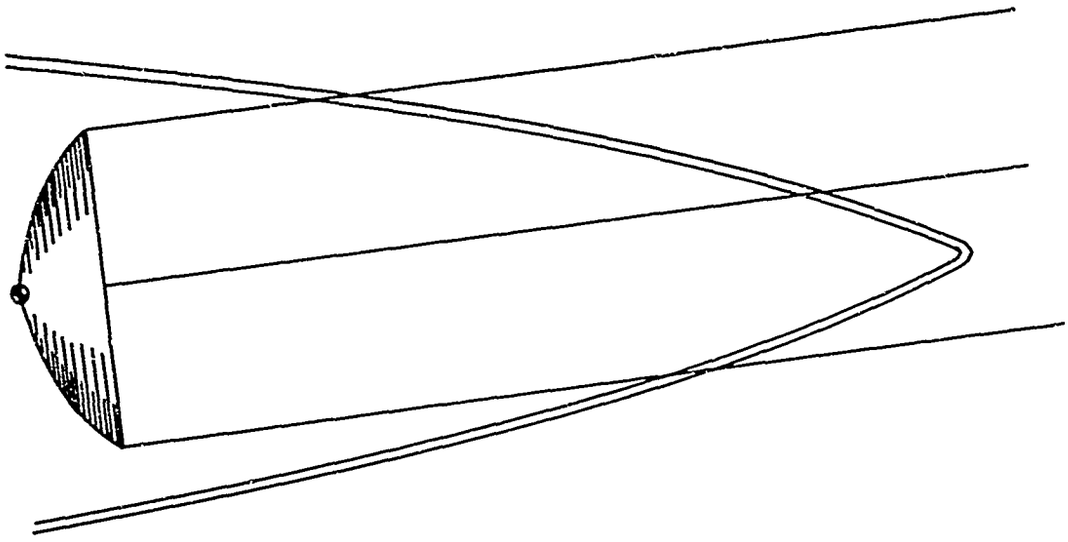

Fig. 5. Antenna with one-half its aperture symmetrically disposed about the radome nose.

For the radomes studied here, the average incidence angles for the two squinted beams (used in computing the differential attenuation error) are taken from the averages of three rays for each beam. These average angles are recorded as θ_1 and θ_2 directly for beams 1 and 2.

A. Radome 1, First-Order Prediction*

This radome is a half-wave plastic ($\epsilon = 4.3$) radome with a 2.1:1 fineness ratio. It houses a conical scan antenna which has a half-power beamwidth of 4.6° in both principal planes. The antenna-radome geometry is shown in Fig. 6.

The modified aperture is found from the formula for the 3 dB beamwidth of a uniform circular aperture as follows:

$$\theta_{3dB} = \frac{58.9}{D/\lambda} \text{ degrees} = 4.6°$$

and

---

* A good discussion of a more rigorous approach to predicting the boresight error of this radome is included in reference 6 in addition to the experimental data.

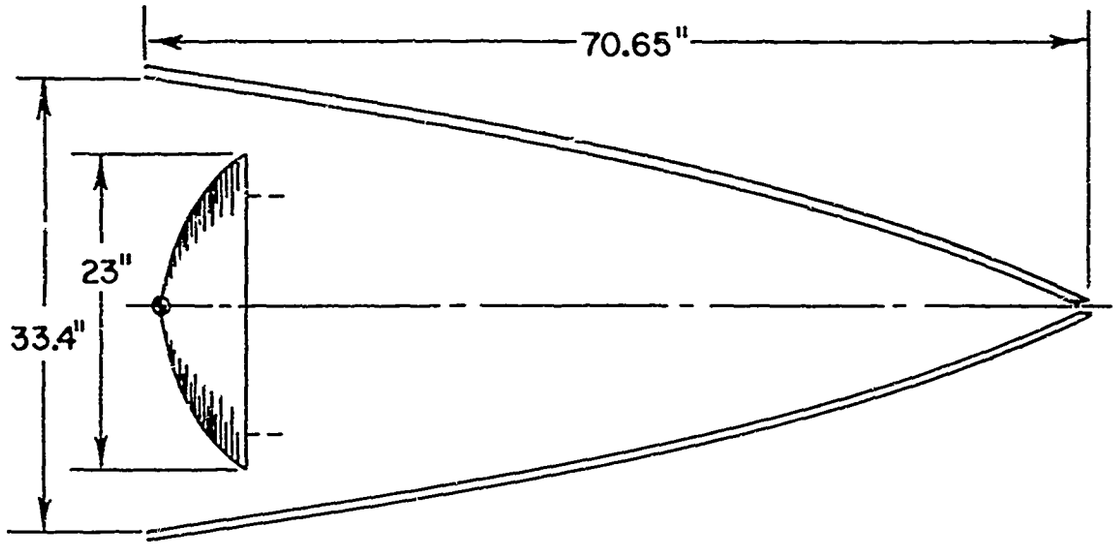

Fig. 6. Radome 1, antenna-radome geometry.

$$\left(\frac{D}{\lambda}\right)_{eq} = \frac{58.9}{4.6} = 12.8 \ .$$

Thus, if we set

$$\frac{D}{\lambda} = \left(\frac{D}{\lambda}\right)_{eq} = 12.8$$

in Eq. (8), the beam-bending portion of Eq. (19) becomes:

$$m_{bb} = (0.217)\,(\theta_U - \theta_L)\,\frac{d}{d\theta}\,(IPD) \ . \tag{31}$$

The slopes of the amplitude patterns at the 3 dB points were measured in each plane and found to be

$$\text{E-plane: } s_E = 12.8 \times 10^{-3} \text{ units/mrad}$$

and

$$\text{H-plane: } s_H = 15.1 \times 10^{-3} \text{ units/mrad} \ .$$

Crossover occurs for $F_0 = 0.707$. Insertion of these values and appropriate nominal values of $|T|$ in the differential attenuation portion of Eq. (19) gives, for the total boresight error,

$$m = (.217)(\theta_u - \theta_L)\frac{d}{d\theta}(IPD) - \begin{Bmatrix} 28.3 \\ 27.1 \end{Bmatrix} (\theta_1 - \theta_2)\frac{d|T|}{d\theta} \begin{Bmatrix} \text{E-plane} \\ \text{H-plane} \end{Bmatrix} . \tag{32}$$

In Eq. (32) the upper multiplier is used for the E-plane (parallel polarization) and the lower multiplier is used for the H-plane (perpendicular polarization).

The particular radome to be analyzed is radome Z - 2i of Reference 6. This radome is 0.39 inch thick and is used at a wavelength of $\lambda_0 = 1.344$ inches. Thus $d/\lambda_0 = 0.29$. If the wall material were of $\epsilon = 4.0$ material, the operating point on Figs. 16 and 17 (Appendix A) would be

$$\Delta\% = \left[\frac{.29}{.2767} - 1\right] \times 100 = +4.8\% .$$

Because the dielectric constant is slightly different from 4.0, the operating frequency point must be adjusted by the per cent change in $\sqrt{\epsilon}$ as discussed in Appendix B. This additional change is found to be

$$\Delta_1\% = \frac{\sqrt{4.3} - \sqrt{4}}{\sqrt{4}} \times 100 = \frac{.074}{2} \times 100 = +3.7\% .$$

Thus the final operating point is

$$\Delta\% = 4.8\% + 3.7\% = 8.5\% .$$

Table I gives the boresight error data calculated for this radome, using Eq. (32) with measured incidence angles from Fig. 6 and data from Figs. 16 and 17 at the + 8.5% operating point.

Figure 7 shows the experimentally measured results for Radome Z - 2i and the first-order prediction of Eq. (32). The predicted error

TABLE I

TABULATED RADOME BORESIGHT DATA
(RADOME Z - 21, Ref. 6, +8.5% POINT ON FIGS. 16 AND 17)

LOOK ANGLE	INCIDENCE ANGLES							BEAM-BENDING BORESIGHT ERROR	DIFFERENTIAL ATTENUATION BORESIGHT ERROR	TOTAL BORESIGHT ERROR
ϕ (deg)	θ_u / θ_1 (deg)	θ_c (deg)	θ_L / θ_2 (deg)	θ_{NOM} (deg)	$\theta_u-\theta_L$ / $\theta_1-\theta_2$ (deg)	$\frac{d}{d\theta}(IPD)\Big\|_{\theta_{NOM}}\begin{Bmatrix}\parallel\\ \perp\end{Bmatrix}$	$\frac{d}{d\theta}T'\Big\|_{\theta_{NOM}}\begin{Bmatrix}\parallel\\ \perp\end{Bmatrix}$	$m_{bb}=(.217)(\theta_u-\theta_L)\frac{d}{d\theta}(IPD)\begin{Bmatrix}\parallel\\ \perp\end{Bmatrix}$ (milliradians - mr)	$m_a=-\left\{\frac{28.3}{27.1}\right\}(\theta_1-\theta_2)\frac{d'T'}{d\theta}\begin{Bmatrix}\parallel\\ \perp\end{Bmatrix}$ (milliradians - mr)	$m_t = m_{bb} + m_a$
5°	75° / 66°	66°	80° / 72°	70°	$\frac{71°}{2}=36°$ / -6°	1.55	0	12.1 mr	0	+12.1 mr (∥)
						1.95	-.0055	15.2 mr	-0.9 mr	+14.3 mr (⊥)
10°	72° / 62.5°	65°	59° / 66°	65°	13° / -3.5°	1.35	0	3.8 mr	0	+ 3.8 mr (∥)
						1.7	-0.0035	4.8 mr	-0.3 mr	+ 4.5 mr (⊥)
15°	66° / 60°	62°	56° / 64°	61°	10° / -4°	1.15	0	2.5 mr	0	+ 2.5 mr (∥)
						1.45	-0.0015	3.1 mr	-0.2 mr	+ 2.9 mr (⊥)
20°	61° / 57°	58°	53° / 61°	59°	8° / -4°	1.15	0	2.0 mr	0	+ 2.0 mr (∥)
						1.4	-0.0015	2.4 mr	-0.2 mr	+ 2.2 mr (⊥)

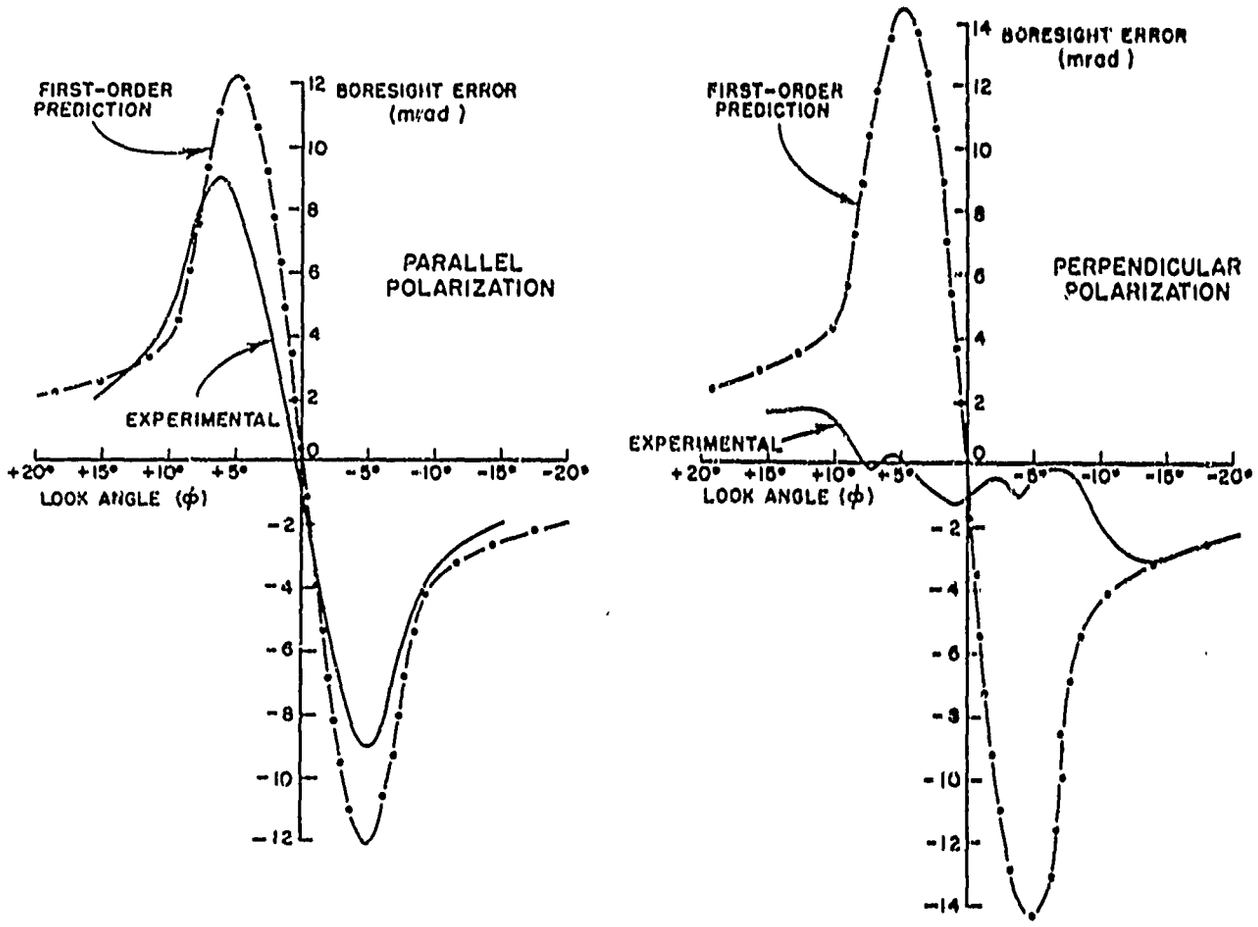

Fig. 7. Experimental and first-order predicted boresight error curves. (Radome Z-2i, Ref. 6, +8.5% point on Figs. 16 and 17)

for parallel polarization agrees quite reasonably with the experimental results; consequently the lack of agreement for perpendicular polarization is surprising.*

The poor prediction for perpendicular polarization probably is a consequence of the approximate nature of the prediction, especially in the nose region, and of physical tolerances in material uniformity and thickness in the radome. The low measured boresight error suggests that the radome was operating at a point such that the beam-bending and differential attenuation errors nearly canceled. Reference to Fig. 16 shows that if the operating point were at -3%, the magnitude of $d|T|/d\theta$ would be large enough to offset the effect of $d(IPD)/d\theta$. This observation is verified by the computed boresight data given in Table II for operation at the -3% point. (Note the change in the nominal value of $|T|$ for perpendicular polarization.) Figure 8 shows the graphical comparison of these results with the measured performance. The agreement for parallel polarization is very good and that for perpendicular quite reasonable.

These results point out several pertinent factors. The radome is very probably operating in a "cancellation" mode, thus justifying the form of Eq. (19) and indicating that loss can be a significant factor in boresight. Radome performance for perpendicular polarization is more sensitive to variation of the radome parameters than for parallel polarization. The off-nose predictions for parallel polarization were quite good for both operating points, suggesting that the beam-bending formulation may be better than the differential attenuation approximation (which was more or less negligible in the parallel polarization computations). The overall results of Eq. (19) are good when one considers the possibility of tolerance slippage (in the radome tested) and the arbitrary method of calculating nose region error.

---

* Correspondence with G. Tricoles (author of Reference 6) elicited the comment that the unusual (non-symmetric) experimental results for perpendicular polarization were probably caused, in part, by experimental error and in part by physical displacement of the curve downward. Mr. Tricoles was furnished the data by another organization.

TABLE II

TABULATED RADOME BORESIGHT DATA
(RADOME 2 - 21, Ref. 6, -3% POINT ON FIGS. 16 AND 17)

LOOK ANGLE	INCIDENCE ANGLES							BEAM-BENDING BORESIGHT ERROR	DIFFERENTIAL ATTENUATION BORESIGHT ERROR	TOTAL BORESIGHT ERROR
ϕ	θ_u / θ_1	θ_c	θ_L / θ_2	θ_{NOM}	$\theta_u - \theta_L$ / $\theta_1 - \theta_2$	$\frac{d}{d\theta}(IPD)'_{\theta_{NOM}} \begin{Bmatrix} u \\ \Delta \end{Bmatrix}$	$\frac{d}{d\theta}\lvert T\rvert_{\theta_{NOM}} \begin{Bmatrix} u \\ \Delta \end{Bmatrix}$	$m_{bb} = (.217)(\theta_u - \theta_L)\frac{d}{d\theta}(IPD) \begin{Bmatrix} u \\ \Delta \end{Bmatrix}$	$m_a = -\left\{\frac{28.3}{26.0}\right\}(\theta_1 - \theta_2)\frac{d\lvert T\rvert'}{d\theta} \begin{Bmatrix} u \\ \Delta \end{Bmatrix}$	$m = m_{bb} + m_a$
(deg)	(deg)	(deg)	(deg)	(deg)	(deg)			(milliradians - mr)	(milliradians - mr)	
5°	75° / 66°	66°	80° / 72°	70°	$\frac{73°}{2} = 36.5°$ / -6°	1.16	-0.001	9.0 mr	-0.2 mr	+8.8 mr (u)
						0.1	-0.012	0.8 mr	-1.9 mr	-1.1 mr (Δ)
10°	72° / 62.5°	65°	59° / 66°	65°	13° / -3.5°	1.12	-0.0005	3.2 mr	0 mr	+3.2 mr (u)
						0.3	-0.008	0.8 mr	- .7 mr	+0.1 mr (Δ)
15°	66° / 60°	62°	56° / 64°	61°	10° / -4°	1.08	0	2.3 mr	0 mr	+2.3 mr (u)
						0.56	-0.0044	1.2 mr	- .5 mr	+0.7 mr (Δ)
20°	61° / 57°	58°	53° / 61°	59°	8° / -4°	1.08	0	1.9 mr	0 mr	+1.9 mr (u)
						0.56	-0.0044	1.0 mr	- .5 mr	+0.5 mr (Δ)

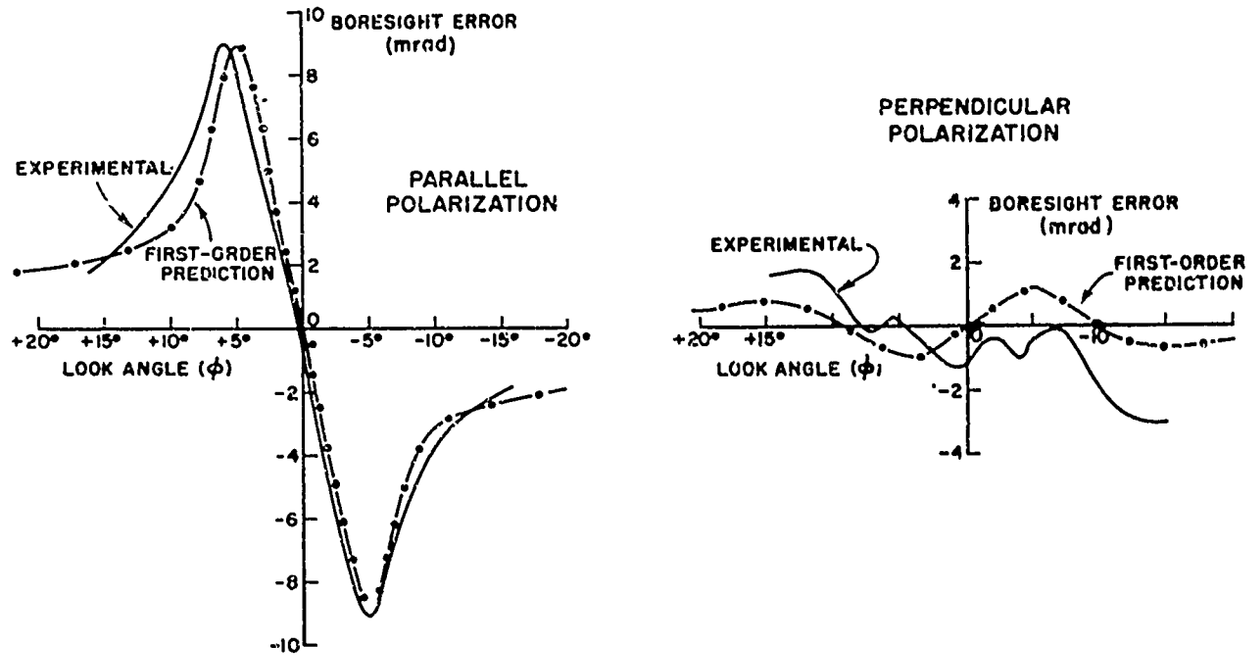

Fig. 8. Experimental and first-order theoretical boresight error curves. (Radome Z-2i, Ref. 6, -3% point on Figs. 16 and 17)

B. Radome 2, First-Order Prediction[12]

This radome is a half-wave wall of fiberglass-polyester ($\epsilon \approx 4.0$) construction designed to operate over the frequency range of 16.5 GHz $\pm$ 3%. The radome houses a conical scan radar antenna which is linearly polarized and has a half-power beam width of 5°. The radome wall thickness is a uniform 0.180 inch. The antenna-radome geometry is shown in Fig. 9. The equivalent aperture dimension for use in Eq. (8) is again found from the formula for the half-power beam width of a uniformly illuminated circular aperture ($\theta_{3dB} = 5°$ in this case):

$$5° = \frac{58.9°}{D/\lambda}$$

$$D/\lambda = \frac{58.9}{5°} = 11.8 \quad .$$

Then, using this value of D/λ in Eq. (8), we find

$$m_{bb} = 0.236\,(\theta_U - \theta_L)\frac{d}{d\theta}(IPD) \quad . \tag{33}$$

We assume that the crossover points of the antenna occur at $F_0 = 0.707$ and, in Eq. (18), use the slope at the half-power point of a uniformly illuminated line source with $D/\lambda = 11.8$. The slope of the amplitude pattern of a uniform line source at the half-power point is given by

$$s = (1.19)\ \frac{D}{\lambda}\ \times 10^{-3} \text{ units / mrad.} \tag{34}$$

In this case we have

$$s = 14.03 \times 10^{-3} \text{ units/mrad.}$$

Use of F_0 and s (given above) in Eq. (18) gives for the differential attenuation boresight error formula

$$m_a = -\frac{25.2}{|T_2|}\ (\theta_1 - \theta_2)\ \frac{\partial |T|}{\partial \theta} \quad .$$

$|T_2|$ is nominally 0.92 for the incidence angles here. The final result for the total boresight error is, therefore,

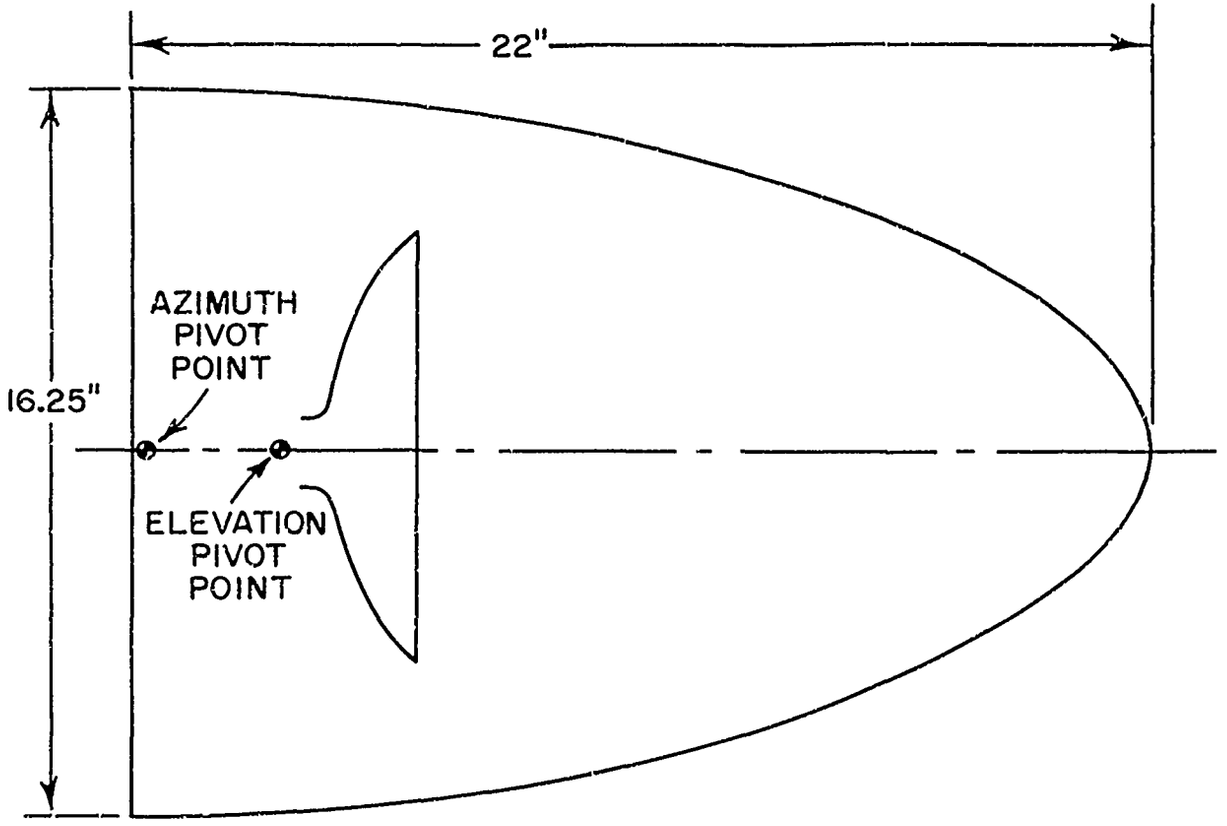

Fig. 9. Radome 2, antenna-radome geometry.

$$(35) \qquad m = (.236)(\theta_U - \theta_L)\frac{d}{d\theta}(IPD) - 27.4\,(\theta_1 - \theta_2)\frac{d|T|}{d\theta} \quad .$$

The dielectric constant is assumed to be $\epsilon = 4.0$, so Figs. 16 and 17 are directly applicable, and no correction for dielectric constant is necessary. The per cent frequency point is found as follows:

$$\frac{d}{\lambda} = \frac{.180}{.716} = 0.251$$

and

$$\Delta\% = \left(\frac{.251}{.2767} - 1\right) \times 100 = -9.4\% \; .$$

Table III presents the boresight data for this radome and Fig. 10 shows the experimental results and first-order predictions from one quadrant for each polarization. The agreement is again reasonable.

IV. RADOME DESIGN FOR MINIMUM BORESIGHT ERROR

Boresight design is discussed for the two principal types of track radars.

A. Phase Monopulse Boresight Design

The first-order theoretical boresight equation (Eq. (29)) is rewritten as

$$(36) \qquad m_P = \frac{2.78}{d/\lambda}\,\frac{\partial(IPD)}{\partial\theta}\,(\theta_1 - \theta_2) \; ,$$

where

m_P = boresight error in mrad,

d/λ = phase center separation of antennas 1 and 2,

θ_1 = average incidence angle of beam 1 (antenna 1), and

θ_2 = average incidence angle of beam 2 (antenna 2) (see Fig. 4).

TABLE III

TABULATED RADOME BORESIGHT DATA
(RADOME IN Ref. 12, -9.4% POINT ON FIGS. 16 AND 17)

LOOK ANGLE	INCIDENCE ANGLES									
θ (deg)	θ_u / θ_1 (deg)	θ_c (deg)	θ_L / θ_2 (deg)	θ_{NOM} (deg)	$\theta_u-\theta_L$ / $\theta_1-\theta_2$ (deg)	$\frac{d}{d\theta}(IPD)\Big\vert_{\theta_{NOM}}$	$\frac{d}{d\theta}\lvert T\rvert\Big\vert_{\theta_{NOM}}$	BEAM-BENDING BORESIGHT ERROR $m_{bb} = (.236)(\theta_u-\theta_L)\frac{d}{d\theta}(IPD)$ (milliradians = mr)	DIFFERENTIAL ATTENUATION BORESIGHT ERROR $m_a = -27.4\,(\theta_1-\theta_2)\frac{d\lvert T\rvert}{d\theta}$ (milliradians = mr)	TOTAL BORESIGHT ERROR $m = m_{bb} + m_a$
5° (u)	63° / 48°	38°	42° / 49°	48°	25° / -1°	0.80	0	4.7 mr	0	+4.7 mr (u)
7° (L)	64° / 46°	37°	43° / 49°	40°	25° / -3°	0.36	-0.0018	2.1 mr	-0.1 mr	+2.0 mr (L)
15°	60° /	47°	19° /	42°	41° /	0.70	0	6.6 mr	0	+6.6 mr (u)
	59° / 36°	44°	2° / 40°	35°	57° / -4°	0.32	-0.0013	4.8 mr	-0.1 mr	+4.2 mr (L)
20°	59° /	48°	28° /	45°	31° /	0.75	0	5.5 mr	0	+5.5 mr (u)
	56° / 40°	45°	20° / 38°	40°	36° / +2°	0.35	-0.0018	3.0 mr	+0.1 mr	+3.1 mr (L)
30°	53° /	44°	34° /	44°	19° /	0.75	0	3.4 mr	0	+3.4 mr (u)
	49° / 38°	40°	28° / 39°	39°	21° / -1°	0.35	-0.0018	1.7 mr	0	+1.7 mr (L)

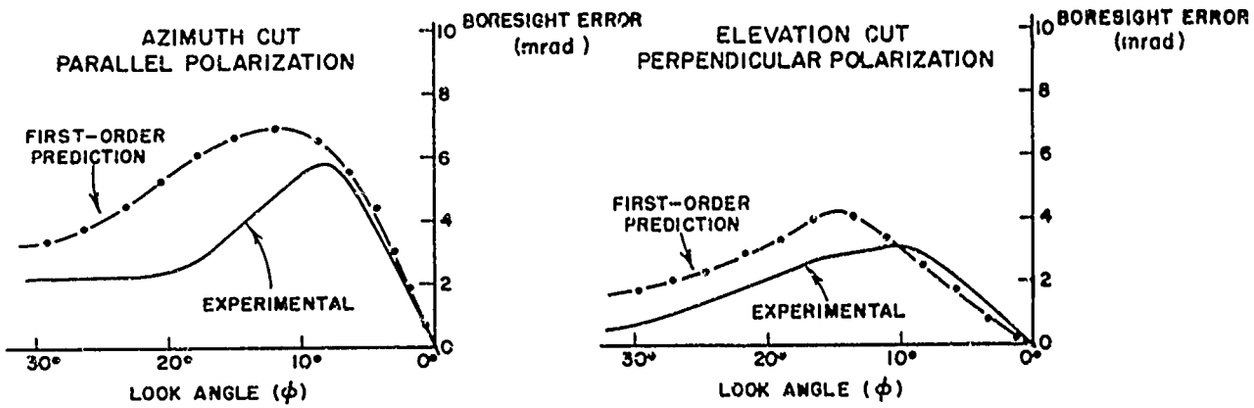

Fig. 10. Experimental and first-order theoretical boresight error curves. (Radome in Ref. 12, -9.4% point on Figs. 16 and 17)

Boresight design and correction for a radome housing a phase monopulse radar thus reduces to minimization of $\partial(\mathrm{IPD})/\partial\theta$.

Polarization control for this type of radar would undoubtedly reduce the boresight error for a constant-wall radome. For thin walls and sandwiches, parallel polarization is preferred; for half-wave walls (and the two-layer investigated here) perpendicular polarization would give less boresight error. Perpendicular polarization designs can be expected to have smaller bandwidth than parallel designs.

B. Amplitude Comparison Boresight Design

The first-order theoretical boresight equation (Eq. (19)) is repeated below:

$$(19) \qquad m_A = \frac{2.78}{D/\lambda} \frac{\partial(\mathrm{IPD})}{\partial\theta} (\theta_U - \theta_L) - \frac{F_0}{2s} \frac{1}{|T_2|} \frac{\partial|T|}{\partial\theta} (\theta_1 - \theta_2) \quad ,$$

where

m_A = boresight error in mrad;

θ_U = incidence angle of a ray emanating normally from the upper edge of the aperture, similarly for θ_L (lower);

F_0 = normalized nominal crossover point of squinted beams 1 and 2;

θ_1, θ_2 = average incidence angles of beams 1 and 2;

D/λ = aperture dimension (of equivalent uniform aperture); and

s = slope of the amplitude pattern at crossover in units/mrad .

For an amplitude comparison radar, the problem of boresight design is one of designing for the best balance between $\partial(\mathrm{IPD})/\partial\theta$ and $\partial|T|/\partial\theta$. A radome wall may be designed such that the $d(\mathrm{IPD})/d\theta$ error and the $d|T|/d\theta$ error are nearly equal in magnitude and opposite in sign. Such a cancellation design is exemplified by the perpendicular polarization results in Table II and shown in Fig. 8.

For constant-wall radomes a cancellation design should be the goal. It is interesting that the magnitude of $d/d\theta\,|T|$ becomes sufficiently large (and negative) for a cancellation design only for high angles of incidence, i.e., about 60° to 70°.

Cancellation designs are possible at high incidence angles for both polarizations for fiberglass ($\epsilon = 4$) thin walls and for all the sandwiches reported in Appendix A. For the ceramic ($\epsilon = 9$) thin wall and the half-wave and two-layer walls studied, good cancellation can be obtained only for perpendicular polarization. The bandwidth of effective cancellation for perpendicular polarization is considerably smaller than for parallel; therefore, maintenance of parallel polarization in conjunction with a cancellation design (for those wall structures which allow it) should allow good, broadband boresight performance. For the high dielectric thin wall and the half-wave radomes, a good cancellation design over a few per cent band could be attained by maintaining perpendicular polarization.

For lower angles of incidence, the magnitude of $d|T|/\partial\theta$ is generally small and a good boresight design results if one designs for a minimum value of $d(IPD)/d\theta$.

C. General

In addition to simply designing a constant-wall radome to minimize $d(IPD)/d\theta$ or to balance $d(IPD)/d\theta$ and $d|T|/d\theta$ effects, it is possible to design a varying wall structure to approximate a desired value of either derivative.

If one were designing for a phase-monopulse or low incidence angle amplitude comparison radar, he could design a tapered wall for a constant IPD over the incidence angles of the antenna rays (normals to the aperture) so that the effective $d/d\theta\,(IPD)$ would be small. For example, to reduce the beam-bending error at a particular look, one could elect to taper the radome so that the IPD's are the same for all antenna rays. In this case, physical points on the radome would correspond to particular incidence angle values. A constant IPD line (horizontal line) is drawn on the IPD curves. The per cent frequency change from the intersection of the horizontal line with the IPD curves for two incidence angles is exactly the necessary per cent change in d/λ for each layer of the wall between the corresponding points on the radome.

The concept of a cancellation design may have more utility as a correction technique than as a design tool. For some wall structures a fairly nominal increase in value of $d|T|/d\theta$ is needed to significantly

reduce the boresight error. Study may reveal methods of designing uniform lossy layers for a required value of $d|T|/d\theta$. Another approach to utilizing loss directs itself to consideration of the high-error region near the radome nose. If the boresight error is positive (away from the nose) then attenuation of the beam closer to the nose will reduce the error. If loss is added at the nose and tapered to zero at the base, the beam passing predominantly through the nose region will be relatively attenuated and the boresight error will be reduced. Lossy paint or tape could be used on the interior of a radome to achieve such a nose-to-base loss taper. The curves of Appendix A serve to indicate how one should proceed in applying loss to design or correction problems.

Polarization control would be very effective in some circumstances, although neither polarization is preferred in all cases. Excellent bandwidth properties are indicated for radomes with parallel polarization only, i.e., little variation of the electrical properties of the wall with change in frequency or wall thickness is indicated. Thus, relaxation of tolerance and corresponding cost reduction are anticipated by-products of maintenance of parallel polarization only.

An example of radome design utilizing the above ideas follows.

D. Example

Suppose the radome for which the incidence angle data are given in Table I (Radome Z - 2i of Reference 6) were designed as a fiberglass sandwich, one for which Figs. 22 and 23 are applicable. It is observed that a relatively large negative value of $d|T|/d\theta$ could be realized for both polarizations by designing at the -4% frequency point for this sandwich. Table IV gives the calculated first-order boresight error for this case and the results can be compared with those of Table II for a good compromise half-wave wall design. The sandwich gives a predicted peak error 3 mrad less for parallel polarization and 3 mrad more for perpendicular (although the peak perpendicular error is still only 3.9 mrad).

With the artificial introduction of loss to give an increase in value of $d|T|/d\theta$ of about 0.02 unit per degree for the 5° position of the antenna, the error at this look could be reduced to about 2.1 mrad for parallel polarization and 1.1 mrad for perpendicular. Since the "down" beam looks more through the nose region than the "up" beam, gradation of loss from the nose backward would undoubtedly help in this case, and perhaps reduce the nose region error nearly to zero.

TABLE IV

TABULATED RADOME BORESIGHT DATA
(RADOME GEOMETRY OF Ref. 6, FIBERGLASS SANDWICH DESIGN, -4% POINT ON FIGS. 22 AND 23)

LOOK ANGLE ϵ (deg)	INCIDENCE ANGLE θ_u / θ_l (deg)	θ_c (deg)	θ_L / θ_s (deg)	θ_{NOM} (deg)	$\theta_u - \theta_L$ / $\theta_l - \theta_s$ (deg)	$\frac{d}{d\theta}(IPD)'_{\theta_{NOM}}$	$\frac{d}{d\theta}\lvert T' \rvert_{\theta_{NOM}}$	BEAM-BENDING BORESIGHT ERROR $m_{bb} = (.217)(\theta_u - \theta_L)\frac{d}{d\theta}(IPD)$ (milliradians = mr)	DIFFERENTIAL ATTENUATION BORESIGHT ERROR $m_a = -\left\{\frac{28.8}{24.6}\right\}(\theta_l - \theta_s)\frac{d\lvert T' \rvert}{d\theta}\left\{\begin{matrix}H\\ \perp\end{matrix}\right.$ (milliradians = mr)	TOTAL BORESIGHT ERROR $m = m_{bb} + m_a$
5°	75° / 66°	66°	80° / 72°	70°	$\frac{71°}{2} = 36.5°$ / -6°	+0.95	-0.011	7.4 mr	-1.9 mr	+5.5 mr (⊥)
						+0.8	-0.017	6.3 mr	-2.4 mr	+3.9 mr (∥)
10°	72° / 62.5°	65°	59° / 66°	65°	13° / -3.5°	+0.72	-0.0065	2.0 mr	-0.7 mr	+1.3 mr (⊥)
						+0.75	-0.010	2.1 mr	-0.9 mr	+1.2 mr (∥)
15°	66° / 60°	62°	56° / 64°	61°	10° / -4°	+0.55	-0.002	1.2 mr	-0.2 mr	+1.0 mr (⊥)
						+0.7	-0.004	1.5 mr	-0.4 mr	+1.1 mr (∥)
20°	61° / 57°	58°	53° / 61°	59°	8° / -4°	+0.55	-0.002	1.0 mr	-0.2 mr	+0.8 mr (⊥)
						+0.7	-0.004	1.2 mr	-0.4 mr	+0.8 mr (∥)

Polarization control itself, without IPD tapering or introduction of loss, can provide a very good boresight design for this radome geometry. If one designs a ceramic sandwich structure (such as that shown in Figs. 26 and 27) at the zero per cent point and maintains parallel polarization, a good cancellation design is the result. The predicted boresight error as tabulated in Table V is quite low.

Figure 11 compares the first-order predicted boresight error of Radome Z - 2i of Reference 6 for the following wall structure:

(1) non-tapered low-loss fiberglass sandwich,

(2) the same sandwich as (1) with a hypothetical $d|T|/d\theta$ artificially introduced (0.02 unit/deg at the 5° position), and

(3) non-tapered low-loss ceramic sandwich designed for parallel polarization only.

V. CONCLUSIONS

A first-order theory of radome boresight error is developed and applied to boresight prediction and design. Boresight error predictions for two radomes with known (measured) errors were sufficiently accurate to justify application of the theory to design problems.

The first-order boresight error was shown to be of the following form for the two basic types of track radar:

(1) Phase comparison: $m = c_1\, d/d\theta(IPD)$ and

(2) Amplitude comparison: $m = c_2\, d/d\theta(IPD) + c_3\, d|T|/d\theta$,

where m is the boresight error in mrad, θ is the incidence angle, IPD is the insertion phase delay, and $|T|$ is the magnitude of the amplitude transmission coefficient.

Radome design curves are included which give $|T|^2$, IPD, $d/d\theta(IPD)$, and $d/d\theta|T|$ for several important radome wall structures over a $\pm$ 20% frequency band.

A "cancellation" boresight design is shown to be possible wherein the radome wall design is chosen so that for amplitude comparison radars the errors resulting from $d/d\theta(IPD)$ and $d/d\theta|T|$ are nearly equal in magnitude but opposite in sign. The result is very low boresight error.

Extension of the cancellation design concept to artificial introduction of loss is discussed.

Polarization control is found to be desirable, although the choice of polarization depends on the radar and radome types. Parallel polarization, as shown by the design curves, is capable of much greater bandwidths of performance than perpendicular. Use of a proper radome wall design with polarization control can give significant reductions in boresight error.

A design example is included which shows a technique of design and the effect of polarization control.

TABLE V

TABULATED RADOME BORESIGHT DATA
(RADOME GEOMETRY OF Ref. 6, CERAMIC SANDWICH DESIGN, PARALLEL POLARIZATION ONLY, 0.0% POINT ON FIGS. 26 AND 27)

LOOK ANGLE	INCIDENCE ANGLES					$\frac{d}{d\theta}(\mathrm{IPD})\Big\|_{\theta_{NOM}}$	$\frac{d}{d\theta}T'\Big\|_{\theta_{NOM}}$	BEAM-BENDING BORESIGHT ERROR	DIFFERENTIAL ATTENUATION BORESIGHT ERROR	TOTAL BORESIGHT ERROR
ϕ	θ_u	θ_c	θ_L	θ_{NOM}	$\theta_u - \theta_L$			$m_{bb} = (.217)(\theta_u - \theta_L)\frac{d}{d\theta}(\mathrm{IPD})$	$m_a = -28.2\,(\theta_1 - \theta_2)\frac{dT'}{d\theta}$ (u)	$m = m_{bb} + m_a$
(deg)	(deg)	(deg)	(deg)	(deg)	(deg)			(milliradians = mr)	(milliradians = mr)	
5°	75° / 66°	66°	30° / 72°	70°	$\frac{71°}{2} = 36°$ / -6°	0.42	-0.012	3.3 mr	-2.0 mr	+1.3 mr (.)
10°	72° / 62.5°	65°	59° / 66°	65°	13° / -3.5°	0.45	-0.006	1.3 mr	-0.6 mr	+0.7 mr (u)
15°	66° / 60°	62°	56° / 64°	61°	10° / -4°	0.5	0	1.1 mr	0	+1.1 mr (.)
20°	61° / 57°	58°	53° / 61°	59°	8° / -4°	0.5	0	0.9 mr	0	+0.9 mr (.)

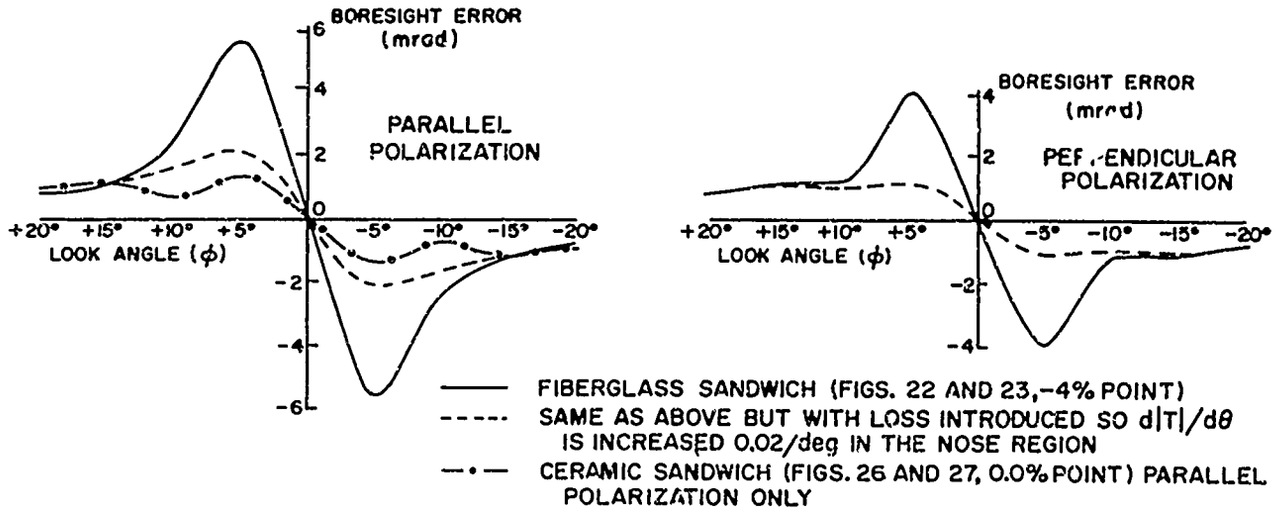

Fig. 11. First-order theoretical boresight error for three example wall designs for the radome shape in Ref. 6.

APPENDIX A
RADOME DESIGN CURVES[13]

Graphs of $|T|^2$, IPD, $d/d\theta|T|$, and $d/d\theta$(IPD) versus frequency for incidence angles of 30°, 40°, 50°, 60°, and 70° are presented in Figs. 12-27 for several radome wall structures. The frequency variation for each wall is $\pm$ 20% about the center frequency. The computation of the data for these curves proceeded as discussed below.

Preliminary thicknesses were assigned each layer and one layer was varied by the computer until maximum transmission was obtained for an incidence angle of 60°. The thicknesses for this condition are the design thicknesses and correspond to the zero per cent frequency variation point. The design thicknesses for each case are shown pictorially on the figure for that case.

In order to demonstrate the meaning of the curves, a short design example will be presented. Suppose one wants to design a two-layer, ceramic-coated, plastic radome for maximum transmission at a 40° angle of incidence for perpendicular polarization (the relevant graph is contained in Fig. 20). The transmission maximum for $\theta = 40°$ occurs at a frequency 4.5% below the center frequency; the thickness for each layer should therefore be 0.955 times its thickness at the zero-per cent point, the thickness given in the illustration in Fig. 20. The design thicknesses for this case should be, then $d_1 = 0.0095\lambda_0$ and $d_2 = 0.2495\lambda_0$. Extension to IPD, $d/d\theta$(IPD) or $d/d\theta|T|$ design problems is clear.

RADOME DESIGN CURVES

THIN WALL PERPENDICULAR POLARIZATION

Fig. 12 (a) Power Transmission Coefficient vs Percent Frequency Change.

(b) IPD vs Percent Frequency Change.

(c) $\frac{d}{d\theta}|T|$ (Units/Degree) vs Percent Frequency Change.

(d) $\frac{d}{d\theta}$(IPD) (Degrees/Degree) vs Percent Frequency Change.

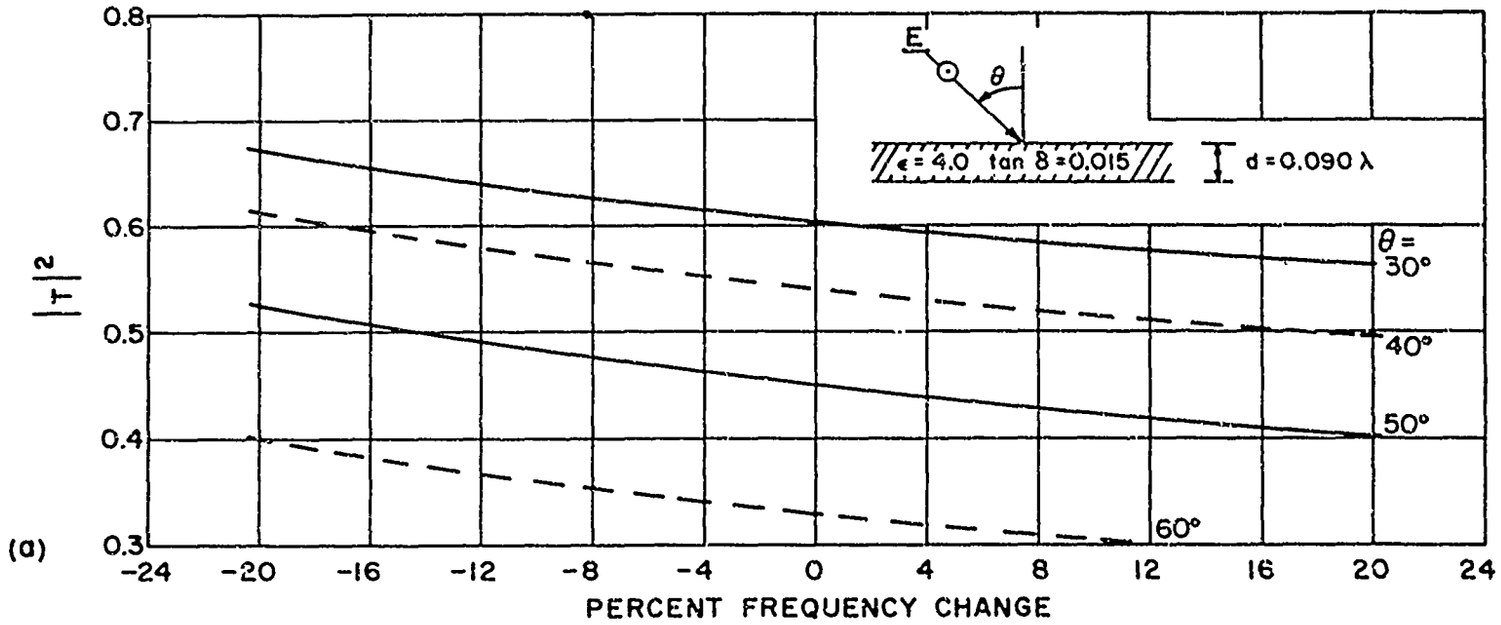

(a)

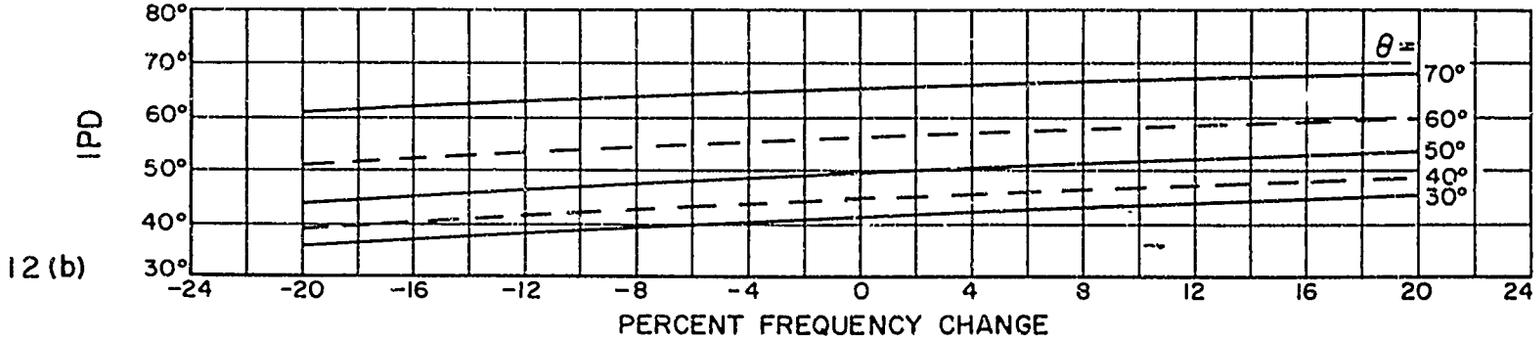
IPD
80°
70°
60°
50°
40°
30°
θ =
70°
60°
50°
40°
30°
-24
-20
-16
-12
-8
-4
0
4
8
12
16
20
24
PERCENT FREQUENCY CHANGE

12 (b)

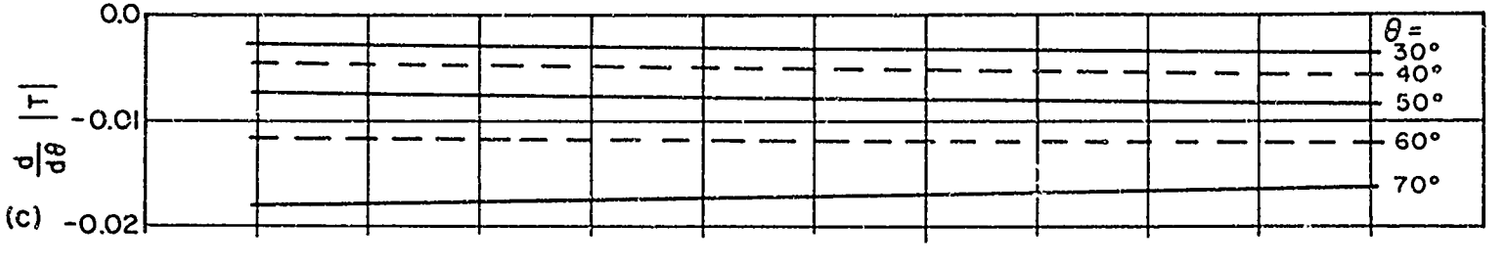
d/dθ |T|
0.0
-0.01
-0.02
θ =
30°
40°
50°
60°
70°

(c)

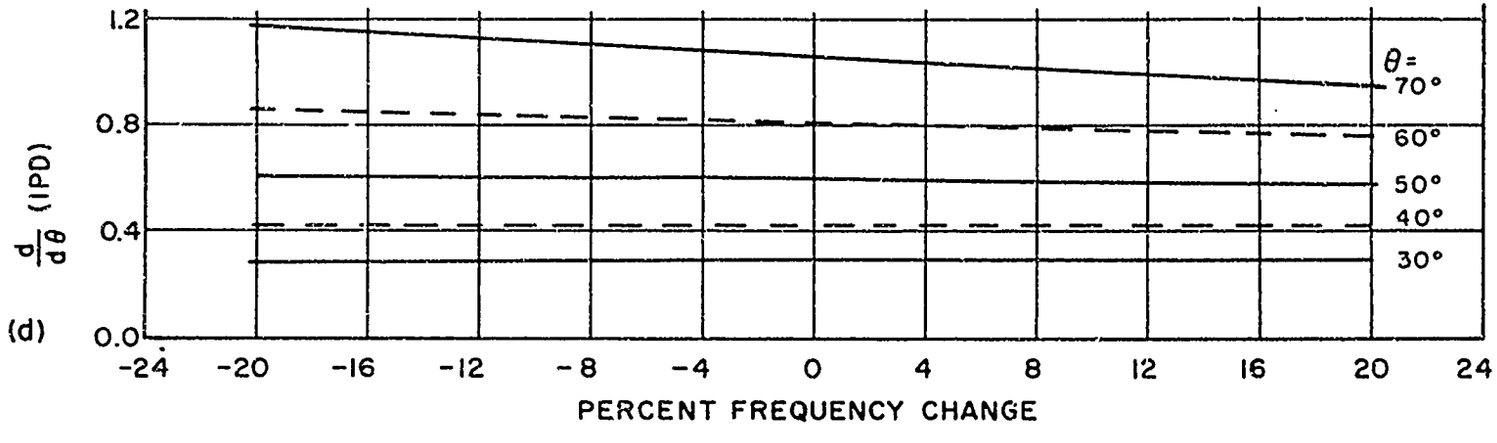
d/dθ (IPD)
1.2
0.8
0.4
0.0
θ =
70°
60°
50°
40°
30°
-24
-20
-16
-12
-8
-4
0
4
8
12
16
20
24
PERCENT FREQUENCY CHANGE

(d)

RADOME DESIGN CURVES

THIN WALL PARALLEL POLARIZATION

Fig. 13 (a) Power Transmission Coefficient vs Percent Frequency Change.

(b) IPD vs Percent Frequency Change.

(c) $\frac{d}{d\theta}|T|$ (Units/Degree) vs Percent Frequency Change.

(d) $\frac{d}{d\theta}(IPD)$ (Degrees/Degree) vs Percent Frequency Change.

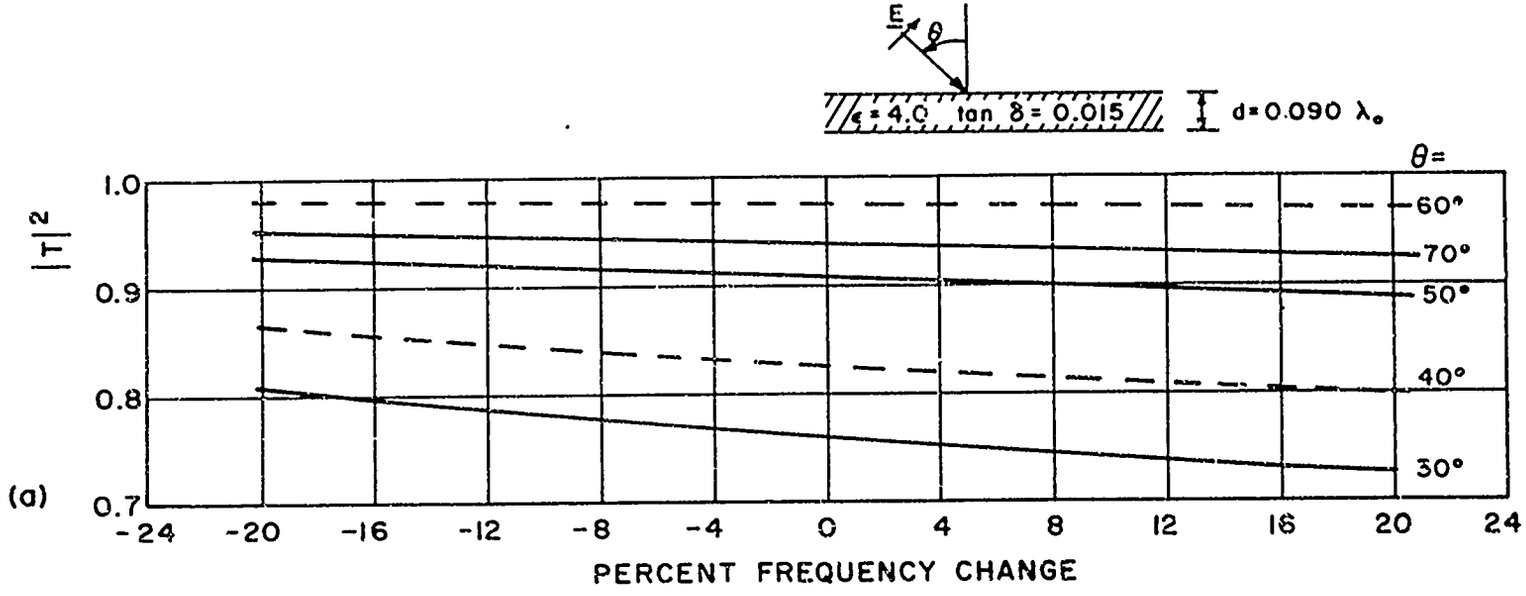

(a)

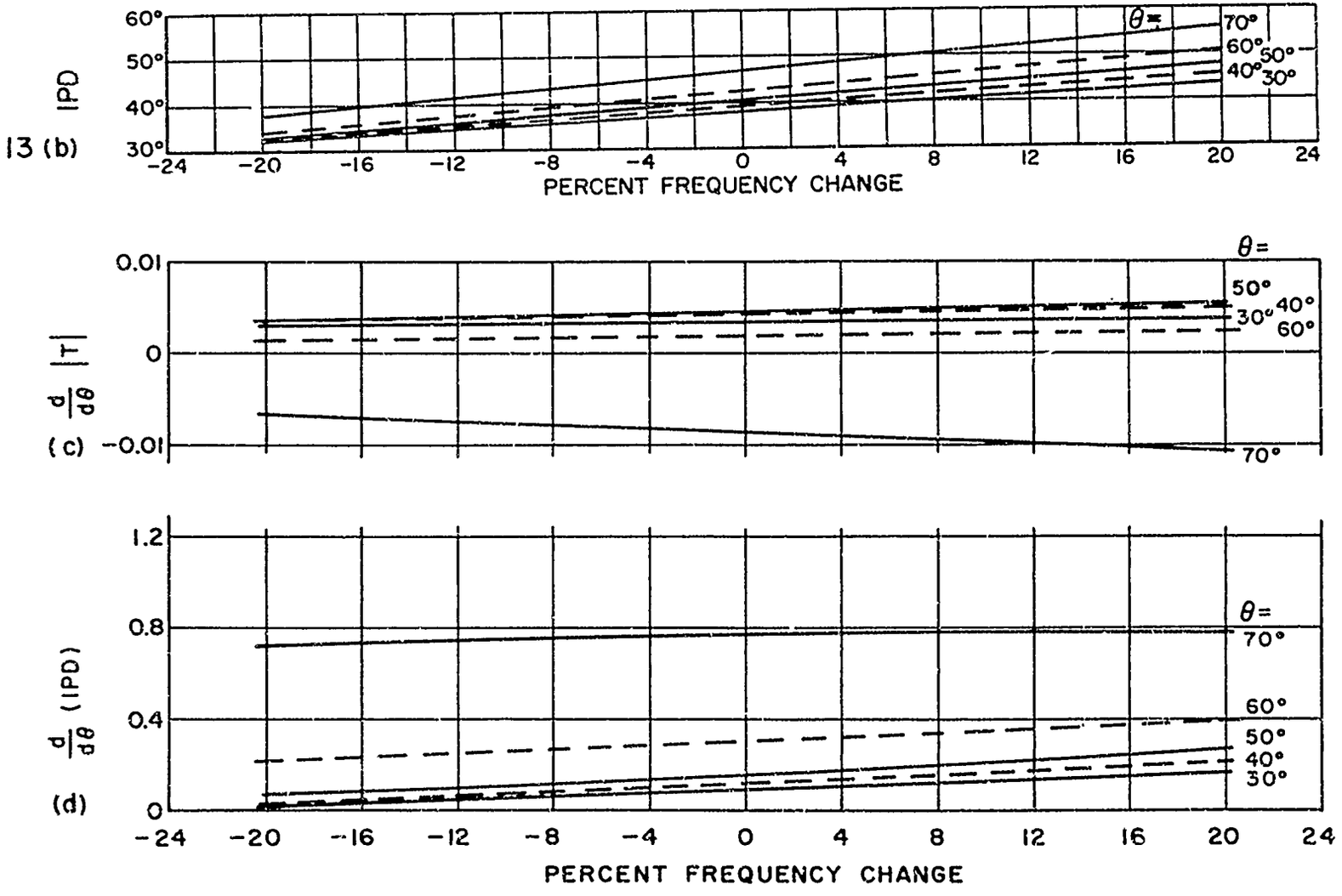
13 (b)
IPD
60°
50°
40°
30°
θ=
70°
60°
50°
40°
30°
-24
-20
-16
-12
-8
-4
0
4
8
12
16
20
24
PERCENT FREQUENCY CHANGE
(c)
$\frac{d}{d\theta}|T|$
0.01
0
-0.01
θ=
50°
30°
40°
60°
70°
(d)
$\frac{d}{d\theta}$ (IPD)
1.2
0.8
0.4
0
θ=
70°
60°
50°
40°
30°
-24
-20
-16
-12
-8
-4
0
4
8
12
16
20
24
PERCENT FREQUENCY CHANGE

RADOME DESIGN CURVES

THIN WALL PERPENDICULAR POLARIZATION

Fig. 14 (a) Power Transmission Coefficient vs Percent Frequency Change.

(b) I P D vs Percent Frequency Change.

(c) $\frac{d}{d\theta}|T|$ (Units/Degree) vs Percent Frequency Change.

(d) $\frac{d}{d\theta}$(I P D) (Degrees/Degree) vs Percent Frequency Change.

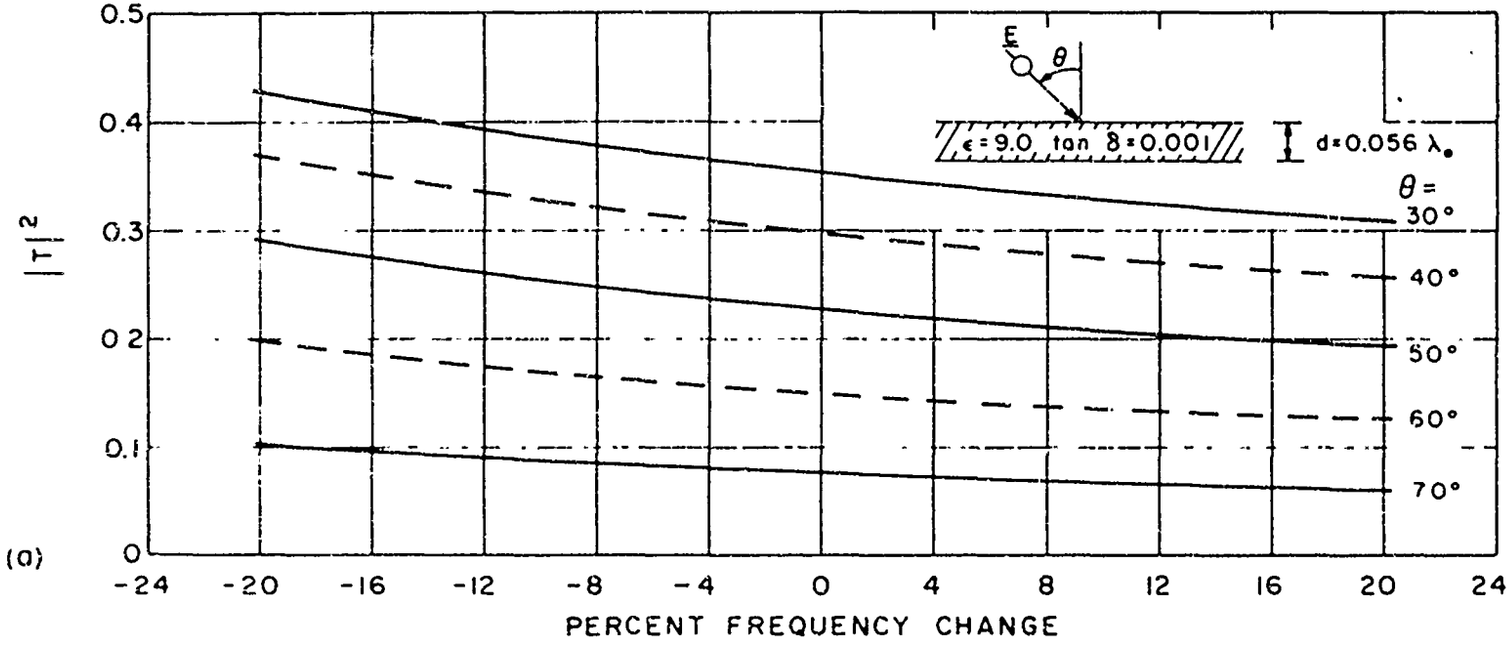

(a)

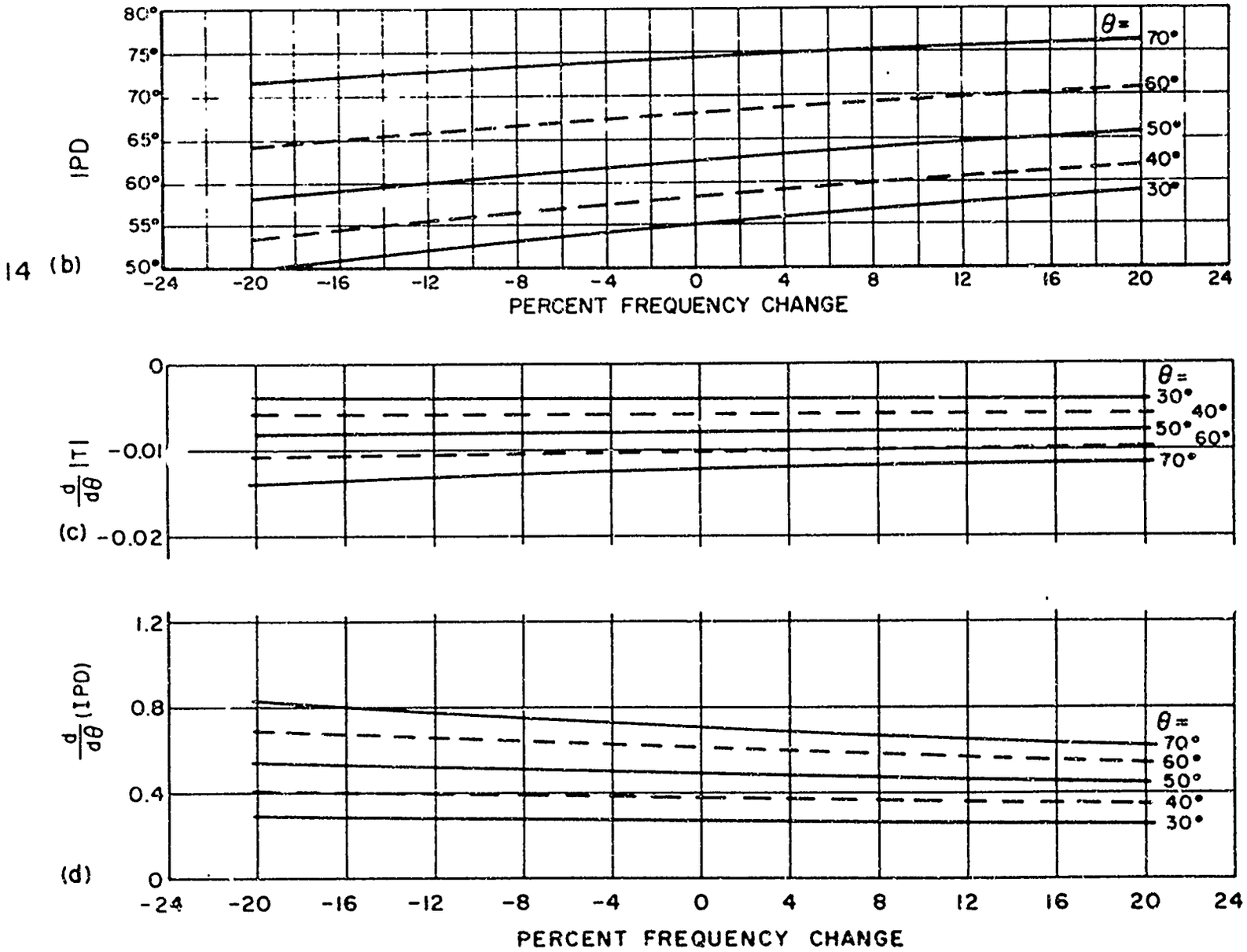
(b)
IPD
80°
75°
70°
65°
60°
55°
50°
θ=
70°
60°
50°
40°
30°
-24
-20
-16
-12
-8
-4
0
4
8
12
16
20
24
PERCENT FREQUENCY CHANGE
(c)
$\frac{d}{d\theta}$ ITI
0
-0.01
-0.02
θ=
30°
40°
50°
60°
70°
(d)
$\frac{d}{d\theta}$ (IPD)
1.2
0.8
0.4
0
θ=
70°
60°
50°
40°
30°
-24
-20
-16
-12
-8
-4
0
4
8
12
16
20
24
PERCENT FREQUENCY CHANGE

RADOME DESIGN CURVES

THIN WALL

PARALLEL POLARIZATION

Fig. 15 (a) Power Transmission Coefficient vs Percent Frequency Change.

(b) IPD vs Percent Frequency Change.

(c) $\frac{d}{d\theta}|T|$ (Units/Degree) vs Percent Frequency Change.

(d) $\frac{d}{d\theta}$(IPD) (Degrees/Degree) vs Percent Frequency Change.

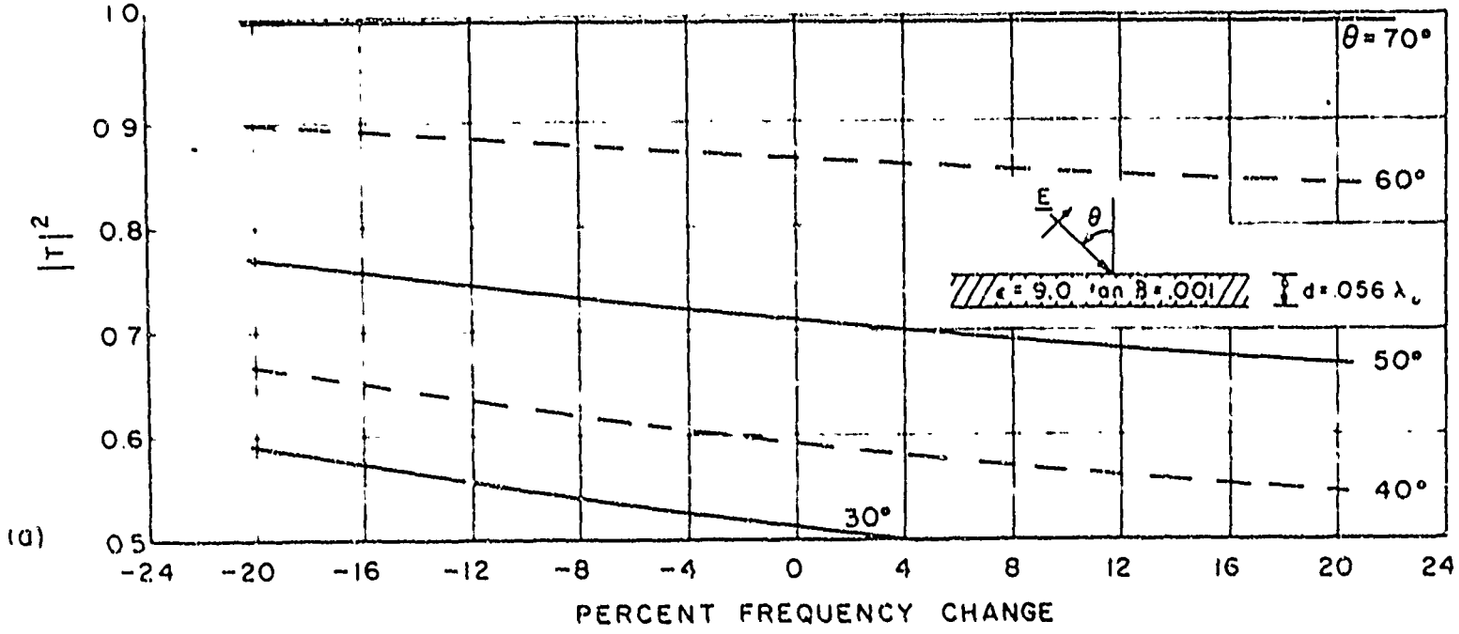

(a)

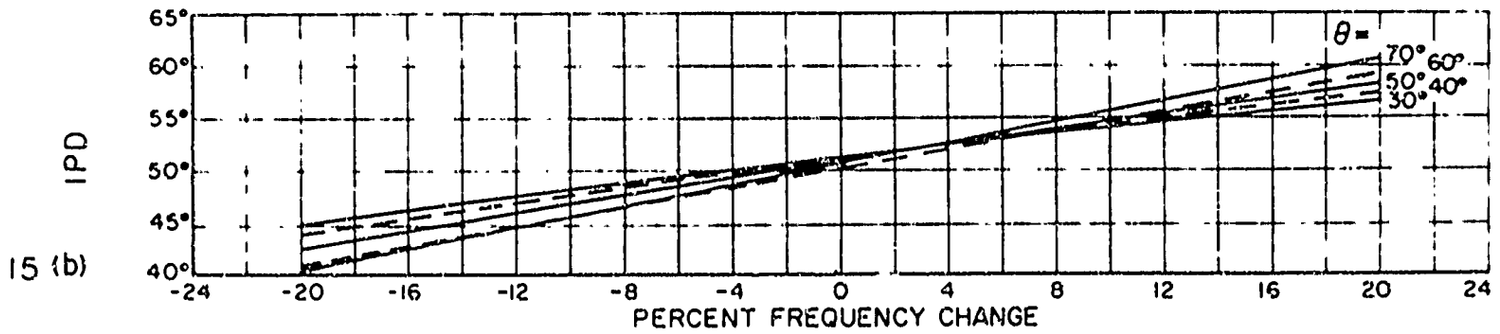
65°
60°
55°
50°
45°
40°
IPD
θ=
70° 60°
50° 40°
30°
-24 -20 -16 -12 -8 -4 0 4 8 12 16 20 24
PERCENT FREQUENCY CHANGE

15 (b)

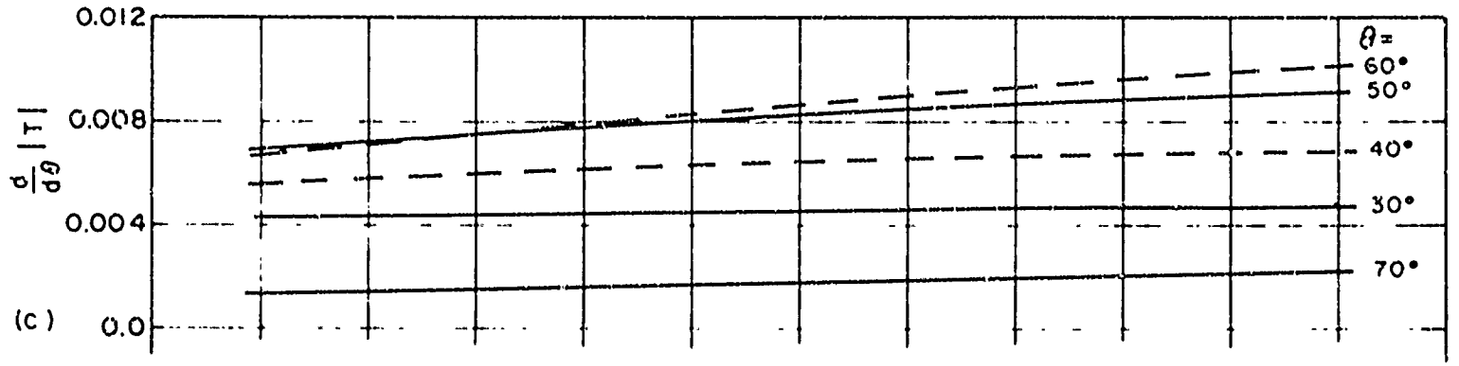
0.012
0.008
0.004
0.0
d/dθ |T|
θ=
60°
50°
40°
30°
70°

(c)

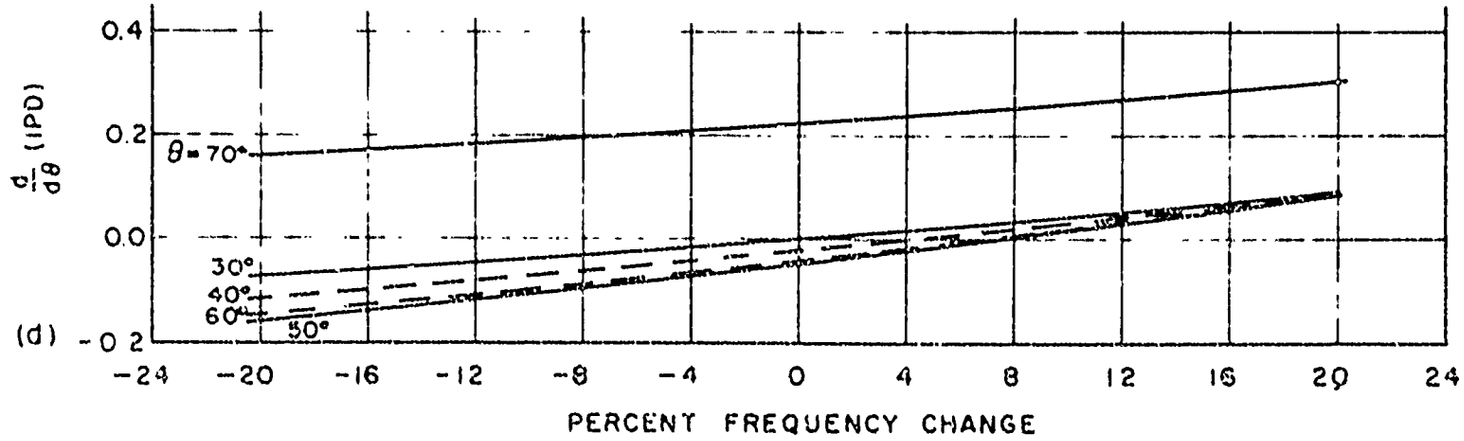
0.4
0.2
0.0
-0.2
d/dθ (IPD)
θ=70°
30°
40°
60°
50°
-24 -20 -16 -12 -8 -4 0 4 8 12 16 20 24
PERCENT FREQUENCY CHANGE

(d)

RADOME DESIGN CURVES

HALF-WAVE WALL PERPENDICULAR POLARIZATION

Fig. 16 (a) Power Transmission Coefficient vs Percent Frequency Change.

(b) IPD vs Percent Frequency Change.

(c) $\frac{d}{d\theta}|T|$ (Units/Degree) vs Percent Frequency Change.

(d) $\frac{d}{d\theta}(IPD)$ (Degrees/Degree) vs Percent Frequency Change.

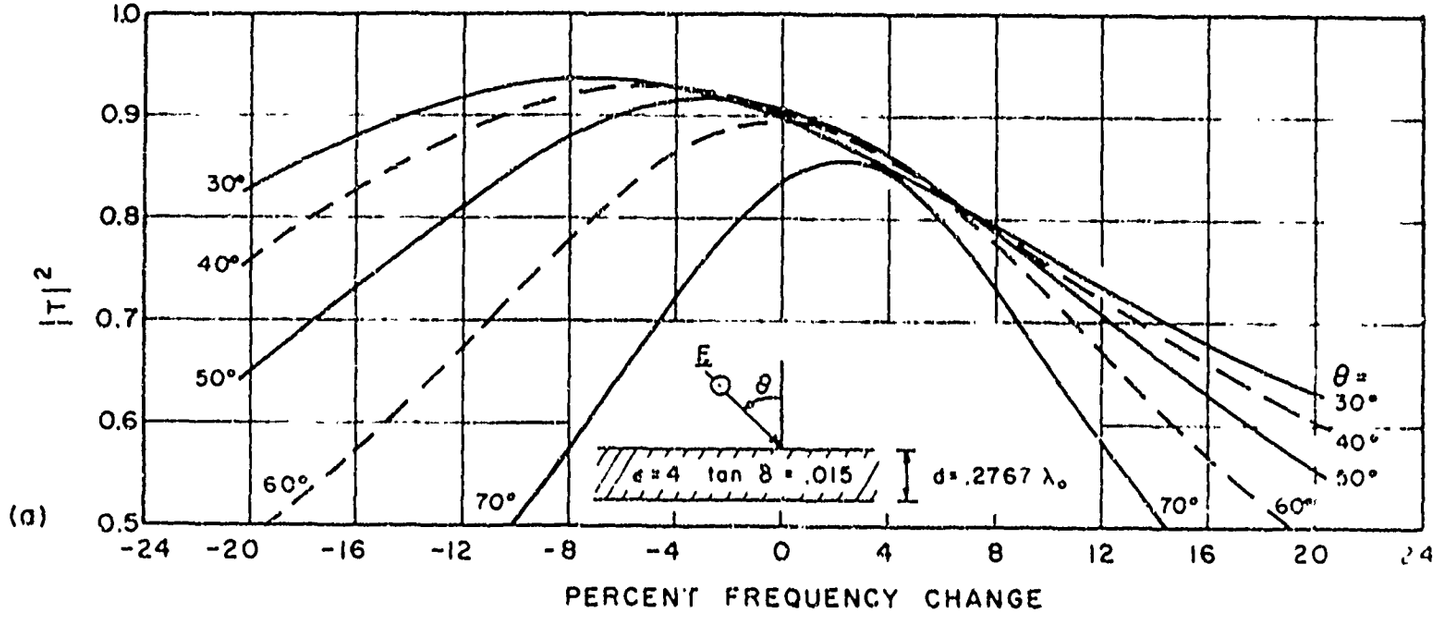

(a)

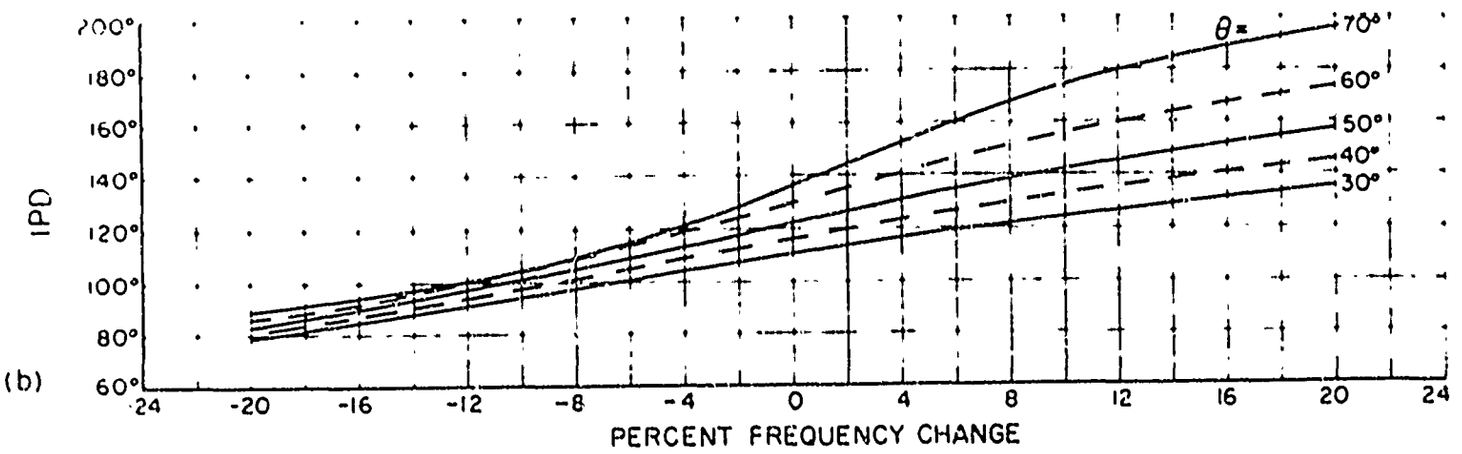
200°
180°
160°
140°
120°
100°
80°
60°
IPD
θ=
70°
60°
50°
40°
30°
-24
-20
-16
-12
-8
-4
0
4
8
12
16
20
24
PERCENT FREQUENCY CHANGE

16 (b)

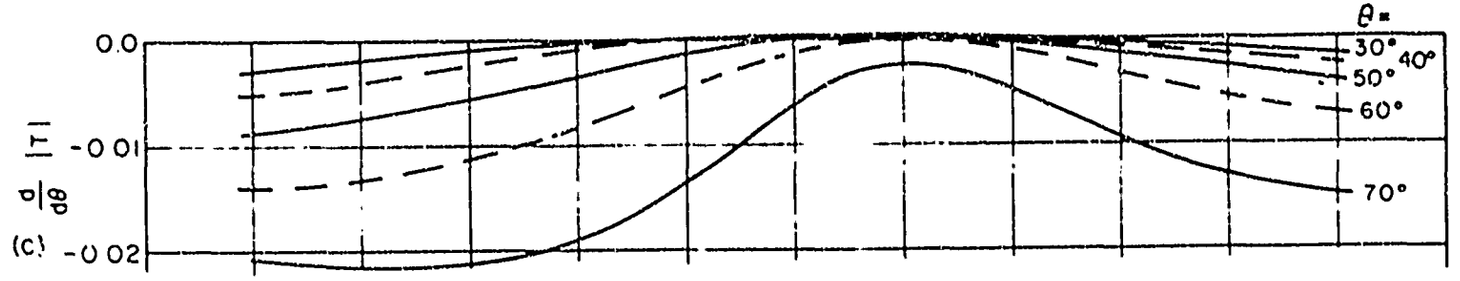
0.0
-0.01
-0.02
d/dθ |T|
θ=
30°
40°
50°
60°
70°

(c)

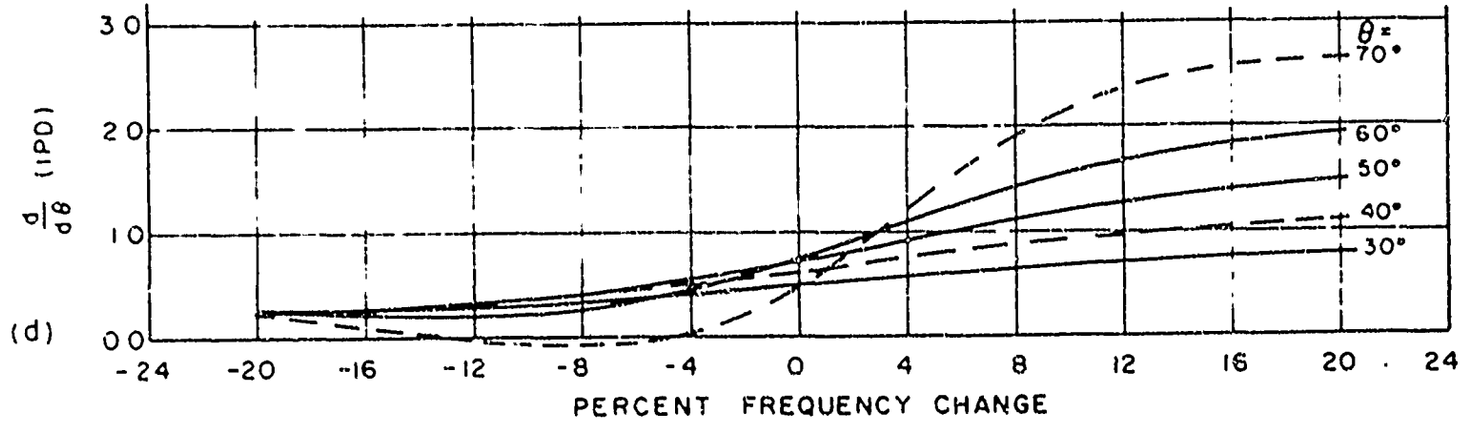
3.0
2.0
1.0
0.0
d/dθ (IPD)
θ=
70°
60°
50°
40°
30°
-24
-20
-16
-12
-8
-4
0
4
8
12
16
20
24
PERCENT FREQUENCY CHANGE

(d)

RADOME DESIGN CURVES

PARALLEL POLARIZATION

HALF-WAVE WALL

Fig. 17 (a) Power Transmission Coefficient vs Percent Frequency Change.

(b) I P D vs Percent Frequency Change.

(c) $\frac{d}{d\theta}|T|$ (Units/Degree) vs Percent Frequency Change.

(d) $\frac{d}{d\theta}$(I P D) (Degrees/Degree) vs Percent Frequency Change.

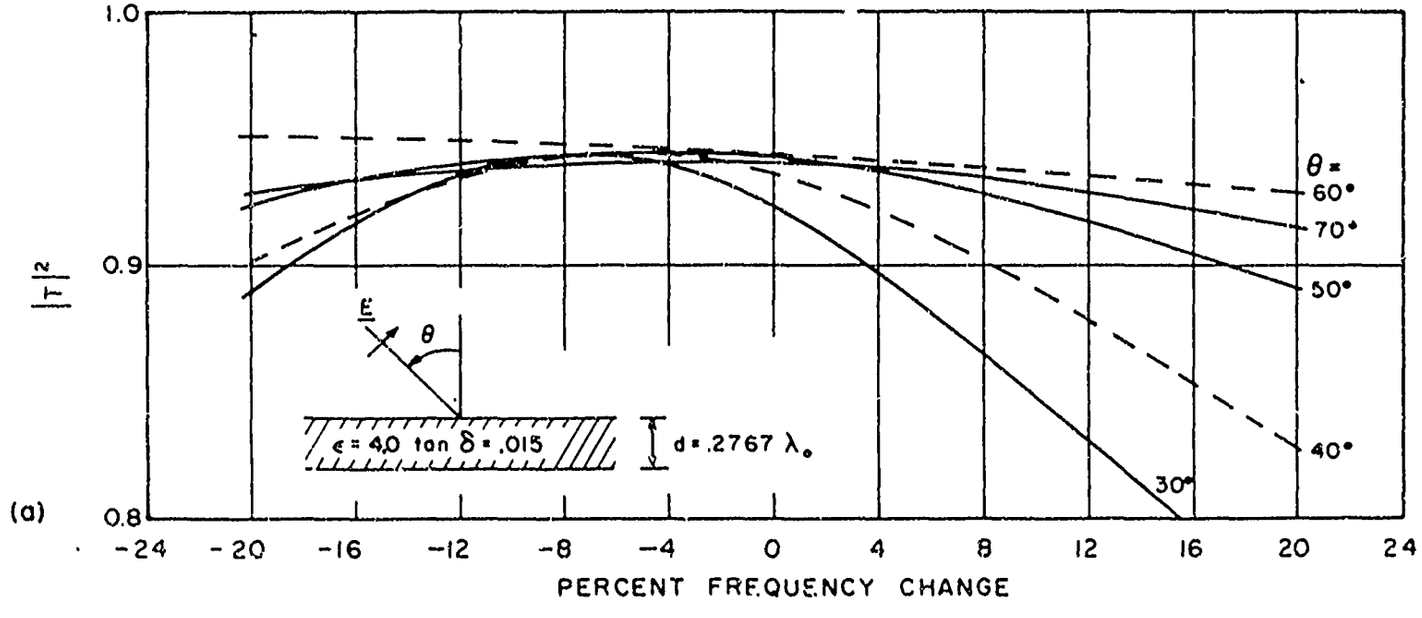

(a)

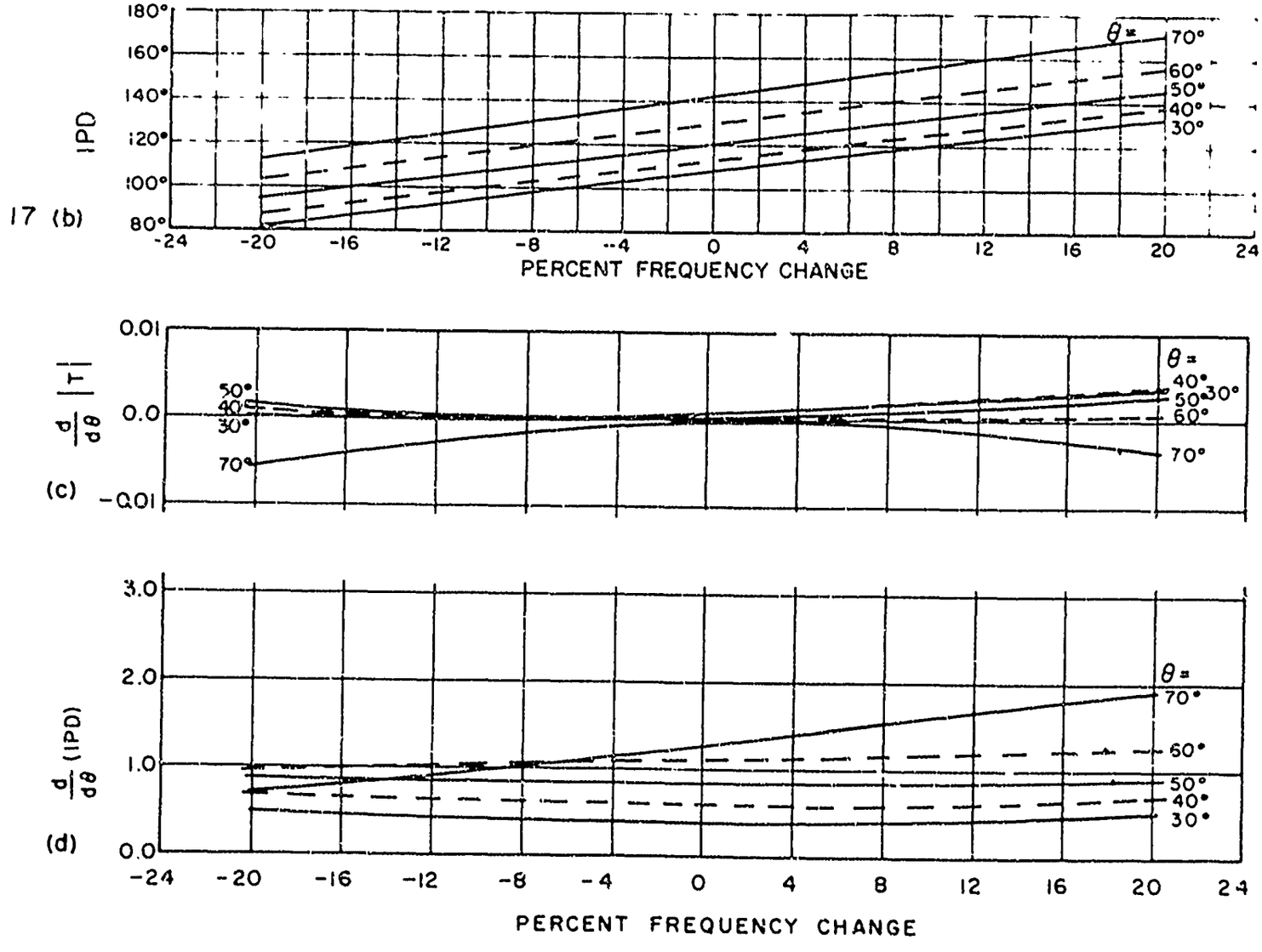
17 (b)
IPD
180°
160°
140°
120°
100°
80°
θ =
70°
60°
50°
40°
30°
-24
-20
-16
-12
-8
-4
0
4
8
12
16
20
24
PERCENT FREQUENCY CHANGE
(c)
$\frac{d}{d\theta}|T|$
0.01
0.0
-0.01
50°
40°
30°
70°
θ =
40°
50°
30°
60°
70°
(d)
$\frac{d}{d\theta}$(IPD)
3.0
2.0
1.0
0.0
θ =
70°
60°
50°
40°
30°
-24
-20
-16
-12
-8
-4
0
4
8
12
16
20
24
PERCENT FREQUENCY CHANGE

RADOME DESIGN CURVES

HALF-WAVE WALL PERPENDICULAR POLARIZATION

Fig. 18 (a) Power Transmission Coefficient vs Percent Frequency Change.

(b) IPD vs Percent Frequency Change.

(c) $\frac{d}{d\theta}|T|$ (Units/Degree) vs Percent Frequency Change.

(d) $\frac{d}{d\theta}$·(IPD) (Degrees/Degree) vs Percent Frequency Change.

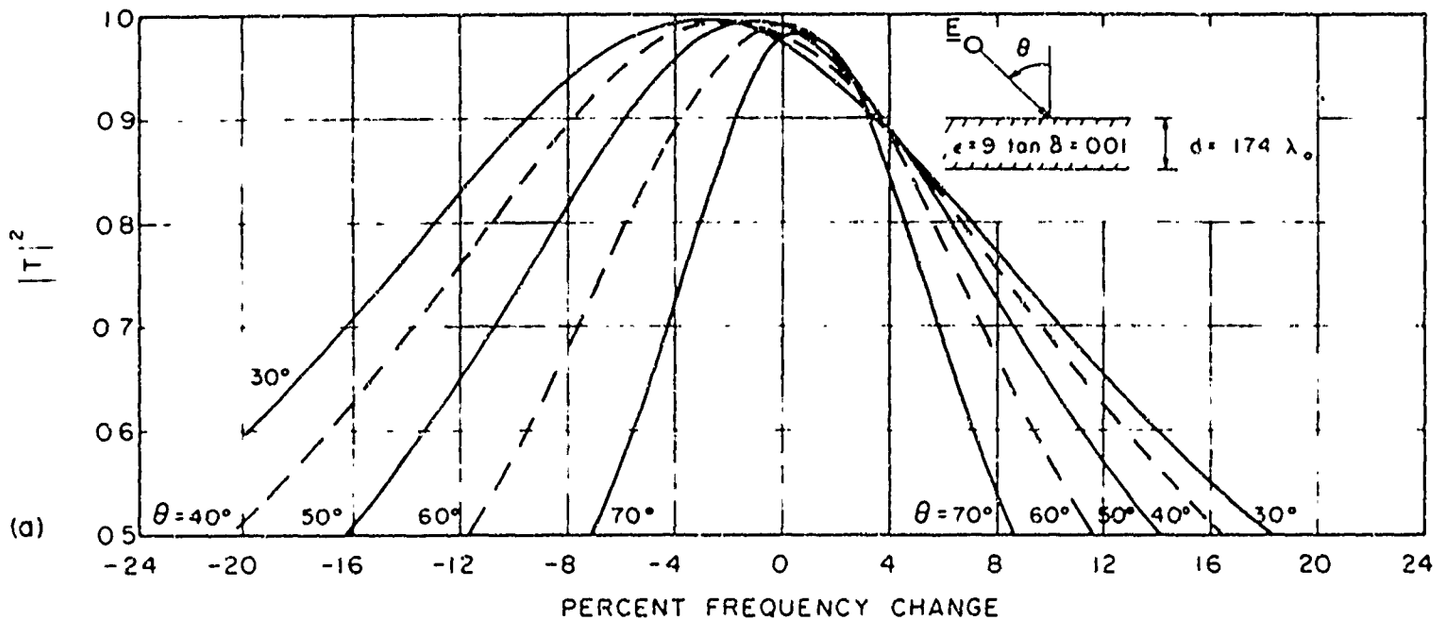

(a)

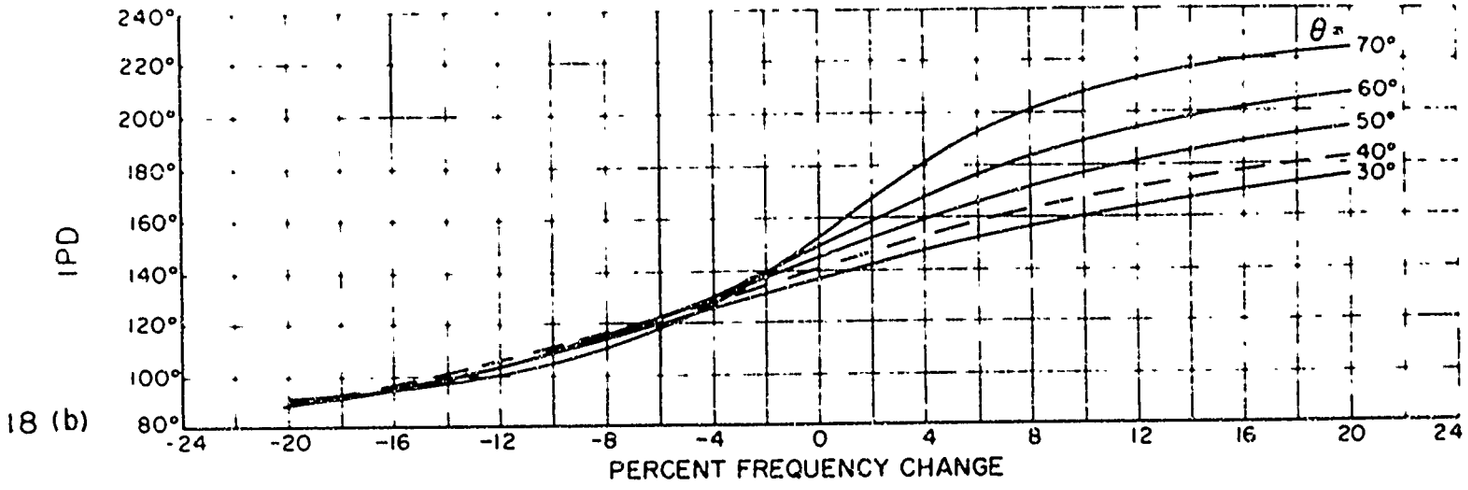
240°
220°
200°
180°
160°
140°
120°
100°
80°
IPD
θ =
70°
60°
50°
40°
30°
-24
-20
-16
-12
-8
-4
0
4
8
12
16
20
24
PERCENT FREQUENCY CHANGE

18 (b)

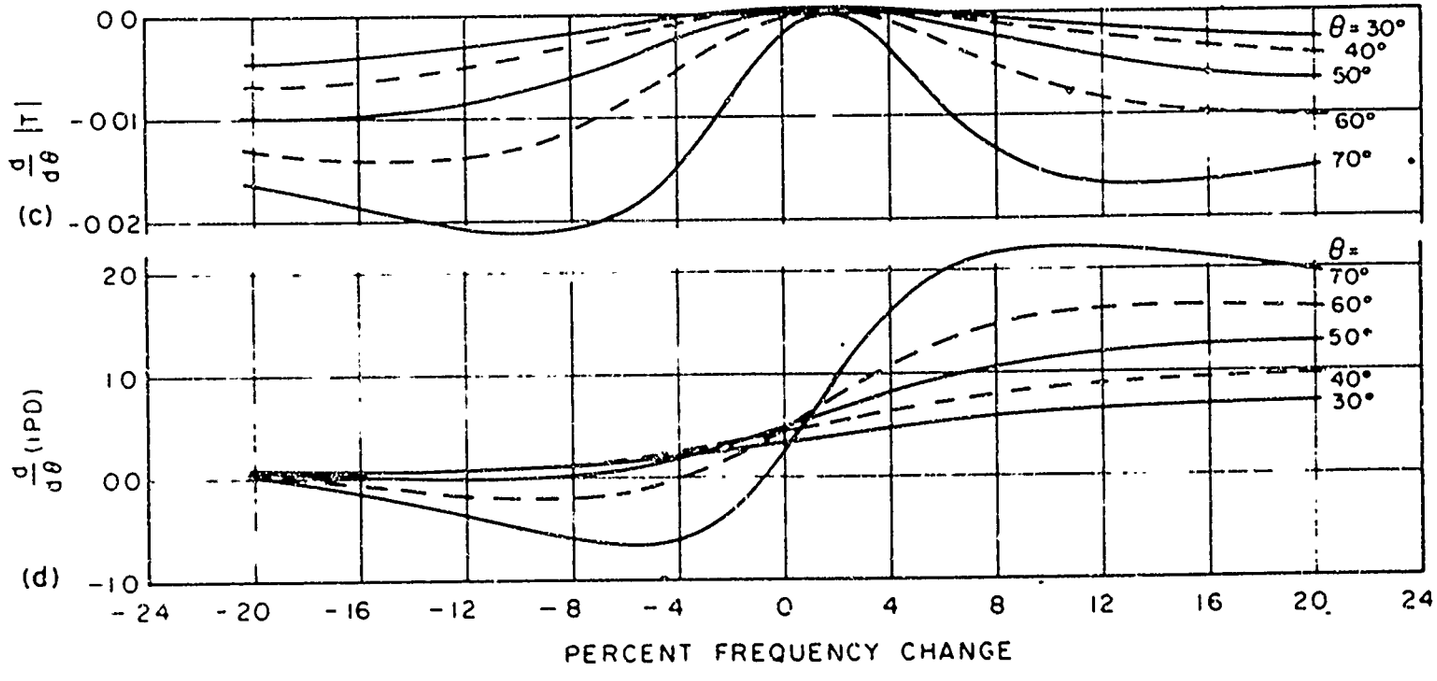
0 0
-0 01
-0 02
d/dθ |T|
(c)
θ = 30°
40°
50°
60°
70°
20
10
0 0
-10
d/dθ (IPD)
(d)
θ =
70°
60°
50°
40°
30°
-24
-20
-16
-12
-8
-4
0
4
8
12
16
20
24
PERCENT FREQUENCY CHANGE

RADOME DESIGN CURVES

HALF-WAVE WALL

PARALLEL POLARIZATION

Fig. 19 (a) Power Transmission Coefficient vs Percent Frequency Change.

(b) I P D vs Percent Frequency Change.

(c) $\frac{d}{d\theta}|T|$ (Units/Degree) vs Percent Frequency Change.

(d) $\frac{d}{d\theta}$(I P D) (Degrees/Degree) vs Percent Frequency Change.

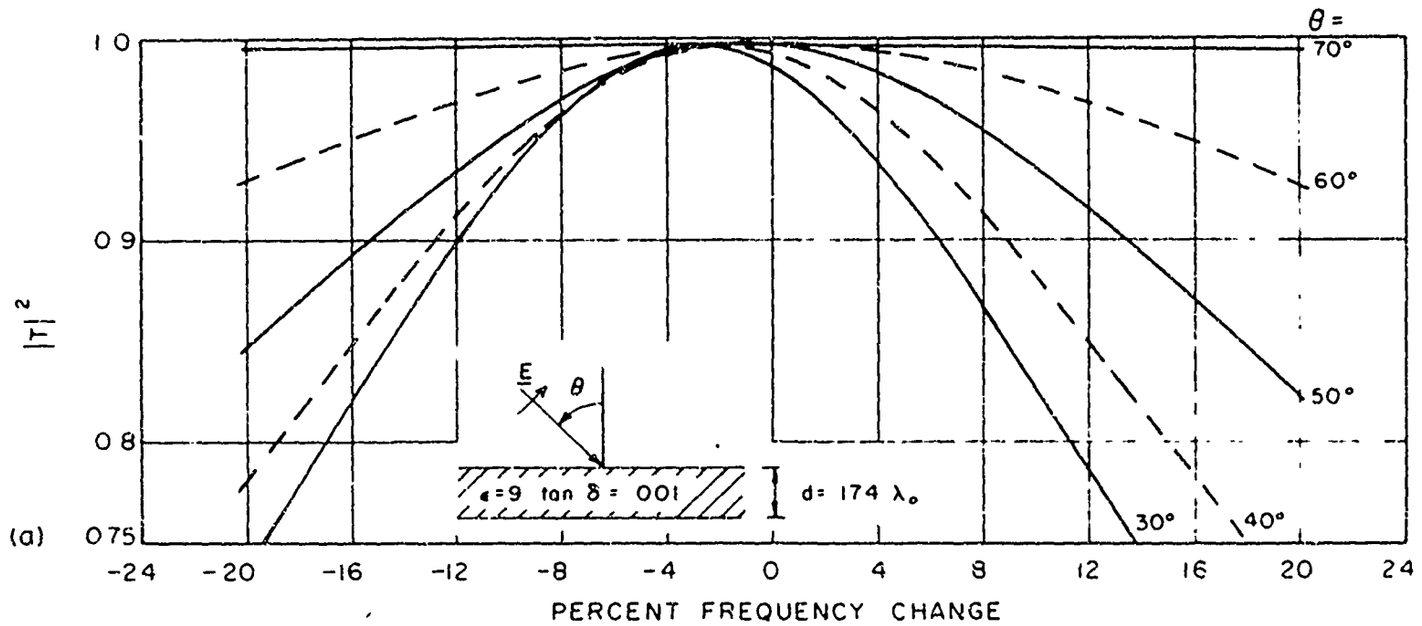

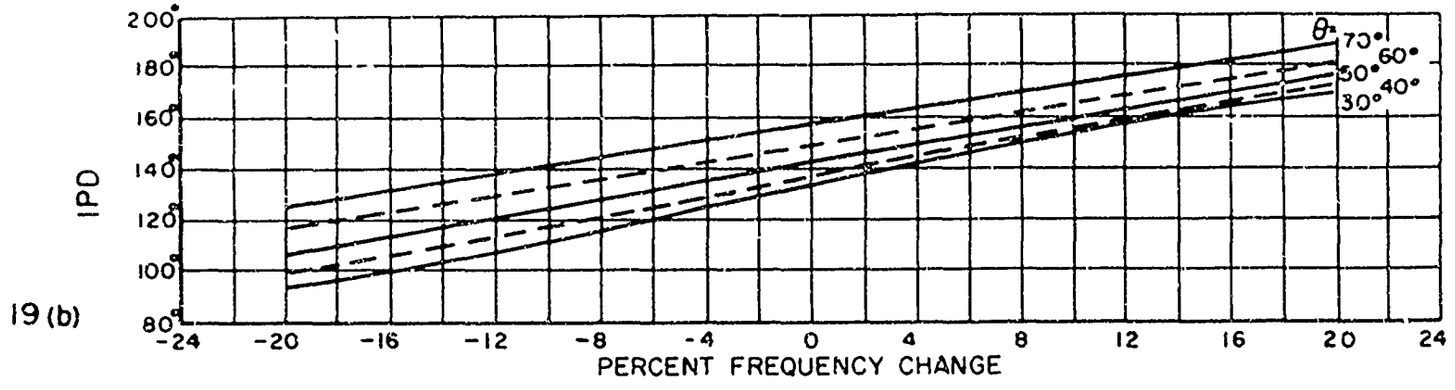
200°
180°
160°
140°
120°
100°
80°
IPD
θ=
70°
60°
50°
40°
30°
-24
-20
-16
-12
-8
-4
0
4
8
12
16
20
24
PERCENT FREQUENCY CHANGE

19 (b)

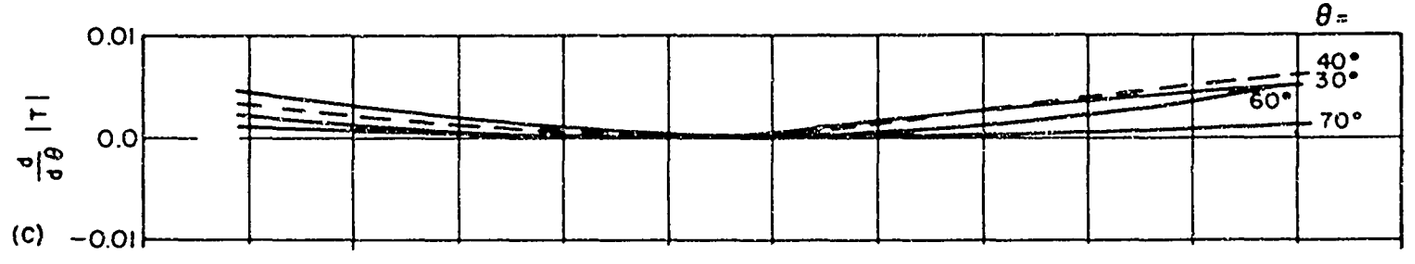
0.01
0.0
-0.01
d/dθ |T|
θ=
40°
30°
60°
70°

(c)

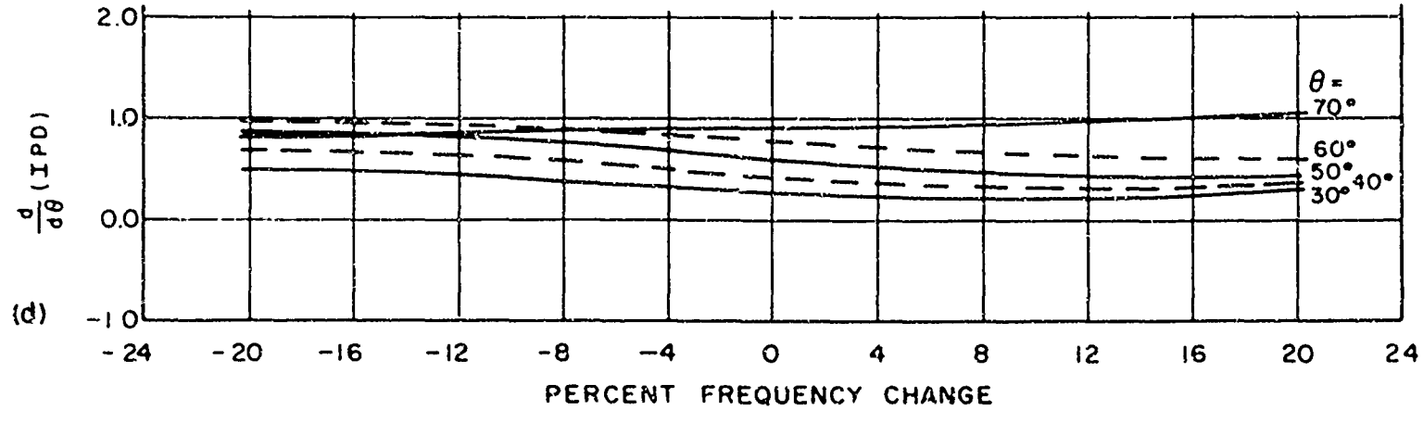
2.0
1.0
0.0
-1.0
d/dθ (IPD)
θ=
70°
60°
50°
40°
30°
-24
-20
-16
-12
-8
-4
0
4
8
12
16
20
24
PERCENT FREQUENCY CHANGE

(d)

RADOME DESIGN CURVES

TWO-LAYER PERPENDICULAR POLARIZATION

Fig. 20(a) Power Transmission Coefficient vs Percent Frequency Change.

(b) I P D vs Percent Frequency Change.

(c) $\frac{d}{d\theta}|T|$ (Units/Degree) vs Percent Frequency Change.

(d) $\frac{d}{d\theta}$(I P D) (Degrees/Degree) vs Percent Frequency Change.

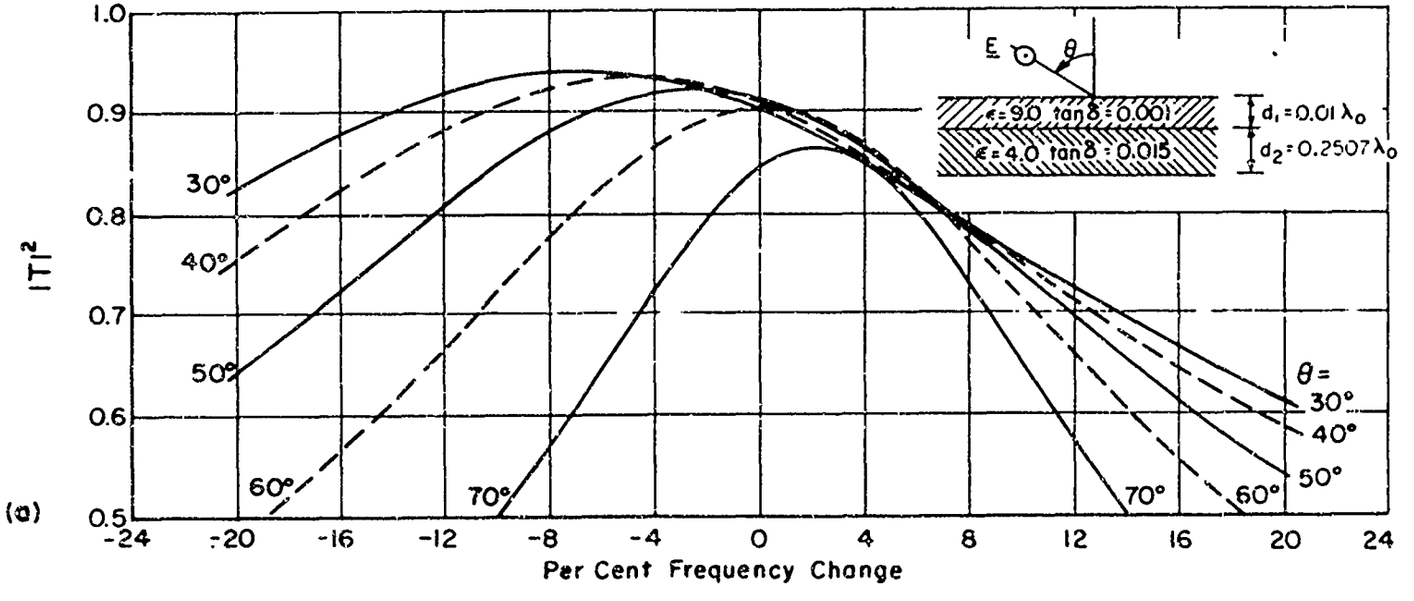

(a)

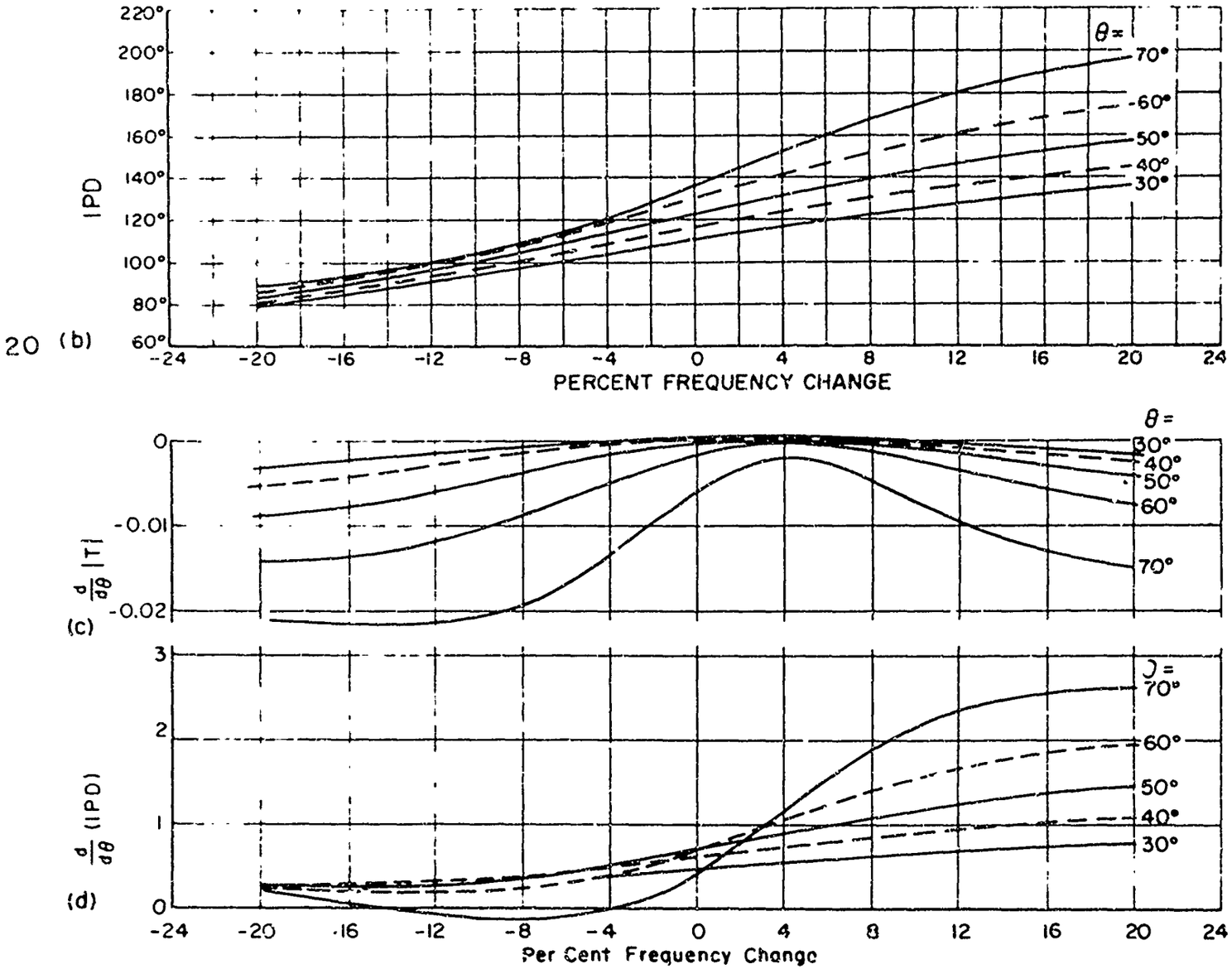
220°
200°
180°
160°
140°
120°
100°
80°
60°
IPD
θ=
70°
60°
50°
40°
30°
-24
-20
-16
-12
-8
-4
0
4
8
12
16
20
24
PERCENT FREQUENCY CHANGE
(b)
0
-0.01
-0.02
$\frac{d}{d\theta}|T|$
(c)
3
2
1
0
$\frac{d}{d\theta}(IPD)$
(d)
Per Cent Frequency Change

RADOME DESIGN CURVES

TWO – LAYER PARALLEL POLARIZATION

Fig. 21 (a) Power Transmission Coefficient vs Percent Frequency Change.

(b) I P D vs Percent Frequency Change.

(c) $\frac{d}{d\theta}|T|$ (Units/Degree) vs Percent Frequency Change.

(d) $\frac{d}{d\theta}$(I P D) (Degrees/Degree) vs Percent Frequency Change.

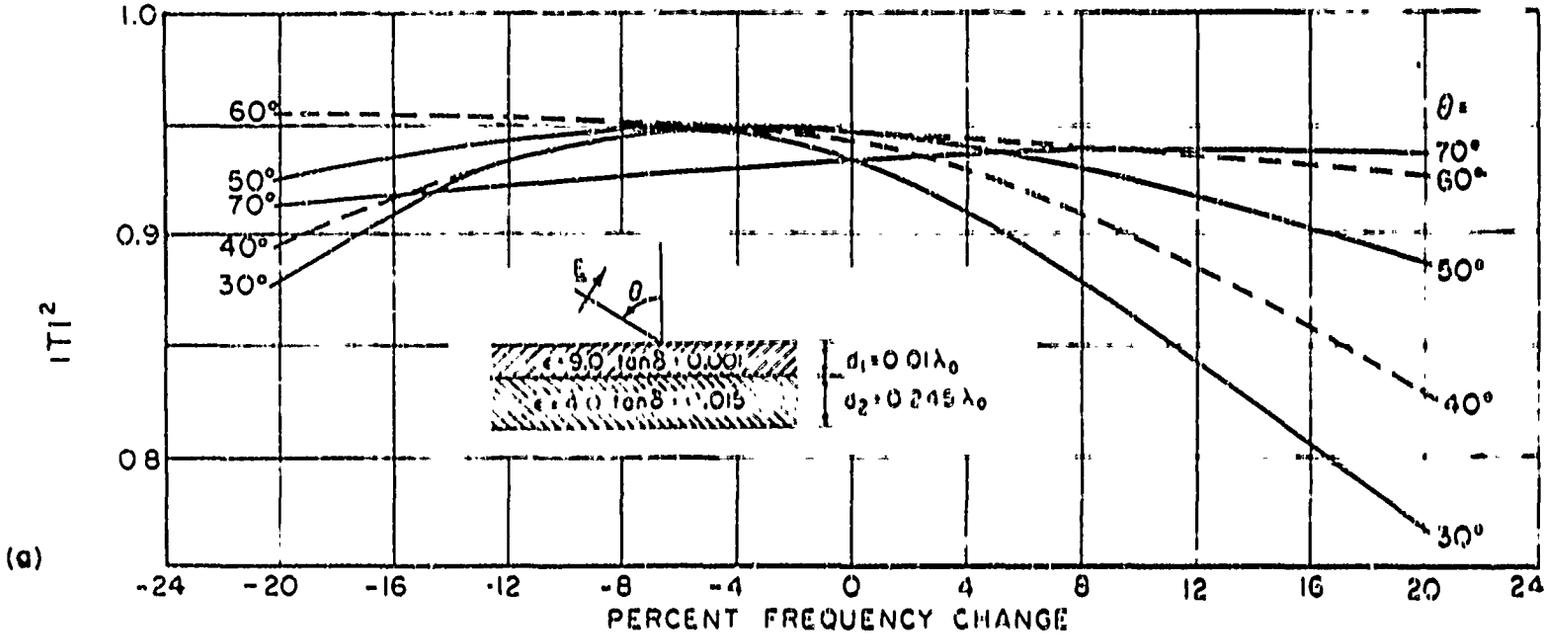

(a)

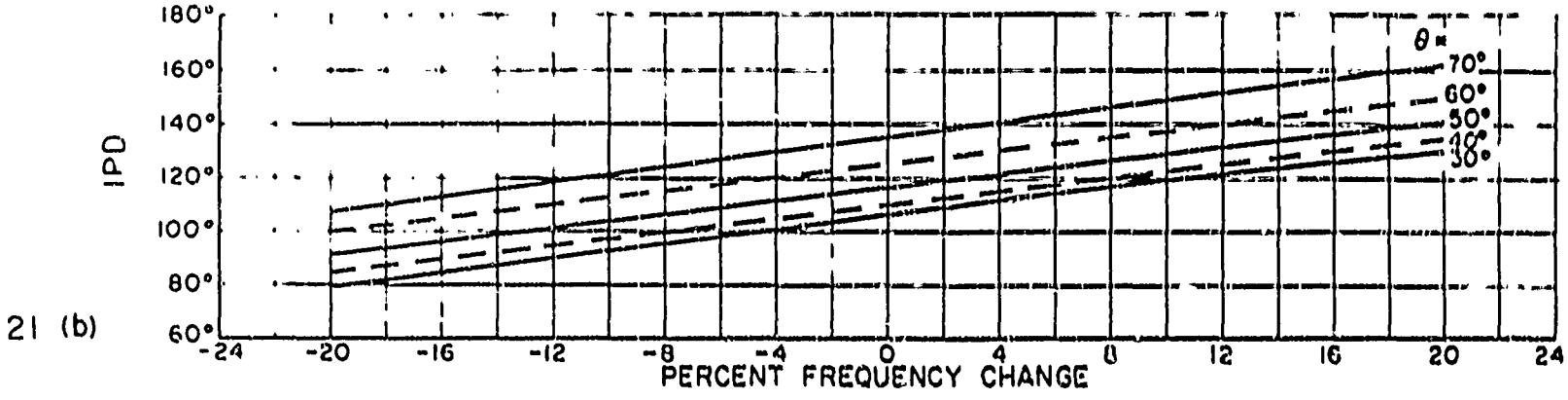
180°
160°
140°
120°
100°
80°
60°
IPD
θ =
70°
60°
50°
40°
30°
-24
-20
-16
-12
-8
-4
0
4
8
12
16
20
24
PERCENT FREQUENCY CHANGE

21 (b)

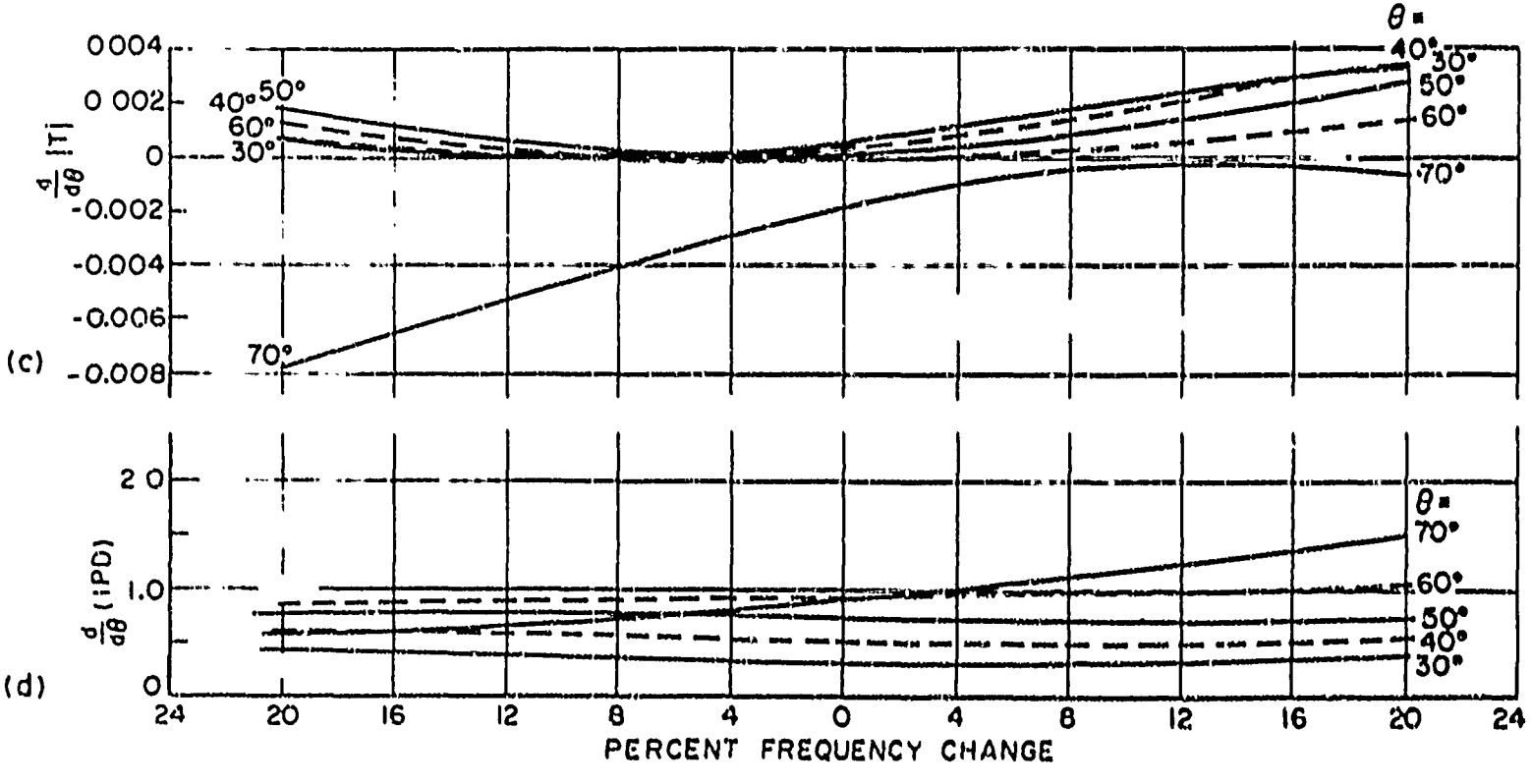
0004
0 002
0
-0.002
-0.004
-0.006
-0.008
d/dθ |T|
40°
50°
60°
30°
70°
θ =
40°
30°
50°
60°
70°
(c)
2 0
1.0
0
d/dθ (iPD)
θ =
70°
60°
50°
40°
30°
(d)
24
20
16
12
8
4
0
4
8
12
16
20
24
PERCENT FREQUENCY CHANGE

RADOME DESIGN CURVES

A-SANDWICH PERPENDICULAR POLARIZATION

Fig. 22(a) Power Transmission Coefficient vs Percent Frequency Change.

(b) I P D vs Percent Frequency Change.

(c) $\frac{d}{d\theta}|T|$ (Units/Degree) vs Percent Frequency Change.

(d) $\frac{d}{d\theta}$(I P D) (Degrees/Degree) vs Percent Frequency Change.

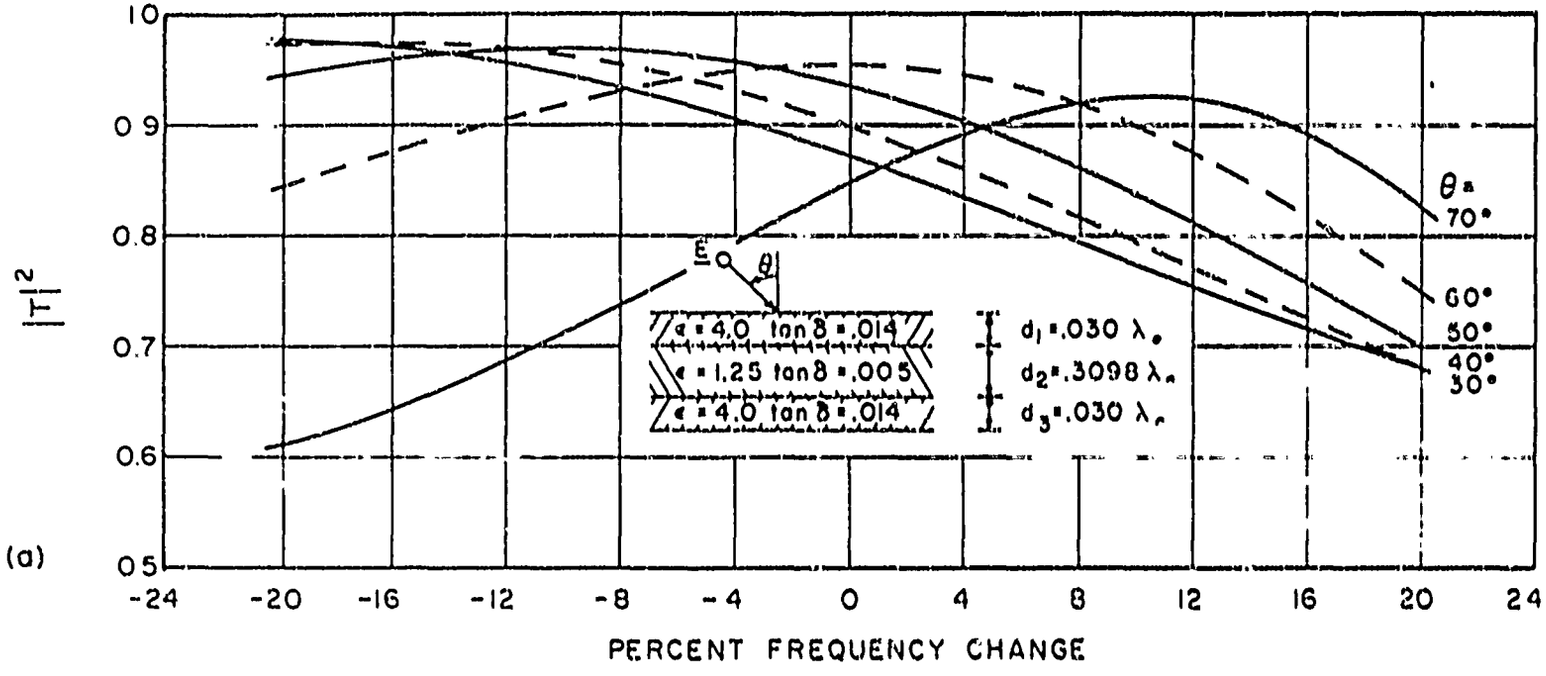

(a)

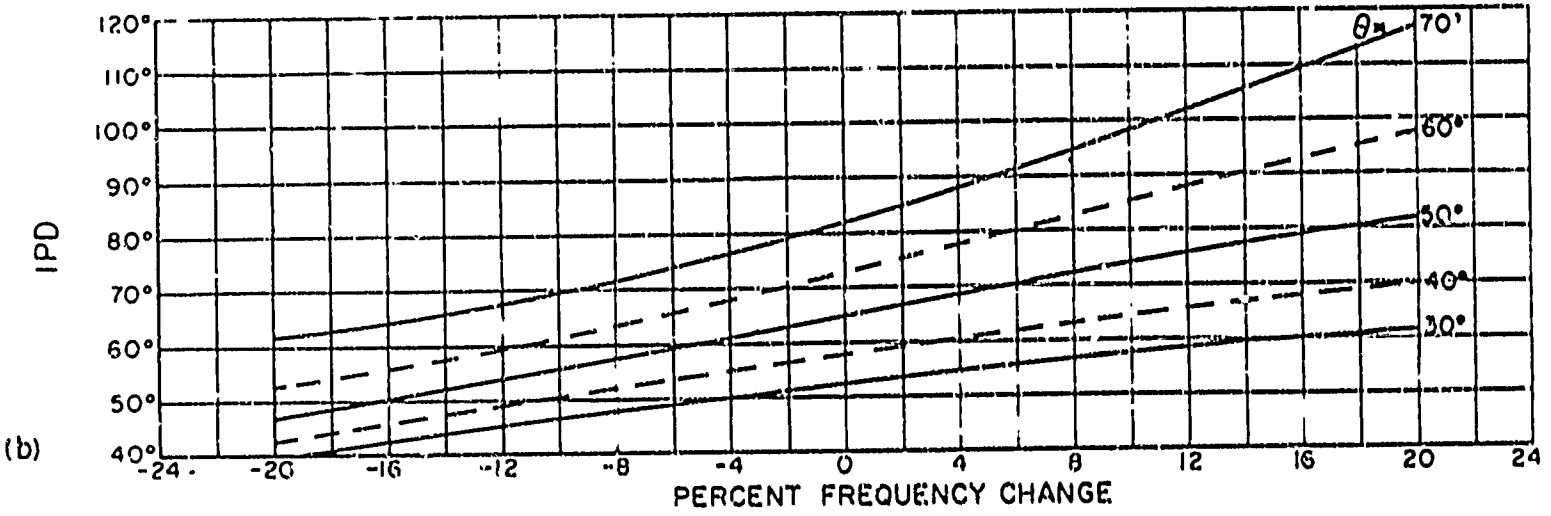
IPD
120°
110°
100°
90°
80°
70°
60°
50°
40°
θ=
70°
60°
50°
40°
30°
-24
-20
-16
-12
-8
-4
0
4
8
12
16
20
24
PERCENT FREQUENCY CHANGE

22 (b)

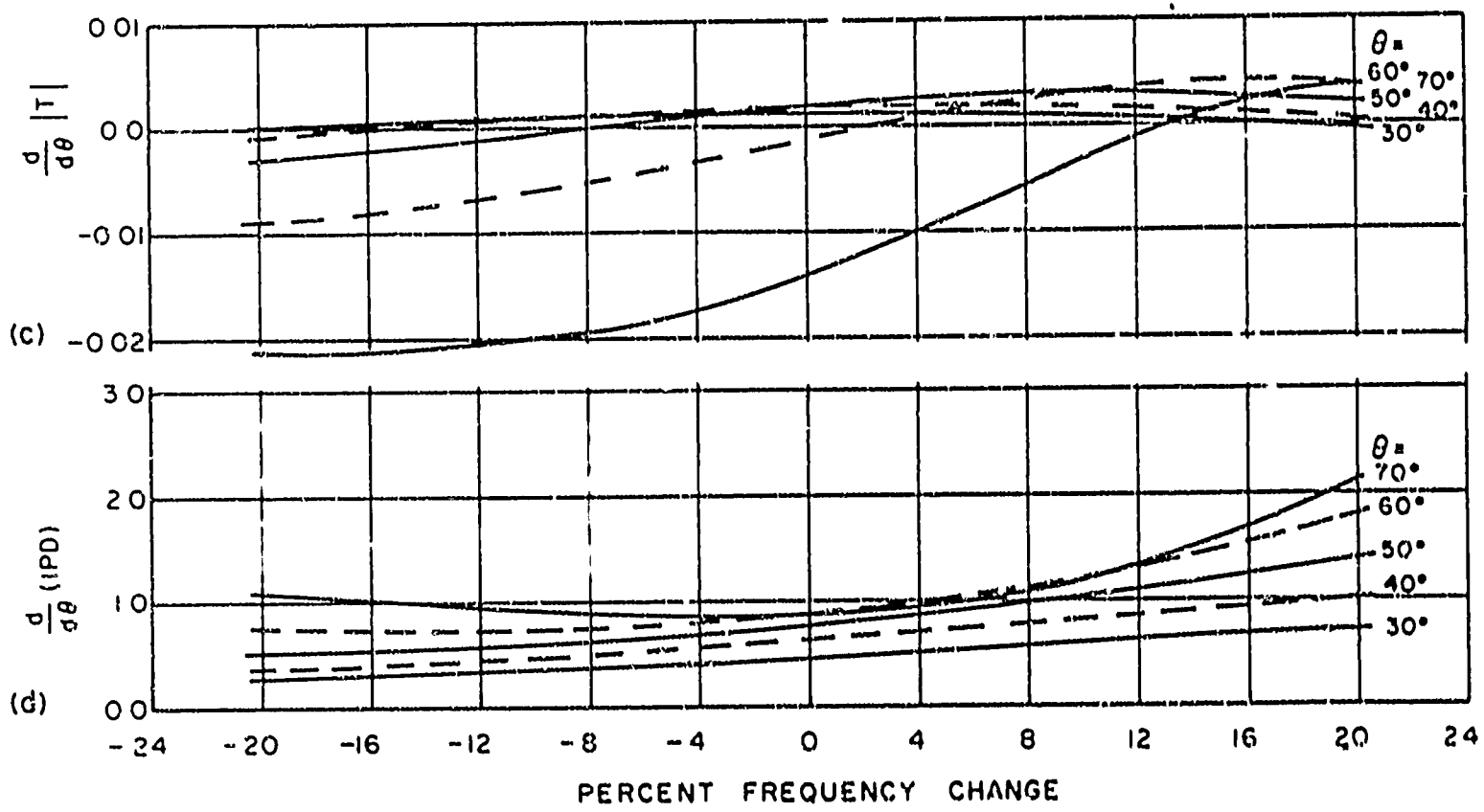
(c)
d/dθ |T|
0 01
0 0
-0 01
-0 02
θ=
60°
70°
50°
40°
30°
(d)
d/dθ (IPD)
3 0
2 0
1 0
0 0
θ=
70°
60°
50°
40°
30°
-24
-20
-16
-12
-8
-4
0
4
8
12
16
20
24
PERCENT FREQUENCY CHANGE

RADOME DESIGN CURVES

A-SANDWICH PARALLEL POLARIZATION

Fig. 23 (a) Power Transmission Coefficient vs Percent Frequency Change.

(b) I P D vs Percent Frequency Change.

(c) $\frac{d}{d\theta}|T|$ (Units/Degree) vs Percent Frequency Change.

(d) $\frac{d}{d\theta}$(I P D) (Degrees/Degree) vs Percent Frequency Change.

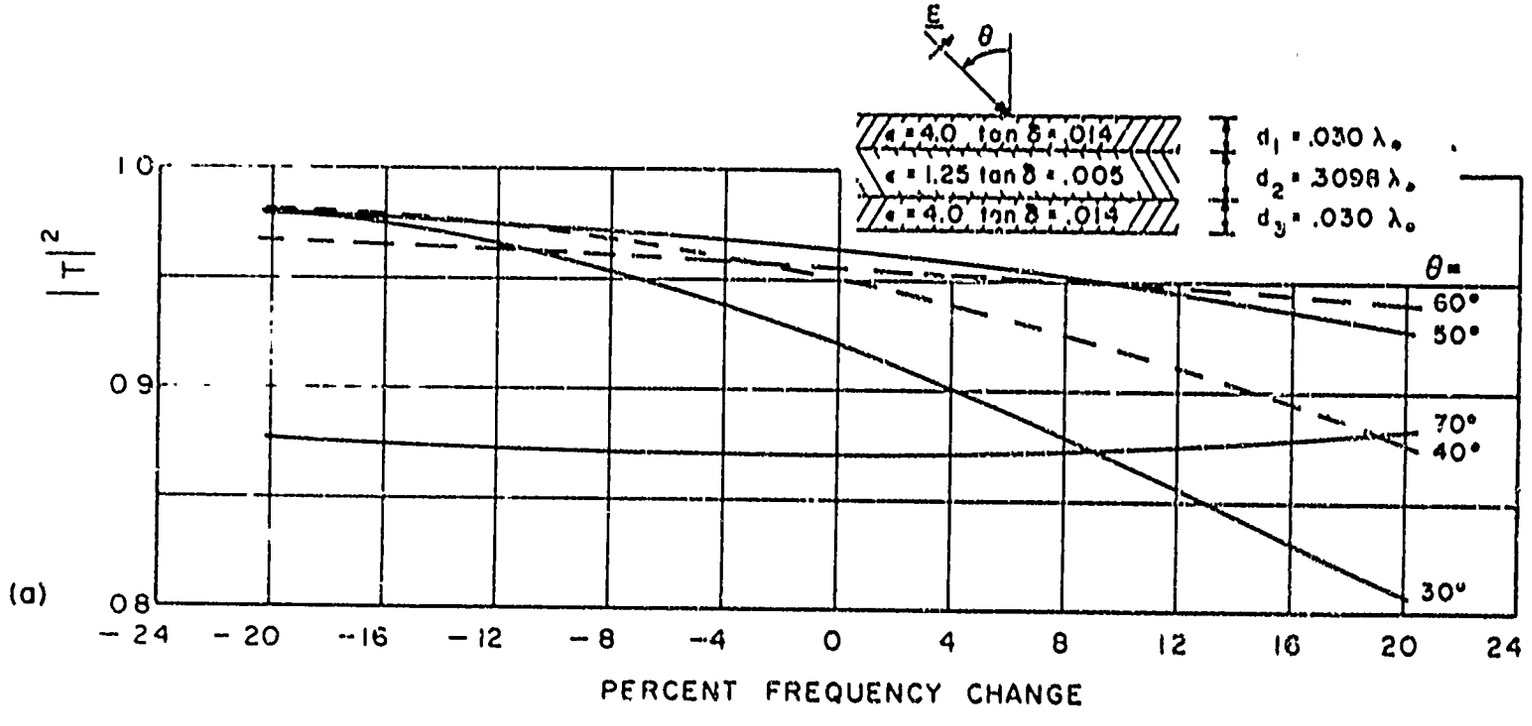

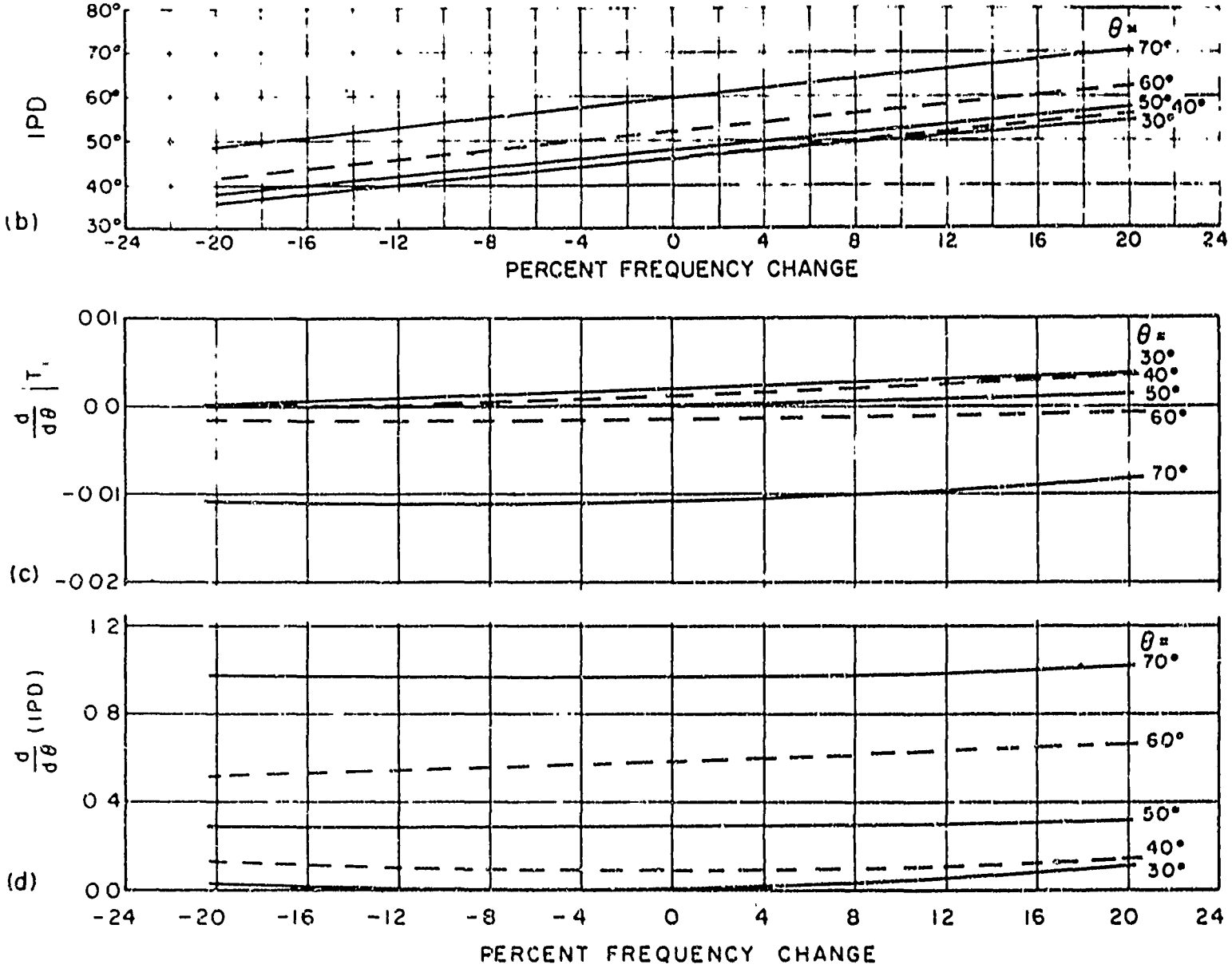
23 (b)
IPD
80°
70°
60°
50°
40°
30°
θ =
70°
60°
50°
40°
30°
-24
-20
-16
-12
-8
-4
0
4
8
12
16
20
24
PERCENT FREQUENCY CHANGE
(c)
d/dθ |T
001
00
-001
-002
θ =
30°
40°
50°
60°
70°
(d)
d/dθ (IPD)
1 2
0 8
0 4
0 0
θ =
70°
60°
50°
40°
30°
-24
-20
-16
-12
-8
-4
0
4
8
12
16
20
24
PERCENT FREQUENCY CHANGE

RADOME DESIGN CURVES

A-SANDWICH PERPENDICULAR POLARIZATION

Fig. 24 (a) Power Transmission Coefficient vs Percent Frequency Change.

(b) IPD vs Percent Frequency Change.

(c) $\frac{d}{d\theta}|T|$ (Units/Degree) vs Percent Frequency Change.

(d) $\frac{d}{d\theta}$(IPD) (Degrees/Degree) vs Percent Frequency Change.

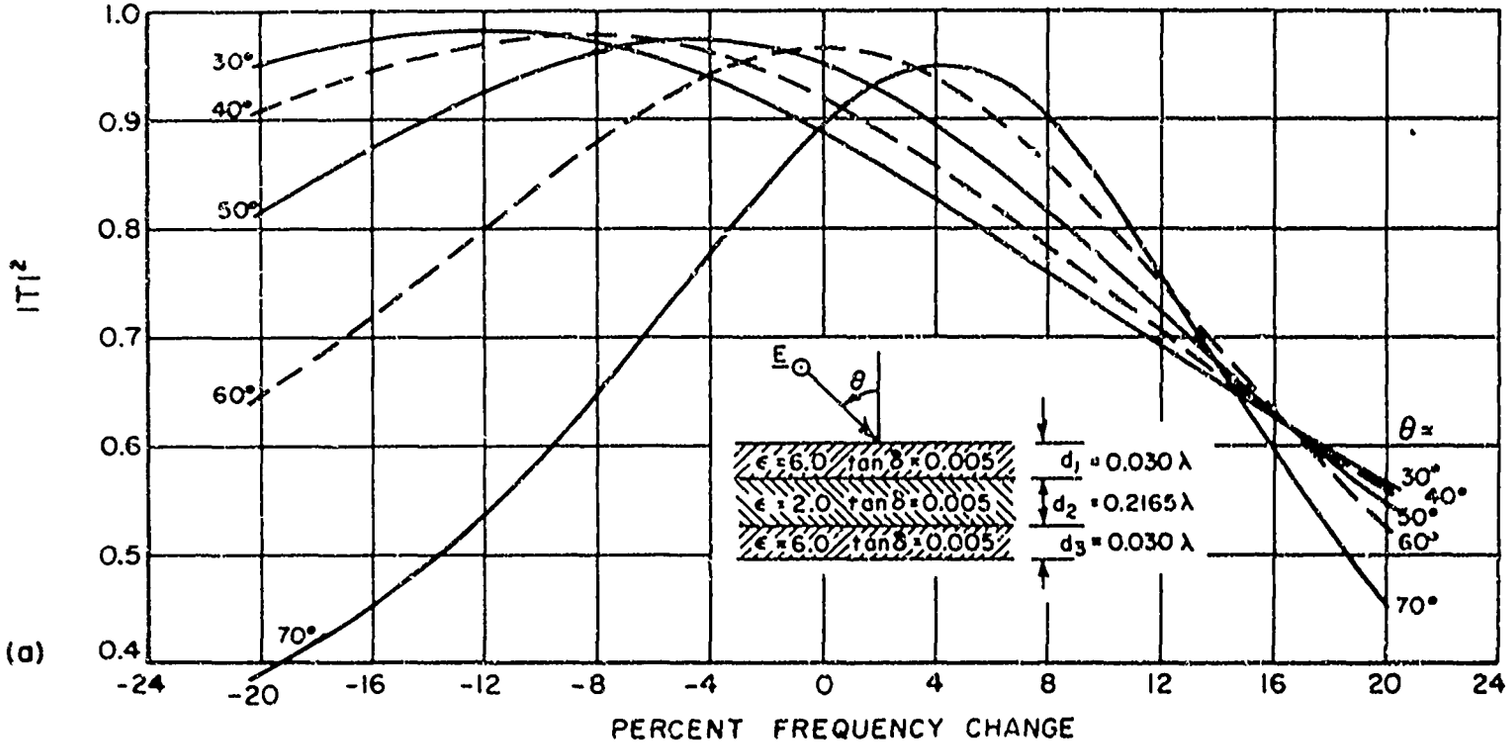

(a)

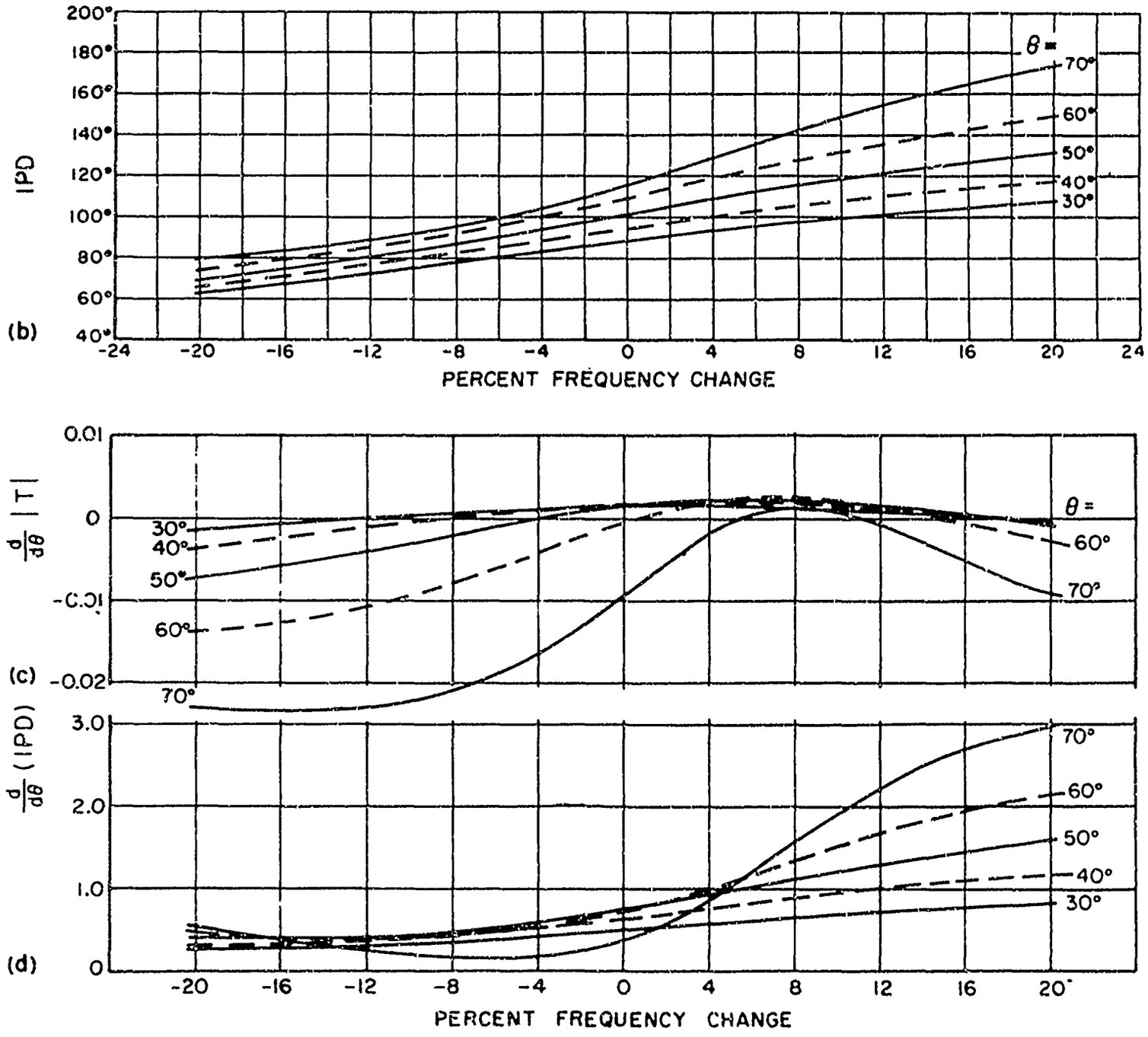
200°
180°
160°
140°
120°
100°
80°
60°
40°
IPD
θ =
70°
60°
50°
40°
30°
-24
-20
-16
-12
-8
-4
0
4
8
12
16
20
24
PERCENT FREQUENCY CHANGE
0.01
0
-0.01
-0.02
d/dθ |T|
θ =
30°
40°
50°
60°
70°
(c)
3.0
2.0
1.0
0
d/dθ (IPD)
70°
60°
50°
40°
30°
(d)
-20
-16
-12
-8
-4
0
4
8
12
16
20°
PERCENT FREQUENCY CHANGE

24 (b)

RADOME DESIGN CURVES

A-SANDWICH PARALLEL POLARIZATION

Fig. 25 (a) Power Transmission Coefficient vs Percent Frequency Change.

(b) IPD vs Percent Frequency Change.

(c) $\frac{d}{d\theta}|T|$ (Units/Degree) vs Percent Frequency Change.

(d) $\frac{d}{d\theta}(IPD)$ (Degrees/Degree) vs Percent Frequency Change.

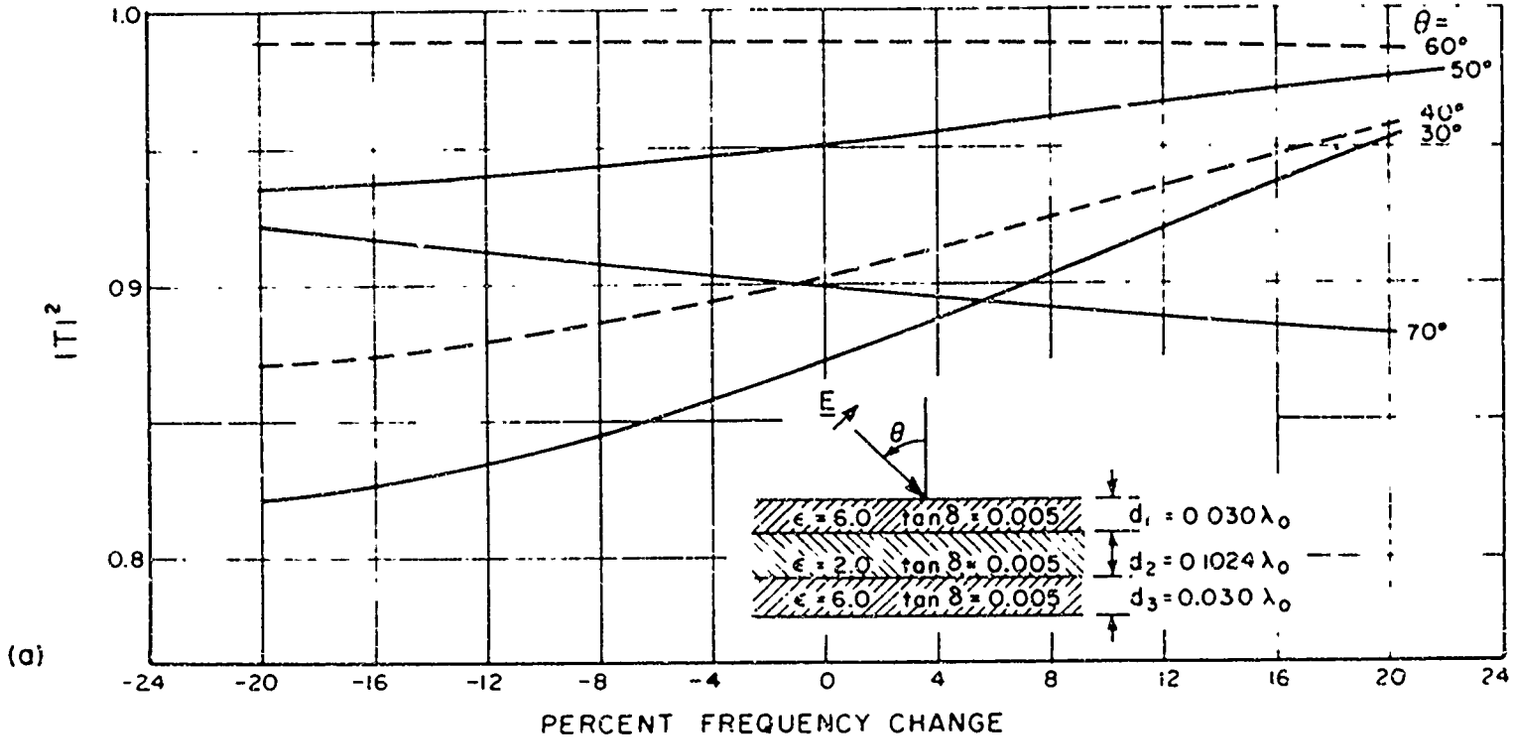

(a)

25 (b)

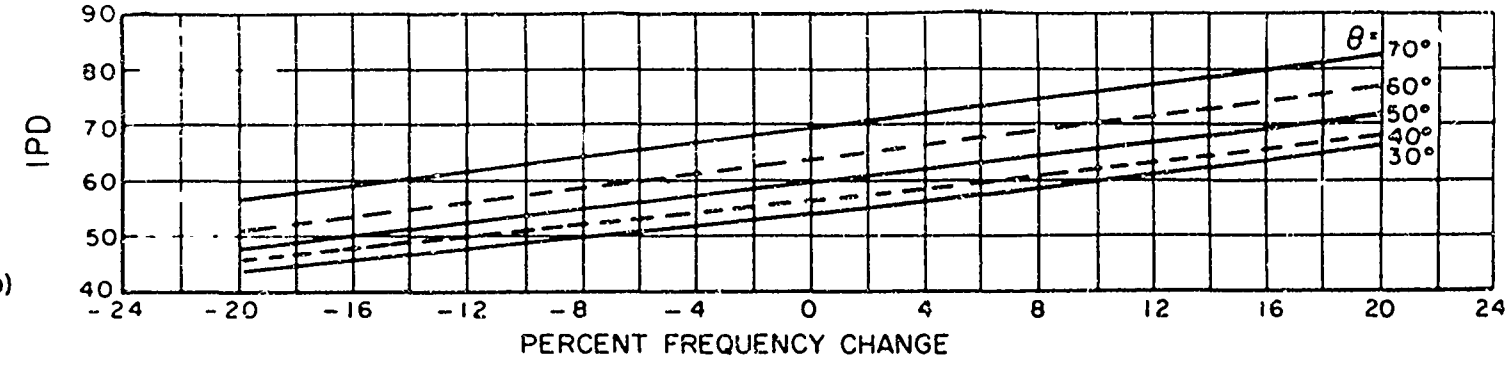
IPD
90
80
70
60
50
40
θ=
70°
60°
50°
40°
30°
-24
-20
-16
-12
-8
-4
0
4
8
12
16
20
24
PERCENT FREQUENCY CHANGE

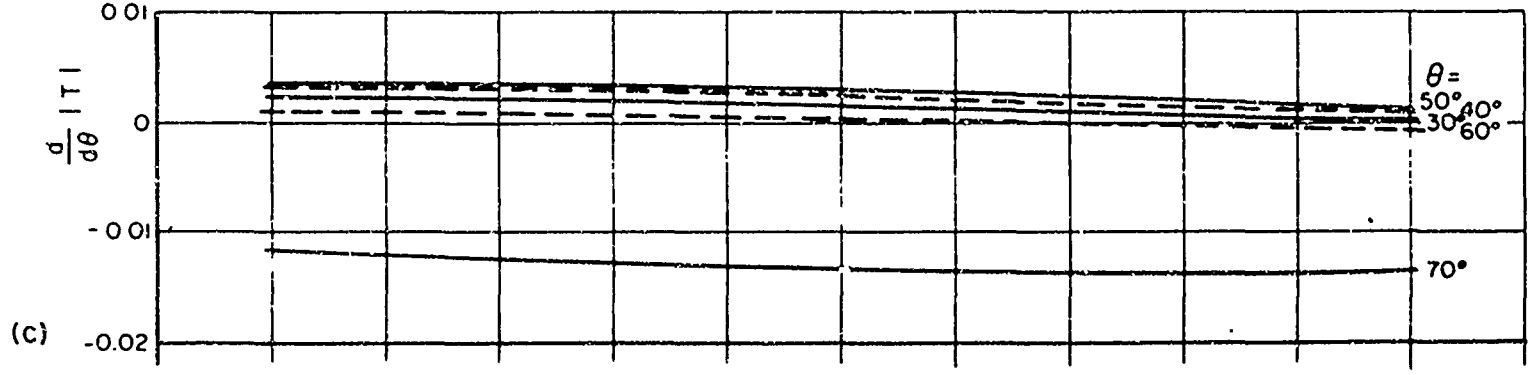
(c)
d/dθ |T|
0.01
0
-0.01
-0.02
θ=
50°
40°
30°
60°
70°

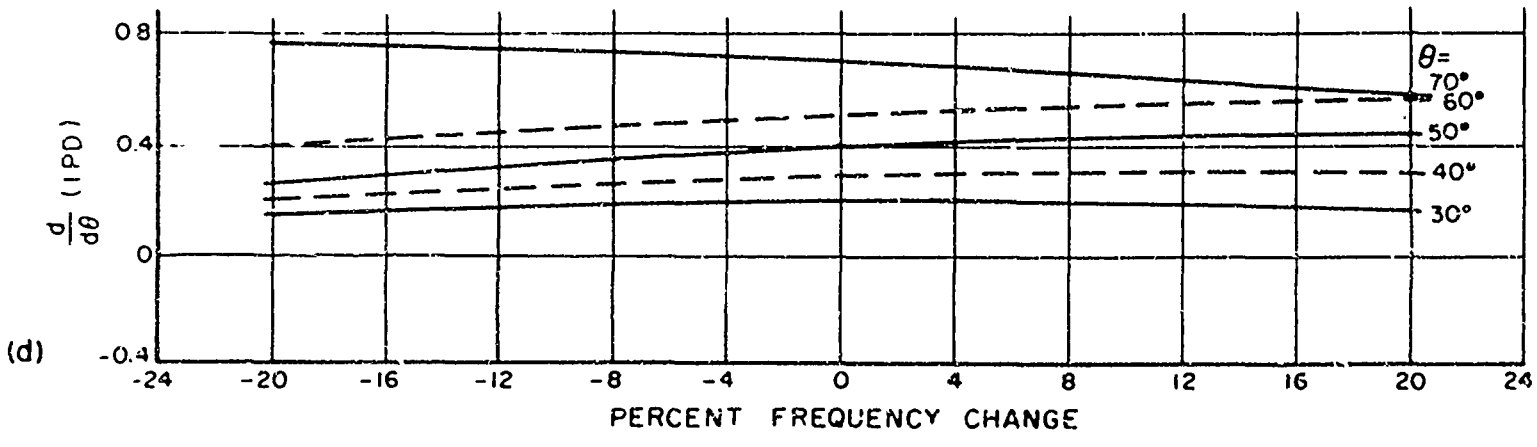
(d)
d/dθ (IPD)
0.8
0.4
0
-0.4
θ=
70°
60°
50°
40°
30°
-24
-20
-16
-12
-8
-4
0
4
8
12
16
20
24
PERCENT FREQUENCY CHANGE

RADOME DESIGN CURVES

A-SANDWICH PERPENDICULAR POLARIZATION

Fig. 26 (a) Power Transmission Coefficient vs Percent Frequency Change.

(b) I P D vs Percent Frequency Change.

(c) $\frac{d}{d\theta}|T|$ (Units/Degree) vs Percent Frequency Change.

(d) $\frac{d}{d\theta}(IPD)$ (Degrees/Degree) vs Percent Frequency Change.

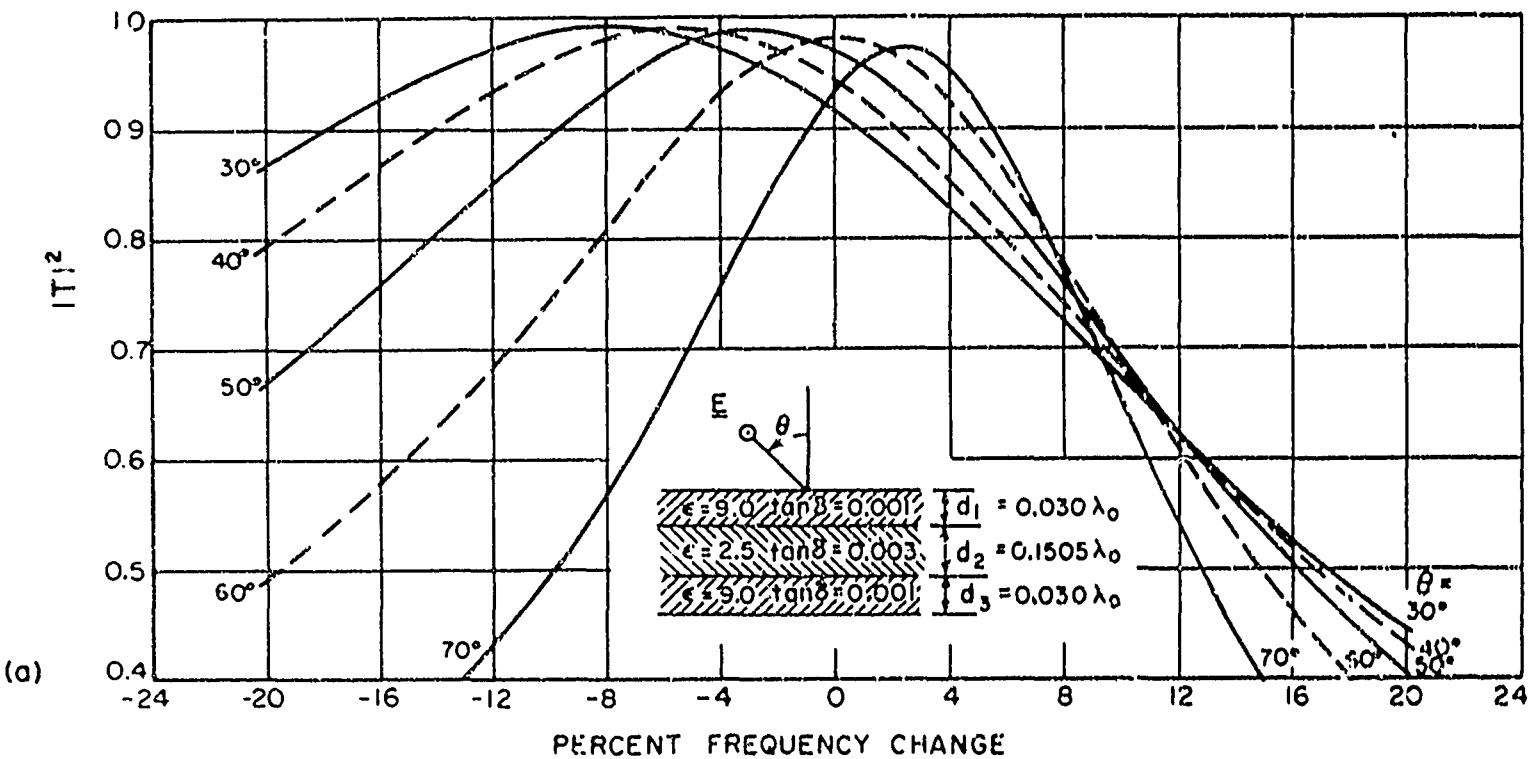

(a)

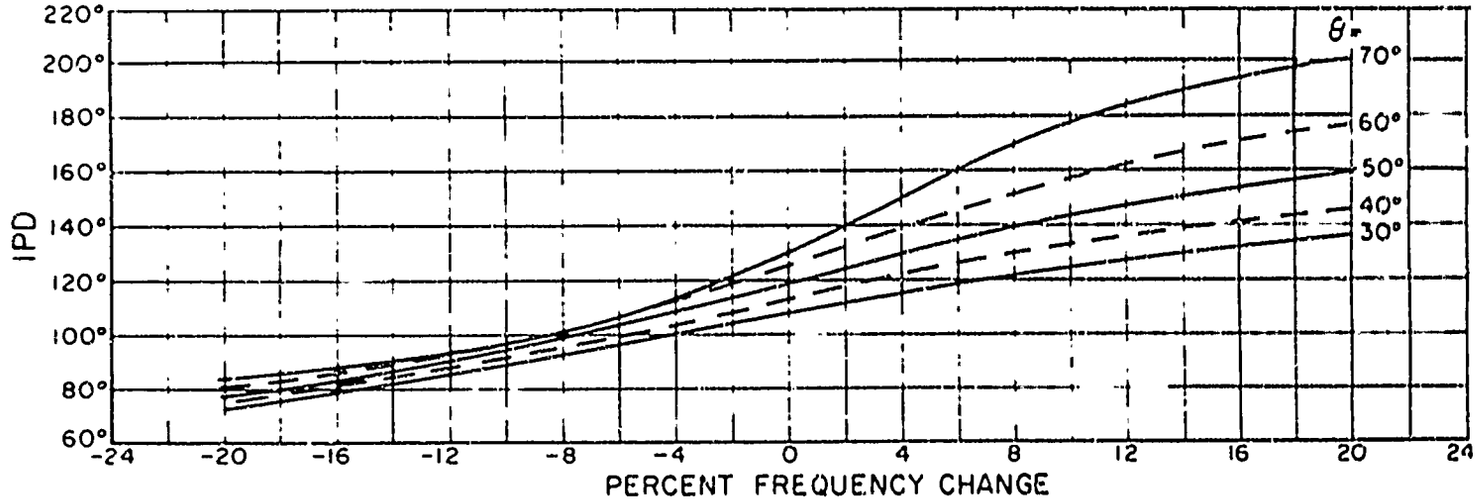
220°
200°
180°
160°
140°
120°
100°
80°
60°
IPD
θ=
70°
60°
50°
40°
30°
-24
-20
-16
-12
-8
-4
0
4
8
12
16
20
24
PERCENT FREQUENCY CHANGE

26 (b)

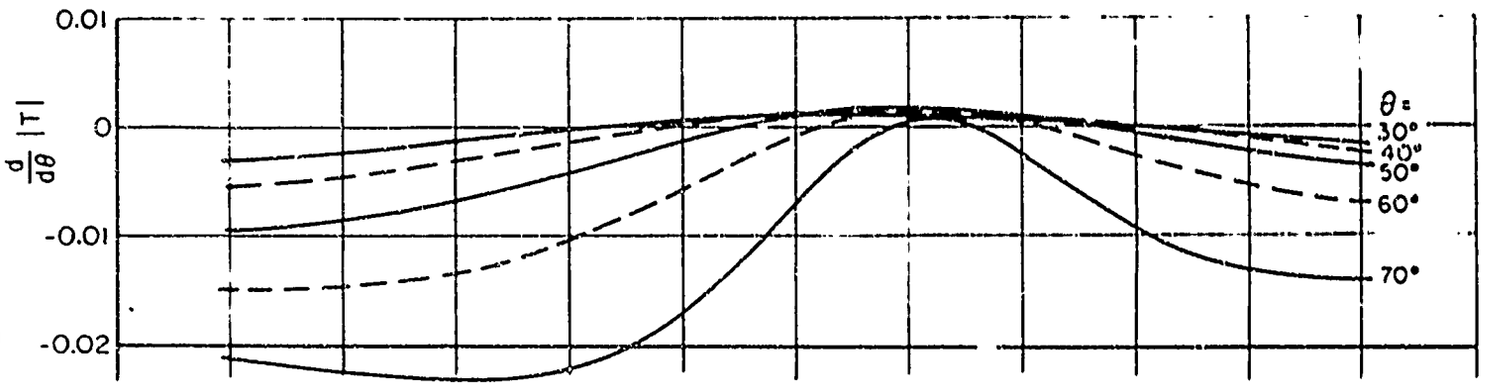
0.01
0
-0.01
-0.02
d/dθ |T|
θ=
30°
40°
50°
60°
70°

(c)

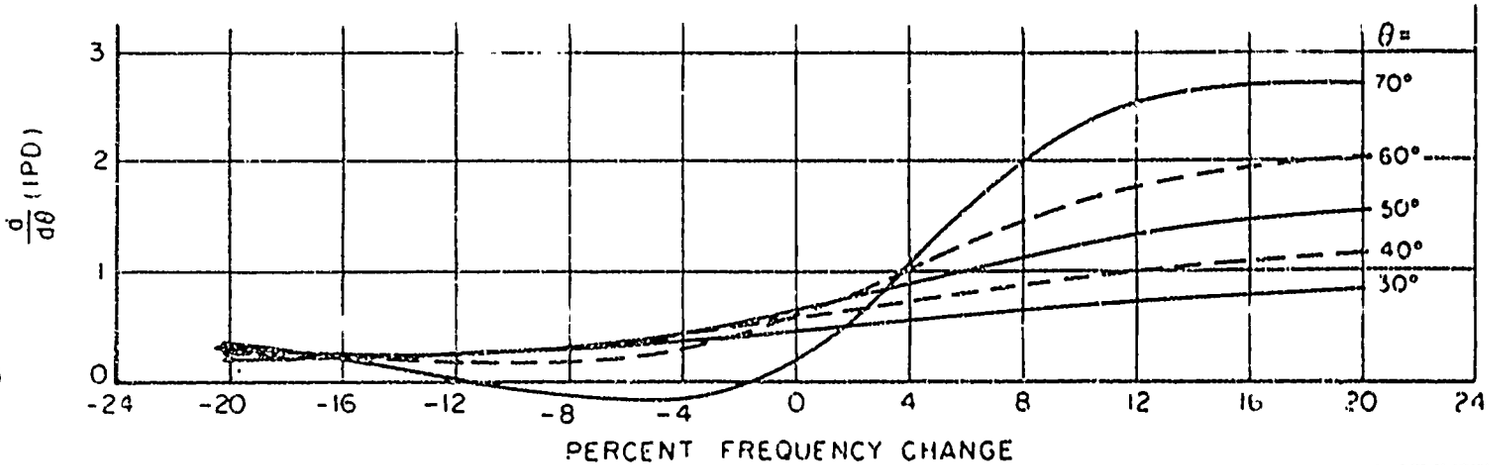
3
2
1
0
d/dθ (IPD)
θ=
70°
60°
50°
40°
30°
-24
-20
-16
-12
-8
-4
0
4
8
12
16
20
24
PERCENT FREQUENCY CHANGE

(d)

RADOME DESIGN CURVES

A-SANDWICH PARALLEL POLARIZATION

Fig. 27 (a) Power Transmission Coefficient vs Percent Frequency Change.

(b) IPD vs Percent Frequency Change.

(c) $\frac{d}{d\theta}|T|$ (Units/Degree) vs Percent Frequency Change.

(d) $\frac{d}{d\theta}(IPD)$ (Degrees/Degree) vs Percent Frequency Change.

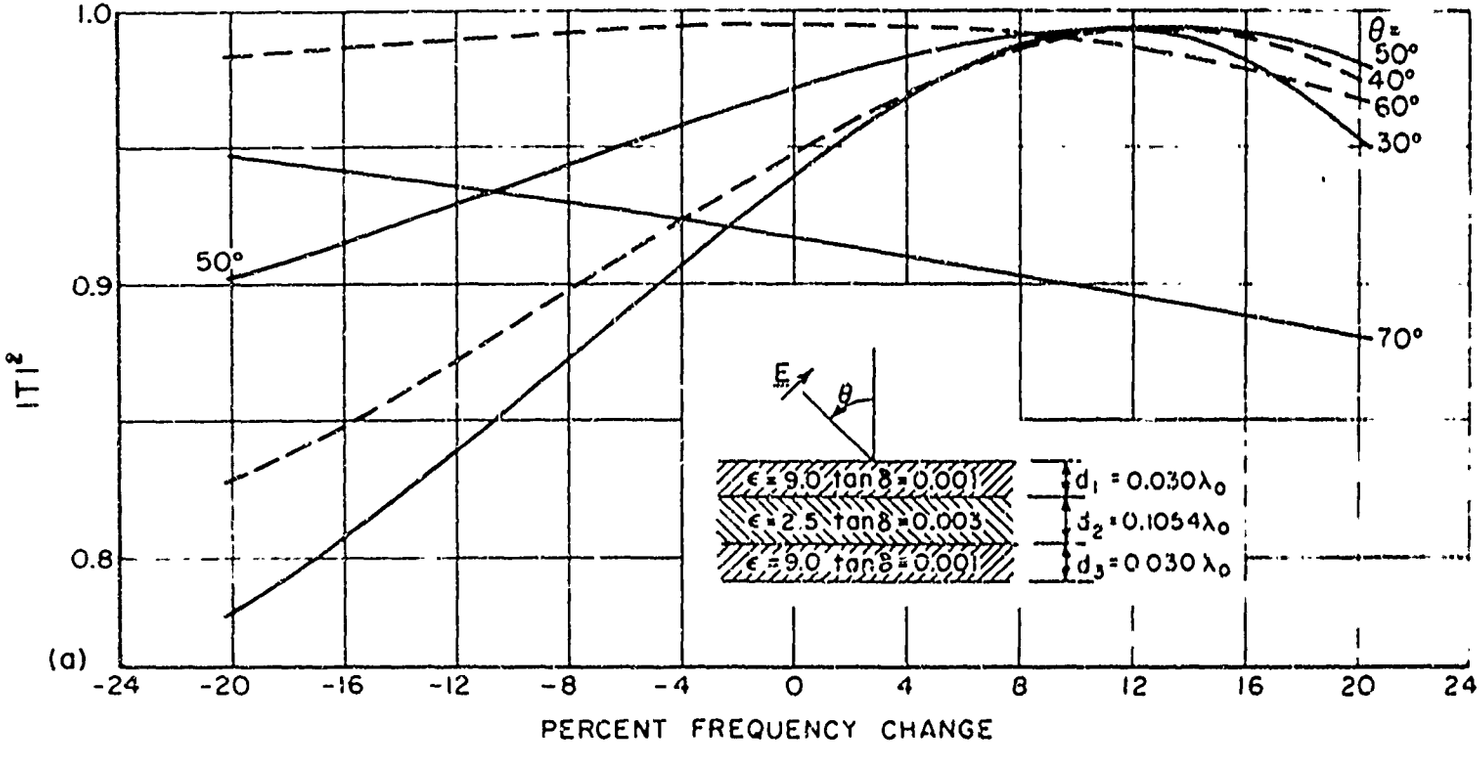

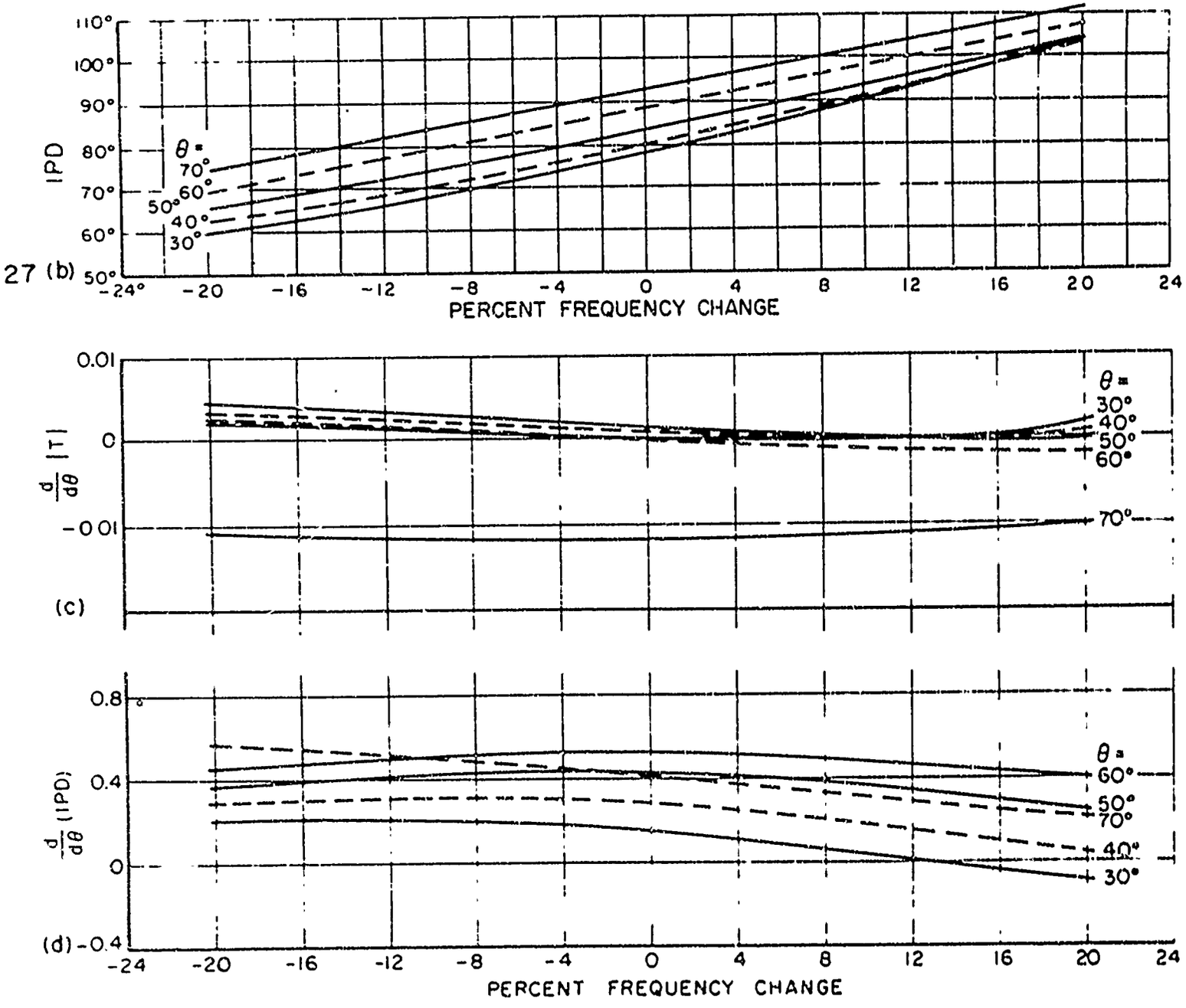
IPD
110°
100°
90°
80°
70°
60°
50°
θ =
70°
60°
50°
40°
30°
-24°
-20
-16
-12
-8
-4
0
4
8
12
16
20
24
PERCENT FREQUENCY CHANGE
(b)
0.01
0
-0.01
d/dθ |T|
θ =
30°
40°
50°
60°
70°
(c)
0.8
0.4
0
-0.4
d/dθ (IPD)
θ =
60°
50°
70°
40°
30°
(d)
-24
-20
-16
-12
-8
-4
0
4
8
12
16
20
24
PERCENT FREQUENCY CHANGE

APPENDIX B
APPLICATION OF THE RADOME DESIGN CURVES TO RADOME WALL STRUCTURES WITH SLIGHTLY DIFFERENT DIELECTRIC CONSTANTS

The radome wall data were computed with frequency as the independent variable because of interest in the bandwidth properties. The thickness in wavelengths of a given layer is d_n/λ_0 and a given per cent change in d_n can be shown to be equivalent to the same, but independent per cent change in frequency as follows:

$$\frac{\Delta\left(\frac{d_n}{\lambda_0}\right)}{\left(\frac{d_n}{\lambda_0}\right)} = \frac{\Delta d_n}{d_n} = \frac{\Delta\left(\frac{d_n}{c} f\right)}{\frac{d_n}{c} f} = \frac{\frac{d_n}{c}\Delta f}{\frac{d_n}{c} f} = \frac{\Delta f}{f} \quad .$$

The phase factor of any given layer of a multilayer is

$$\beta d_n = 2\pi \frac{d_n}{\lambda_0} \sqrt{\mu_n \epsilon_n - \sin^2 \theta} \quad ,$$

where μ_n and ϵ_n are the relative constants of the layer and θ is the angle of incidence of a plane wave on the multilayer. Let $\mu_n = 1$ and estimate the effect of an increment in ϵ_n by ignoring $\sin^2 \theta$ relative to ϵ_n. Then, to establish an equivalence between a change in d_n (and therefore the frequency) and a change in ϵ_n, independent of each other, we write

$$\Delta\left(\frac{d_n}{\lambda_0}\sqrt{\epsilon_n}\right) = \frac{\sqrt{\epsilon_n}}{\lambda_0}\Delta d_n = \frac{d_n}{\lambda_0}\Delta\sqrt{\epsilon_n}$$

$$\frac{\Delta d_n}{d_n} = \frac{\Delta\sqrt{\epsilon_n}}{\sqrt{\epsilon_n}} = \frac{\Delta f}{f} \quad .$$

Thus, a small per cent change in $\sqrt{\epsilon_n}$ is approximately equivalent to the same per cent change in frequency on the design curves (approximate because $\sin^2\theta$ and the effect of a change in ϵ_n on the interface reflections were neglected).

Thus, if the performance of a multilayer with given dimensions is known at one value of $\Delta f/f$ and it is required to find that for a given per cent change in the square root of the dielectric constant of each layer, it is necessary only to change the frequency by the same percentage and make the observation.

REFERENCES

1. Tice, T.E. (Editor), "Techniques for Airborne Radome Design," WADC-TR-57-67, (September 1957). (AD 142 001).

2. Boyce, W.E.L., and Hartig, E.O., Chapter 3, "Techniques for Airborne Radome Design," WADC-TR-57-67, (September 1957), Edited by T.E. Tice. (AD 142 001).

3. Boyce, W.E.L., "The Angular Error Characteristics of a Radome As a Function of the Polarization of the Field Incident on the Radome," Proceedings of the OSU-WADC Radome Symposium, Vol. II, (June 1955), pp. 205-230.

4. Snyder, R.C., "An Empirical Analysis of Conical-Scan Boresight and Transmission Characteristics of a Streamlined Thin-Wall Missile Radome," Proceedings of the OSU-WADD Symposium on Electromagnetic Windows, WADD-TR-60-274, Vol. I, (June 1960), pp. 238-248.

5. Pressel, P.I., and Mathis, H.F., "Improved Boresight Prediction Technique," Proceedings of the OSU-WADC Radome Symposium, WADC-TR-57-314, Vol. I, (1957), pp. 126-133.

6. Tricoles, G., "A Physical Optics Radome Error Prediction Method," Proceedings of the OSU-WADC Radome Symposium, WADC-TR-57-314, Vol. II, (1957), pp. 35-54.

7. Tricoles, G., "A Radome Error Prediction Method Based on Aperture Fields and Rays: Formulation and Application," Proceedings of the OSU-WADD Symposium on Electromagnetic Windows, WADD-TR-60-274, Vol. I, (1960), pp. 267-286.

8. Wolin, S., "Theory of Lossy High-Incidence Radomes," Report NADC-EL-5116, U.S. Naval Air Development Center, Johnsville, Pennsylvania, (15 January 1952).

9. DiToro, J.A., "Graphs of Transmission and Phase Data of Plane Dielectric Sheets for Radome Design," Report NADC-EL-5313, U.S. Naval Air Development Center, Johnsville, Pennsylvania, (1 July 1953). (AD 45 316).

10. Schetne, H.A., Chapter 4, "Techniques for Airborne Radome Design," WADC-TR-57-67, (September 1957), Edited by T.E. Tice. (AD 142 001).

11. Pressel, P.I., "Boresight Prediction Technique," Proceedings of the OSU-WADC Radome Symposium, Vol. I, (August 1956), pp. 33-40.

12. Augustine, R.J., "Boresight Correction of a Streamlined K_u Band Radome," Proceedings of the OSU-WADC Radome Symposium, Vol. II, (1957), pp. 87-97.

13. Van Doeren, R.E., "Design Curves for Transmission and Boresight Analysis of Several Radome Wall Structures," Report 1804-3, 21 May 1965, Antenna Laboratory, The Ohio State University Research Foundation; prepared under Contract Number NOw-64-0293-d, Department of the Navy, Bureau of Naval Weapons, Washington, D.C. (AD 623 656).

UNCLASSIFIED

Security Classification

DOCUMENT CONTROL DATA - R&D

(Security classification of title, body of abstract and indexing annotation must be entered when the overall report is classified)

1. ORIGINATING ACTIVITY (Corporate author)	2a. REPORT SECURITY CLASSIFICATION
Antenna Laboratory, Department of Electrical Engineering, The Ohio State University Research Foundation, Cols., O.	Unclassified
	2b. GROUP

3. REPORT TITLE

A First Order Approach to Radome Boresight Analysis and Design

4. DESCRIPTIVE NOTES (Type of report and inclusive dates)

Technical

5. AUTHOR(S) (Last name, first name, initial)

Van Doeren, R.E.

6. REPORT DATE	7a. TOTAL NO. OF PAGES	7b. NO. OF REFS
15 March 1966	74	13

8a. CONTRACT OR GRANT NO.	9a. ORIGINATOR'S REPORT NUMBER(S)
Contract NOw-64-0293-d	Antenna Laboratory 1804-6
b. PROJECT NO.	
c. TASK	9b. OTHER REPORT NO(S) (Any other numbers that may be assigned this report)
d.	

10. AVAILABILITY/LIMITATION NOTICES

Release to Defense Documentation Center (DDC) without Restriction. Release by the Office of Technical Service, Department of Commerce, is approved.

11. SUPPLEMENTARY NOTES	12. SPONSORING MILITARY ACTIVITY
	Department of the Navy Bureau of Naval Weapons Washington, D.C. 20360

13. ABSTRACT

A simplified first-order theory of radome boresight error is derived and applied to prediction and design problems. Reasonable predictive results are obtained for radomes with known boresight error. The dependence of boresight error on the derivatives of IPD and $|T|$ with respect to incidence angle is shown and the significance of polarization in light of the theory is discussed. Polarization control is shown to reduce boresight error when used with an appropriate radome wall design.

The possibility of a "cancellation" design for a radome, wherein the errors due to phase tapering and to differential attenuation tend to cancel each other is pointed out. The concept of artificially introduced loss to achieve such cancellation is discussed. A design example is included. Radome design curves giving $|T|^2$, IPD, $d/d\theta$(IPD), and $d/d\theta\,|T|$ for several important radome wall structures are also included.

DD FORM 1 JAN 64 1473

UNCLASSIFIED

Security Classification

UNCLASSIFIED

Security Classification

14. KEY WORDS	LINK A		LINK B		LINK C	
	ROLE	WT	ROLE	WT	ROLE	WT
Radar						
Monopulse						
Radome design						
Radome correction						
Boresight error						
Multilayer transmission						
Polarization						
Polarization control						
Polarization effects						

INSTRUCTIONS

1. ORIGINATING ACTIVITY. Enter the name and address of the contractor, subcontractor, grantee, Department of Defense activity or other organization *(corporate author)* issuing the report.

2a. REPORT SECURITY CLASSIFICATION. Enter the overall security classification of the report. Indicate whether "Restricted Data" is included. Marking is to be in accordance with appropriate security regulations.

2b. GROUP: Automatic downgrading is specified in DoD Directive 5200.10 and Armed Forces Industrial Manual. Enter the group number. Also, when applicable, show that optional markings have been used for Group 3 and Group 4 as authorized.

3. REPORT TITLE: Enter the complete report title in all capital letters. Titles in all cases should be unclassified. If a meaningful title cannot be selected without classification, show title classification in capitals in parenthesis immediately following the title.

4. DESCRIPTIVE NOTES: If appropriate, enter the type of report, e.g., interim, progress, summary, annual, or final. Give the inclusive dates when a specific reporting period is covered.

5. AUTHOR(S): Enter the name(s) of author(s) as shown on or in the report. Enter last name, first name, middle initial. If military, show rank and branch of service. The name of the principal author is an absolute minimum requirement.

6. REPORT DATE: Enter the date of the report as day, month, year, or month, year. If more than one date appears on the report, use date of publication.

7a. TOTAL NUMBER OF PAGES: The total page count should follow normal pagination procedures, i.e., enter the number of pages containing information.

7b. NUMBER OF REFERENCES: Enter the total number of references cited in the report.

8a. CONTRACT OR GRANT NUMBER. If appropriate, enter the applicable number of the contract or grant under which the report was written.

8b, 8c, & 8d. PROJECT NUMBER: Enter the appropriate military department identification, such as project number, subproject number, system numbers, task number, etc.

9a. ORIGINATOR'S REPORT NUMBER(S). Enter the official report number by which the document will be identified and controlled by the originating activity. This number must be unique to this report.

9b. OTHER REPORT NUMBER(S): If the report has been assigned any other report numbers *(either by the originator or by the sponsor)*, also enter this number(s).

10. AVAILABILITY/LIMITATION NOTICES. Enter any limitations on further dissemination of the report, other than those imposed by security classification, using standard statements such as:

(1) "Qualified requesters may obtain copies of this report from DDC."

(2) "Foreign announcement and dissemination of this report by DDC is not authorized."

(3) "U. S. Government agencies may obtain copies of this report directly from DDC. Other qualified DDC users shall request through

_____."

(4) "U. S. military agencies may obtain copies of this report directly from DDC. Other qualified users shall request through

_____."

(5) "All distribution of this report is controlled. Qualified DDC users shall request through

_____."

If the report has been furnished to the Office of Technical Services, Department of Commerce, for sale to the public, indicate this fact and enter the price, if known.

11. SUPPLEMENTARY NOTES: Use for additional explanatory notes.

12. SPONSORING MILITARY ACTIVITY: Enter the name of the departmental project office or laboratory sponsoring *(paying for)* the research and development. Include address.

13. ABSTRACT: Enter an abstract giving a brief and factual summary of the document indicative of the report, even though it may also appear elsewhere in the body of the technical report. If additional space is required, a continuation sheet shall be attached.

It is highly desirable that the abstract of classified reports be unclassified. Each paragraph of the abstract shall end with an indication of the military security classification of the information in the paragraph, represented as *(TS), (S), (C), or (U).*

There is no limitation on the length of the abstract. However, the suggested length is from 150 to 225 words.

14. KEY WORDS: Key words are technically meaningful terms or short phrases that characterize a report and may be used as index entries for cataloging the report. Key words must be selected so that no security classification is required. Identifiers, such as equipment model designation, trade name, military project code name, geographic location, may be used as key words but will be followed by an indication of technical context. The assignment of links, rules, and weights is optional.

UNCLASSIFIED

Security Classification